# SYSTEM APPLICATION TO NON-DESTRUCTIVE STUDY OF COUPLED FLOW IN POROUS MEDIA

by
Mesut Pervizpour

A Dissertation
Presented to the Graduate Committee
of Lehigh University
in Candidacy for the Degree of
Doctor of Philosophy
in
Civil and Environmental Engineering

**Lehigh University**
**January 2000**

This dissertation is accepted in partial fulfillment of the requirements for the degree of Doctor of Philosophy.

_____
(Date)

_____
Sibel Pamukçu
(Ph.D. Advisor.)

_____
Gerard P. Lennon
(Committee Chair)

_____
Scott A. Raschke

_____
Richard Sause

_____
Fazil Erdoğan
(Mechanical Engineering Dept.)

_____
Hugo S. Caram
(Chemical Engineering Dept.)

# Acknowledgements

I have been fortunate to work with many good people. I wish to thank a few.

I wish to thank the members of my Graduate Committee for their support, intellectually and emotionally through the years of my presence at Lehigh University. Dr. Sibel Pamukcu who has taught and advised me through my Ph.D. program has helped me develop as a researcher and a teacher in my field. Dr. Gerry Lennon, my committee chair, has been a source of support with a methodological and thorough knowledge of the applications in the field. Dr. William Schiesser, a true gentleman, has been a great source of insight and support with his ability in mathematical modeling and numerical solution of partial differential equations.

Finally, thanks to my parents and my sister for being supportive, patient and understanding during the entire time and most of all for believing in me. Surely, if it were not for their sacrifices and understanding, this course of study would never have been completed.

# Contents

# List of Tables

# List of Figures

**Abstract**

A non-destructive system approach is developed and applied to the study of coupled flow in porous media subject to hydraulic and thermal gradients. The approach makes use of the transient pressure and temperature responses of the saturated porous media under applied gradients to obtain the flow related soil parameters. An experimental one-dimensional set-up is developed to apply the gradients and measure the real time pressure and temperature responses of the system along the sample. The analytical governing equations for the transient development of the fluxes of a multi-component system are derived based on conservation equations and nonequilibrium thermodynamics theories. The analytical model is then used to form the appropriate numerical simulation environment, which is constructed to solve the governing set of partial differential equations. The soil parameters defining the heat and fluid flow in porous media are obtained by constructing an optimization environment, which obtains the parameters by minimizing the objective function. The objective function is defined as the sum of the least squares of the experimental and numerical responses of the system.

# Chapter 1

# Introduction

The heat and mass transfer problem is studied and developed extensively in fields ranging from chemistry, material science to micro-electronics. Similar concepts are also studied in geotechnical engineering in the hydro-geothermal problems related to radioactive waste burial facilities, other waste impoundments, or constructed heat barriers.

The design, life span, and performance of such earth facilities and their effects on the surrounding ground depends on the rate of the heat and mass transfer in soil. Some performance related issues for such facilities can be listed as: emanation of gas from buried tailings, surface dust, surface run-off and groundwater contamination, decay and leakage of the constructed barrier and their impact on the quality of the surrounding life. The changes in the hydro and thermal characteristics of the soil subject to elevated values of pressure and temperature may cause failure in terms of leakage, excessive deformation or instability of the near by ground and supported structures. The overall performance of these underground facilities is measured by their ability to withstand such impacts over their life cycle.

The advancement of monitoring equipment and subsurface measurement techniques have direct impact on the understanding and evaluation of the existing facilities, as well as the design of the new ones. The advantage of monitoring the performance of a constructed facility over its entire life cycle should improve their design and help schedule effective maintenance and preventive measures. Presently,

information gathering and processing is limited to indirect observations or random sampling for the hydro-thermal problems of the subsurface.

In this study, a direct approach to monitoring, and data acquisition and processing is considered to address the heat and mass transfer problem in porous media. Of particular interest is the coupled flow in porous media as a result of elevated temperature and pressure in subsurface. A testing scheme with on-line monitoring is designed to allow continuous observation of the transient response of a test sample to induced temperature and pressure perturbations.

To accomplish this, a non-destructive testing environment had to be constructed to record the transient temperature and pressure response of the sample and be able to verify its repetition in multiple applications. The irreversible thermodynamics concepts are used in developing the pertinent analytical model to represent the governing physical system. A numerical solution of the analytical model simulated the experiments. The collocation of the numerical and experimental responses provided the means to estimate the soil parameters under the given transient event.

## 1.1 Background

The problem of soil subjected to elevated temperatures and the resulting heat and material flow has been one of the most studied topics in geomechanics. The two commonly used models for the study of soil water flow are the mechanistic and the thermodynamic models. The mechanistic model is based on the coupling of Darcy's law with conservation of water mass, and the thermodynamic model is related to the principles applied to equilibrium or consecutive equilibrium states.

The mechanistic models are developed for both isothermal and nonisothermal, and saturated and partially saturated medium. Karl Terzaghi [37] developed the consolidation theory for an isothermal saturated deforming soil based on the effective stress concept. Biot [4] developed the three-dimensional consolidation concept based on linear elasticity and the generalized form for the porous media. In his formulation, he used the relations between the four terms; modulus of elasticity, Poisson's ratio,

the compressibility of the fluid and the hydraulic conductivity [5], [6].

One of the first works on coupled thermal and fluid flow in partially saturated media was by Philip and DeVries [29], expressing the vapor flux for a rigid soil in terms of volumetric water content and temperature gradients within the soil.

Narasimhan and Witherspoon [26], developed the model for water flow in partially saturated deforming soil based on the assumption of small strains. Dakshanamurthy and Fredlund [7] developed a model for moisture flow in partially saturated deformable soil subject to hydraulic and thermal gradients. In this model, heat flow is due to conduction only, where the water vapor flux is neglected, and the temperature effect is included in terms of the increase in soil air pressure.

The use of thermodynamics principles in soil was introduced by Sposito's early works on soil swelling under isothermal conditions and the more complete recent work on thermodynamics of soil solutions [35]. However, the major advance was the development of the theory of irreversible (non-equilibrium) thermodynamics. The theory studies the rate of change of entropy of a system. Entropy is a state function, as the internal energy and the enthalpy of a system. The change of entropy is divided in to two parts; entropy flow and local entropy production. The entropy flow component is due to convective flow carried through the boundaries of a system and the heat conduction through its walls. The local entropy production is a source and also a positive definite term indicating that the system is not in equilibrium, which is the main cause of flows.

Onsager [27], [28] introduced the concept of coupled flow based on a hypothesis that all the potential functions causing direct flow will also cause coupled flows. His theory stated that all fluxes such as mass, heat, electrical current can be related linearly to the corresponding thermodynamic forces. The positive nature of the entropy production term restricts the form and value of the cross coefficients and causes them to be equal. This outcome allowed determination of the cross coupled terms by measuring only one of the cross terms.

The application of irreversible thermodynamics to coupled flow in soil systems was introduced by Taylor and Cary [36]. The study developed non-equilibrium expressions for heat and water vapor flow in soil and verified that the cross-coupling

terms were equal. Later, analytical expressions for the coupled fluxes based on the irreversible thermodynamics or theory of mixtures for multicomponent systems were formulated by others [31], [8], [13], [24].

Since then, the multi-phase heat and mass transfer for saturated and unsaturated porous media has become a well understood problem for the researchers [9], [25], [32], [35], [29],[39].

## 1.2 Scope

The specific manner a typical heat and mass transfer problem is handled determines the applicability of the thermodynamics method to soils. This handling may include utilization of the analytical expressions, experimental methods or the numerical schemes and algorithms in analyzing and explaining the observed or designed phenomena. The analytical, experimental and numerical components are seldom applied simultaneously as a unified system capable of addressing the phenomenon at hand.

The analytical formulas are highly detailed and often expressed for general cases. These formulations often deal with parameters that may not be appropriate for direct use in a unified system approach consisting of experimental and numerical components as well. In an integrated system, the solution requires measurable parameters.

A well planned unified system should take advantage of the initial experiments to determine a relevant set (and combination) of coefficients and terms used in the analytical representation of the tested event. The next step is the numerical solution of the analytical equations to determine the required characteristics. In this way, redundancies due to the large number of built-in coefficients and terms involved in the numerical solution of the system can be reduced without oversimplifying the problem.

The research to be discussed here is based on this unified system approach with

experimental, analytical and numerical components. A unique experiment, its equipment, and an accompanying methodology is designed to serve this purpose. The analytical expressions are formulated using principles of non-equilibrium thermodynamics that represent the system with easily measurable terms. The numerical solution of these formulas are collocated with the experimental results in a parameter identification and optimization process to obtain the desired coupled coefficients.

A nondestructive approach is considered here to test the classical heat and mass transfer problem. The tests are conducted by applying various types and combinations of the temperature and pressure gradients. The transient response of a saturated porous medium is measured in terms of temperature and pressure flux. The non-destructive test is achieved by closed material boundaries and pulse like gradient applications to minimize possible deformation to the porous skeleton and preserve the original physical properties of the medium.

A set of coupled governing equations were derived and used in the numerical generation of the temperature and pressure profiles in the direction of the applied gradients. These simulations utilized initial sets of estimated coupled coefficients. The profiles were then compared to the experimental profiles generated under the same boundary conditions. A parameter estimation routine was performed by minimizing the error between the experimentally and numerically generated responses, to obtain the coupled coefficients that will satisfy the experimental data.

The components of this unified system are designed to conform to each other within the system. For example, the nondestructive experimental approach capability is utilized to allow to test under closed material boundary conditions which improves gradient control. The analytical formulas express the transient state of the coupled flow allowing conformance with the transient state experimental measurements. The numerical simulation of the analytical model is based on the solution of the governing equations by discretizing the spatial derivative and integrating the resulting ODE in time which is also referred to as; the Method of Lines [33]. A parameter identification approach is built-in the simulation routine that collocates the simulated results and the experimental measurements. The parameter identification routine performs search-and-optimization to determine the coupled flow parameters

satisfying an error term.

## 1.3 Contents

This study is presented in the following four main chapters and a conclusion chapter. Chapter 2 describes the design and operation of the nondestructive experimental set-up. The governing equations are derived in Chapter 3. First, the multi-phase form of coupled equations for heat and mass transfer are obtained. Then, transient coupled and uncoupled expressions for hydraulic and thermal components are derived from the general expressions. Chapter 4 discusses the selected numerical solution method including its advantages and applicability to the problem in hand. Also provided in this chapter are sample solutions of the typical forms of the governing equations of the system.

The parameter identification - estimation approach utilizing a quasi-newton quadratic search-and-optimization method is discussed in Chapter 5. The examples of the application of the method to the numerical and experimental responses obtained are shown. The final list of the soil parameters obtained for each case are discussed in Chapter 5 also.

A brief discussion of the relevance and importance of the method developed and the required improvements and further applications are discussed in Chapter 6.

# Chapter 2

# Experimental Approach

A unified system of experimental testing, analytical modeling, simulation and parameter identification were applied to the coupled flow problem in porous media. A unique system approach was needed to overcome the experimental limitations in acquiring a set of parameters that conform with the analytical and numerical components. The experimental component of the system had to be well represented by an analytical model. The measured parameters were then put in the model to obtain the desired coupled coefficients.

The experimental method was designed to be flexible for continuous improvement of the testing methodology, measurement techniques, and the quality and repeatability of the data by feedback from the analytical model. Such a design required complete understanding of analytical limitations and capabilities of the numerical solution method. This requirement forced the experimental improvements to be incremental and concurrent with the development of the analytical and numerical components.

The experimental set-up is designed to work with the transient state response of the system. The transient response is defined as the temperature and pressure distribution along the deformable saturated porous media, in the same direction as the applied gradient or force. The real time temperature and pressure measurements are used to model the transient state behavior when solving for the coupled coefficients.

A one-dimensional and a triaxial experimental set-ups were designed and constructed to observe the system response under the applied thermal and hydraulic gradients. The unified system approach presented in here is validated using only the one-dimensional set-up.

## 2.1 Nondestructive testing approach

It is desired to construct a testing environment where minimal disturbance is introduced to the original state, constituents and the skeleton of the porous media. A non-destructive test is required to achieve the minimal disturbance which in turn provides better quality data and higher rate of success in repeatability.

Use of the closed material boundaries and the pulse like gradient applications are two of the possible conditions that can be induced to minimize the disturbance and changes to the skeleton of the porous media. The advantage of applying these conditions on a two-phase system (solid-liquid) is the elimination of the material flux and thereby minimization of the disturbance by deformation or particle seepage.

The elimination of the flux prevents us from using steady state flux and gradient relationships to obtain the pertinent coupled coefficients. Consequently, transient state response is selected as an alternative which can provide information not only for the final equilibrium state, but also allows in-depth look to the development of the process itself.

Another precaution to ensure as little disturbance as possible, is to operate the system at low levels of stresses. These conditions qualify the testing environment as non-destructive and permit application of various types and combinations of gradients on a single specimen in repeated experiments. This approach was also found to eliminate the variations observed in measurements when un-identical specimens are used typically.

The implementation of the non-destructive test and the analysis of the transient response of the system allow shorter duration experiments without the requirement

to achieve a steady state condition. The analytical model and the numerical simulation, in the following chapters are integral parts of the nondestructive approach discussed. They complement the experimental method by cloning the experimental pressure and temperature responses numerically.

## 2.2 Soil specimen

The system referred to in this dissertation is the two-phase solid-fluid specimen of soil. The soil samples were prepared to obtain a desired range of permeability so that the fluid saturation could be achieved in reasonable duration of time.

### 2.2.1 Constituents and composition

The soil particle sizes range from clay to sand size. The diameter of the particles is between $0.005 \leqslant D \leqslant 1$mm. The typical particle size distribution curve is shown in Figure 2.1. The mixture was prepared by mixing 15% Georgia kaolinite (LL=42%, PL=30%) with 40% silt, 25% medium sand and 20% coarse sand by weight at a water content of approximately 20%. As stated previously, the proportions and the size distribution were pre-selected to obtain a permeability in the range of $10^{-4}$ to $10^{-6}\,\mathrm{cm}\,/\,\mathrm{s}$.

### 2.2.2 Sample tube

An acrylic cylindrical tube with an ID of 2.5 cm, and a length of 21 cm is used as a mold during sample preparation and as a sample holder during the transient coupled flow tests. The acrylic tube permits easy instrumentation for temperature and pressure measurements (Figure 2.2).

The thermocouple locations are drilled and plugged with silicon glue to prevent their clogging during soil placement. The pressure sensor connections are 0.25 in Swagelog quick connects which are leak proof. The front end surface of the quick connects are covered with Nylon filters with an opening size of 5 or 10 $\mu$m, prior to

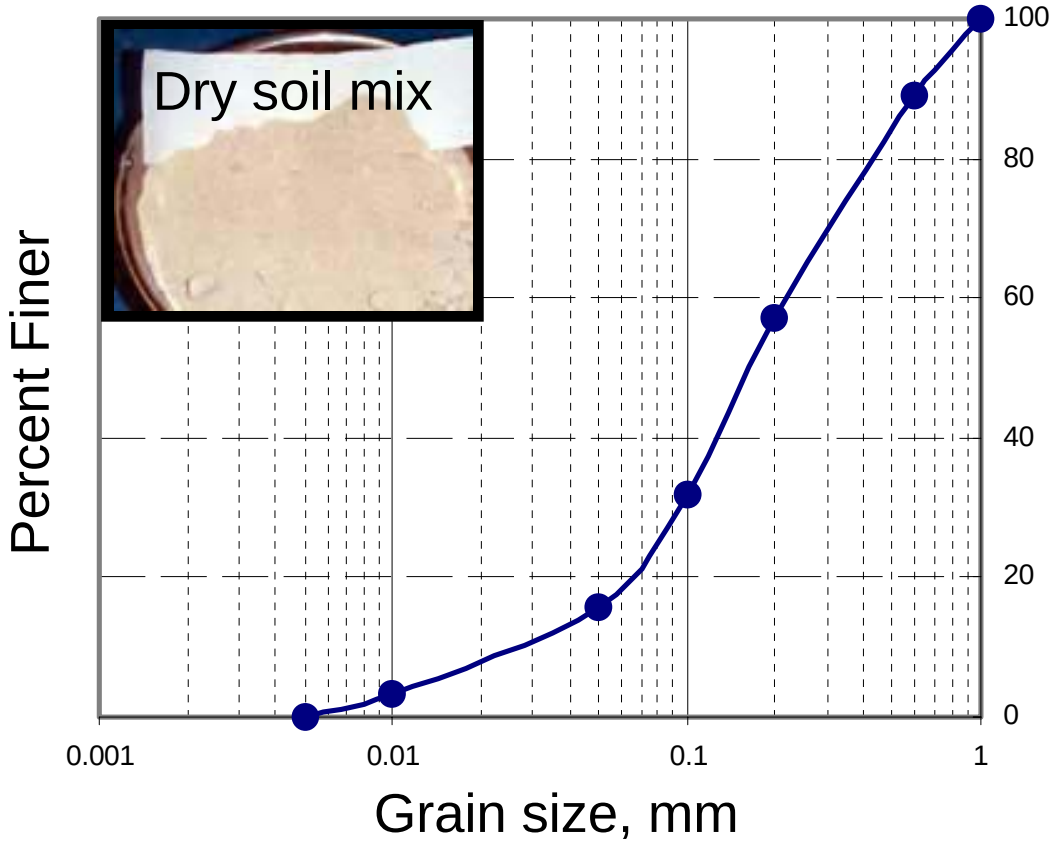


Figure 2.1: Particle size distribution curve of the soil mixture.

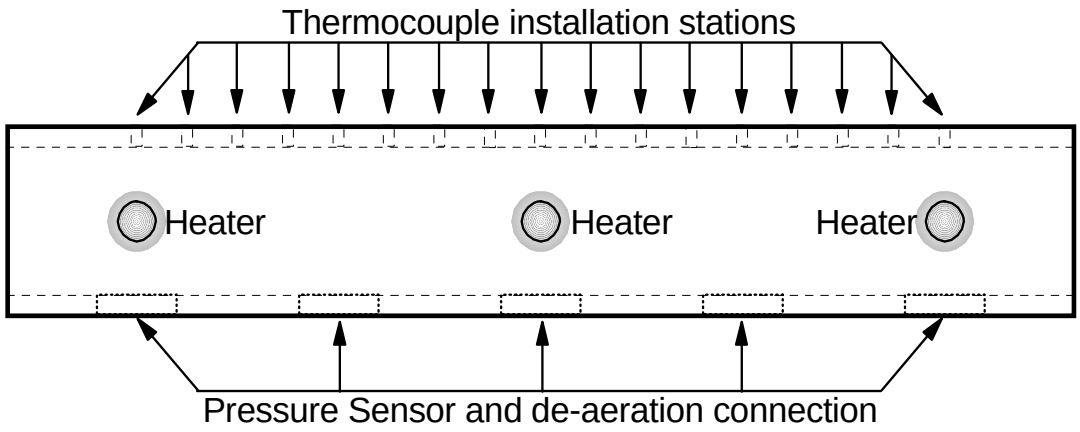


Figure 2.2: Cylindrical sample test tube.

their installation. Initially, porous stones were used as interfaces between the soil and the transducers. However, porous stones used at different pressure measurement stations had variable resistances and response rates owing to slight differences in their thicknesses. They caused an undesirable pressure drop across the two faces. Therefore, the Nylon filter with a thickness of few microns is adapted instead. This replacement proved to correct the response magnitude and the lag time problem caused by the earlier use of the porous stones.

The empty tube with all the connections installed and securely plugged, is mounted on a one-dimensional consolidometer (Figure 2.3) base. Porous stones and filter papers are used as separators at both ends of the sample. The soil is filled from top and compacted in four layers. The extension segment and the piston within the top platen is connected and an initial seating pressure of 5psi is applied to the sample.

At this point the specimen is ready for consolidation. Prior to the initial saturation and pressure increments for consolidation, the thermocouples are inserted to assure good contact with soil.

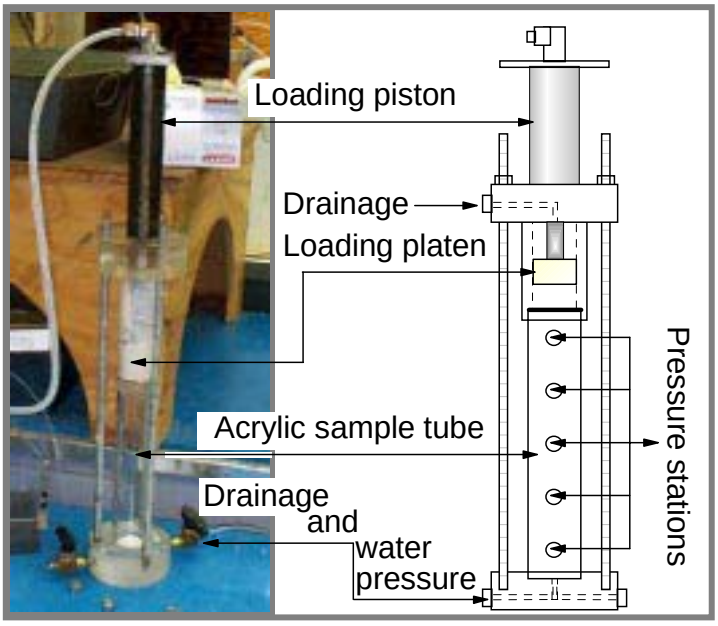


Figure 2.3: One-dimensional consolidometer

### 2.2.3 Sensor installation

Alumel-Chromel type fine wire thermocouples are initially guided into 1/8 in teflon tubes which are sealed with silicon on the inner surface to eliminate leakage. A metal pin of same diameter as the thermocouple is then used to provide an insertion hole for the thermocouple head that is to be positioned at the center of the specimen. The surrounding of the thermocouple location is sealed with several applications of water resistant silicon glue.

After the glue is set, de-aired water is connected to every quick connect along the sample tube to fill their housing with water. Pre-filling the housings with water helped to avoid back flush of soil particles into the quick connects during consolidation. Then the back saturation valve at the bottom of the consolidometer is opened. Following this step, an initial pressure of 5psi is applied to drive water up along the sample while pushing the air out of the pores.

### 2.2.4 Sample consolidation

The one-dimensional consolidation set-up is shown in Figure 2.3. Back pressure was applied to replace the air from the pores with de-aired water. The back pressure was applied in steps of 1psi up to 5psi. The back pressure application is terminated when a constant rate of flow is measured at the top platen drainage for a period of 24h. Then the bottom platen drainage valve is closed and consolidation pressure applied with drainage allowed at the top only.

Step wise pressure increments are applied over several periods of hours to achieve the desired consolidation level. The end of each consolidation step is reached when the out flow at the top ceases. The consolidation pressure is applied in the following sequence: 5, 10, 15, 20, 40 and 80psi as required to achieve the targeted permeability range. The non-standard length of the sample tube and the granular nature of the soil reduced the overall effectiveness of the consolidation owing to increased wall friction. Therefore, the tube is tapped several times at the beginning of each pressure increment to help to overcome the initial wall resistance between the acrylic surface and the particles.

At the completion of consolidation, the sample tube is detached from the consolidometer base and placed in the coupled flow test set-up.

### 2.2.5 Initial measurements

The soil sample weight and volume measurements are taken before and after consolidation. The acrylic tube dimensions and the weight are measured prior to each test including the porous stone and the filter papers. Water content measurements are made for the initial soil mixture and the soil sample after the consolidation period.

Density, porosity, void ratio and other relevant soil properties are calculated from these measurements.

Additional measurements include the particle size distribution and hydraulic conductivity. Furthermore, conventional consolidation tests are performed on soil samples of the initial mixture and a segment of the consolidated test soil trimmed from the extension section of the one-dimensional consolidometer.

## 2.3 Experimental set-up

A coupled flow test apparatus is constructed to obtain experimentally the pressure and temperature response of the system under applied gradients. Three different set-ups are constructed: one triaxial and two one-dimensional set-ups. The triaxial set-up components were the first to be designed and constructed which conformed to the testing requirements under the applied hydraulic and thermal gradients. Two variations of the one-dimensional set-up were constructed. The second generation test equipment had improved control over the two end boundaries of the soil sample.

In this chapter, the final form of the one-dimensional set-up and testing protocol used with this set-up will be covered in detail and the relevant improvements will be discussed. Although the triaxial set-up was not used for testing purposes in this work, its system design and various components were utilized in the one-dimensional tests. Therefore the triaxial set-up will be described briefly for future use purposes.

### 2.3.1 One-dimensional set-up

The design and construction of the second generation set-up was done to improve the control of boundary conditions and to capture detailed transient response measurements. A picture of the test station is shown in Figure 2.4.

One major advantage of this equipment is the use of the same sample tube in sample preparation and testing as well, without the need of extraction or further handling of the soil sample. Another advantage is the ability to apply either single or combined gradients on the same sample. The design of the system permits flexibility on the type and combination of the tests to be run without changing the physical or sensorial arrangements.

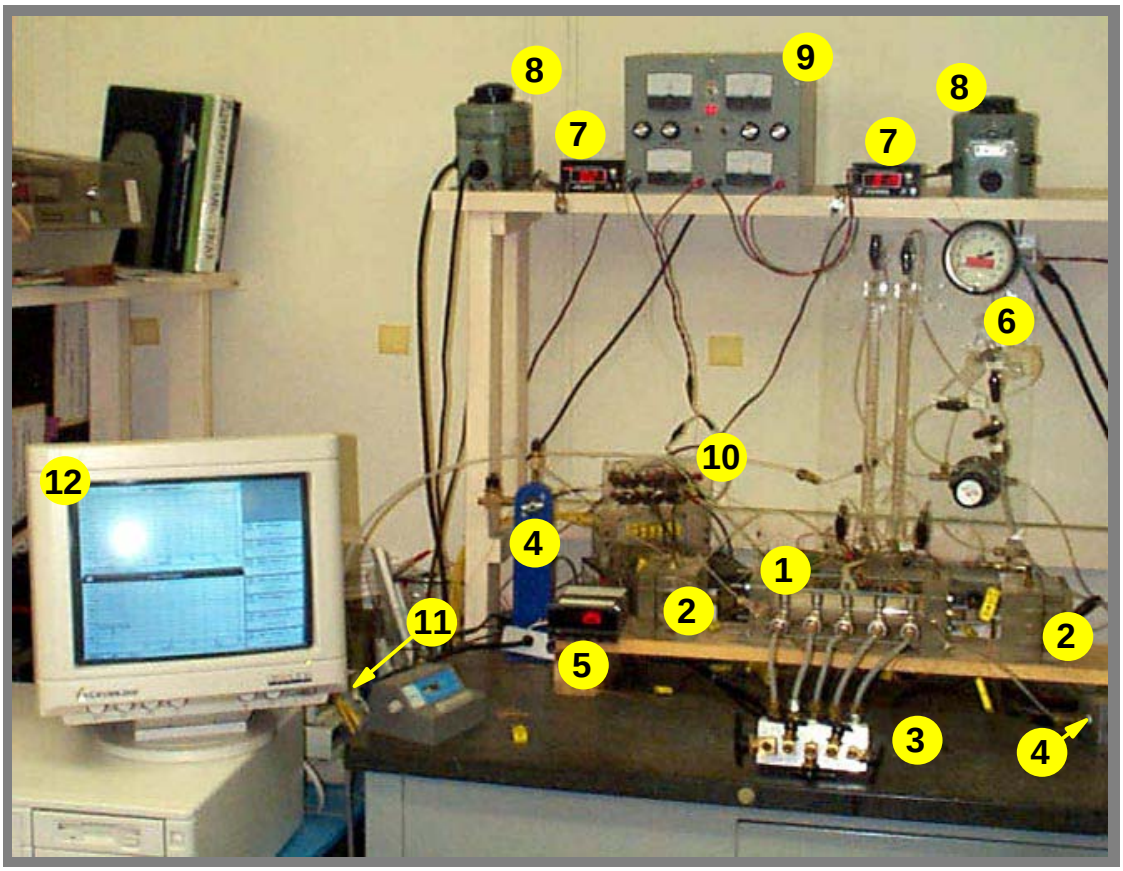


Figure 2.4: Coupled flow complete test station.

The items numbered on figure 2.4 are:

| No. | Description | No. | Description |
|---|---|---|---|
| 1 | Test cell | 7 | Heater control unit |
| 2 | Reservoir | 8 | Heater power unit |
| 3 | Pressure block | 9 | Pressure transducer power supply |
| 4 | Boundary pressure | 10 | Thermocouple connection board |
| 5 | Pressure gauge | 11 | Thermocouple cold junctions |
| 6 | Hydraulic control panel | 12 | PC - Data acquisition |

The test equipment consists of the following components: 1) sample tube, 2) two water reservoirs, 3) instrumentation, 4) heat sources at the boundaries and within the sample, and 5) flow control panel. The inflow, outflow and the hydraulic gradient controls are performed from the control panel via burettes and pressure regulators. A pressure and de-aeration control unit is used during the initial de-aeration of the system. It is a rigid aluminum block for pressure sensor connections.

As shown in Figure 2.4, the system is made of different components. Next the whole system is described in detail in the following sequence of components: the test cell unit, the measurement and sensory environment, boundary conditions and their control, and the data acquisition.

### Coupled flow test cell

The coupled flow test cell shown as 1 in Figure 2.4, is detailed in Figure 2.5. Three different views of the cell and an actual image is included to show its various parts. The center unit has the soil sample and it is instrumented for temperature and pressure measurements at stations along its length. This unit also has three ports for internal heat source. There are a total of seven pressure transducers, five on the sample tube and one at each boundary. The ends of the sample tube is connected to two end plates and each plate is connected to a reservoir with a ball valve. The separation of the sample tube from the reservoir was necessary in order to control the material boundary conditions without introducing volume change effects due to the adjustments made in fluid reservoirs. Thermocouple stations are conveniently placed across the pressure ports, on the other side of the sampling tube where the temperature along the center line of the sample is measured.

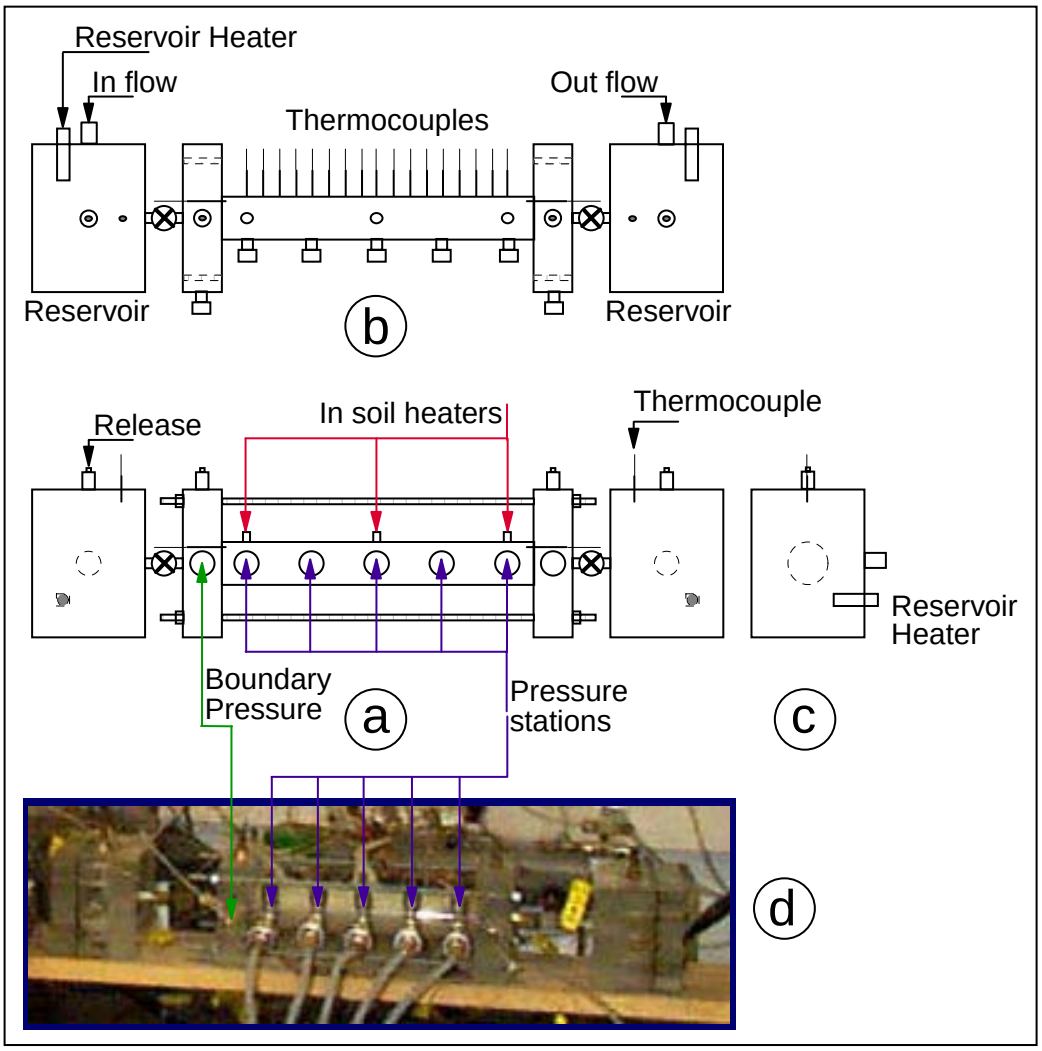


Figure 2.5: One-dimensional setup, a) front, b) top, c) side view, d) picture of setup.

**Pressure connections** The pressure transducers are connected to the sample tube by means of T connectors and quick connects (Figure 2.6a) via the pressure transfer block (Figure 2.6b). The T-shaped connections are necessary to allow de-

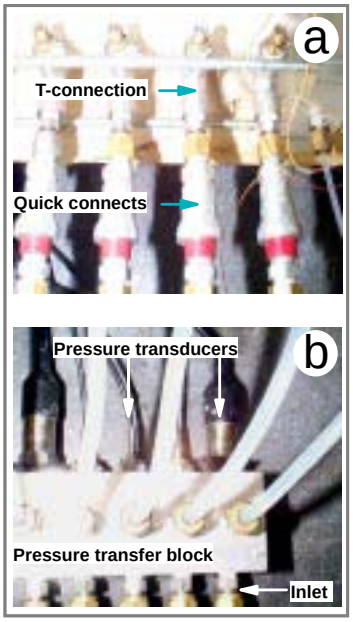


Figure 2.6: Pressure measurement stations, a) quick connects, b) pressure transfer block.

aeration at the connection and to eliminate the entrapped bubbles that effect the fluid pressure measurements. The transfer block is also used as the de-aeration station of the pressure transducers prior to attaching them to the test apparatus.

**Thermocouple connections** The thermocouples are inserted from the opposite side of the sample tube (Figure 2.7) to the sample center line at 19 locations (including the boundaries). Thermocouple wires were mounted in 1/8 in teflon tubes and sealed with water resistance silicon adhesive. The fixture was then used as a stance and to prevent the leakage by the wires which was installed prior to the consolidation phase as described before. Figure 2.7a, shows three additional locations

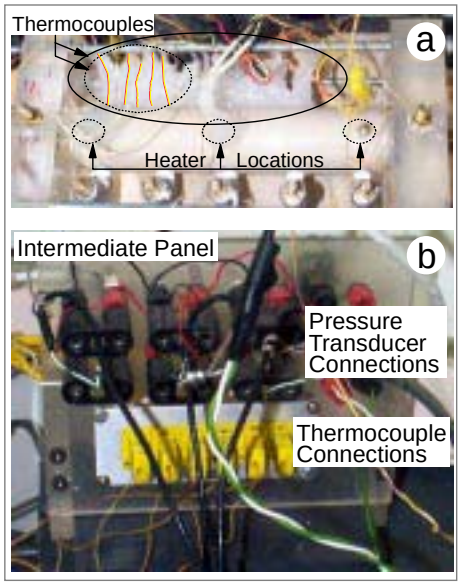


Figure 2.7: Temperature system, a) measurement stations, b) intermediate panel.

along the sample tube where rod type heaters would be embedded into the sample prior to consolidation. Figure 2.7b, is the intermediate connection panel where the thermocouples, and transducers' wiring are plugged for connection to the cold junction or the daughter boards of the data acquisition system.

### Sensoral system

The various sensors, their types, specifications, justification for their selection and their relevant usage are described in this section. In this study, only two types of physical measurements were made for simulation purposes: pressure and temperature. Thermocouples and pressure transducers were selected to obtain on-line, real-time measurements.

**Pressure transducers** A total number of eight pressure transducers were used with two of them located at the boundaries, five along the length of the sample and one to monitor the applied hydraulic pressure. Five different liquid filled type

transducers are used. These transducers sense through diaphragm action with output ranges of $15 - 150$psi. The output of the self-amplified transducers were from $0 - 6$ to $0 - 10\,\mathrm{V}$ in full-range.

The applied pressure is measured by one pressure transducer and monitored through a readout box and recorded along with others via the data acquisition system. The boundary and the other sensors along the sample provided the transient state measurements.

Three levels of calibration were applied to these sensors. First, each sensor was calibrated individually. Prior to sample preparation, the empty sample tube equipped with transducers was set-up in the apparatus and filled with de-aired water. The response of all the sensors were recorded and the system was calibrated as a whole to account for losses at connections and other system induced effects with respect to the pressure at the application point. The third level was conducted at the end of each test when equilibrium was reached and the signals obtained from all sensors were again checked relative to the input signal to account for drift and other sources of measurement errors.

**Thermocouples** $36\,\mathrm{in}$ long, fine wire ($D = 0.010\,\mathrm{in}$) gauge= 30, Alumel-Chromel type (5TC-TT-K-30-36), teflon coated K-type thermocouples, were selected for their size, range and durability. A maximum number of 22 installed thermocouples were available for use, but due to the channel limitations on the data acquisition system, only 9 were related from the remaining of the 16 total channels at a time.

**Data acquisition system**

A PC based data acquisition and supporting peripheral was constructed to measure and control the parameters of the system. A high resolution 16 bit digital I/O, multi-function, 16 channel card with inputs for: T/C, mV, V, mA, was selected for this purpose. The WB-FAI-B PC-card based data acquisition module were supplemented with external terminal boards with isothermal plates, (item 11 on Figure 2.4), for the thermocouple measurements. Other specifications of this card

are listed in Table 2.1. The 16 available channels were allocated to the measurement

Table 2.1: Data acquisition card specifications

| **Board** | **Channels** | **Resolution** | **Input Type** | **Max. Rate** |
|---|---|---|---|---|
| WB-AAI-B | 8 and 16 diff. | 16 bit | mV, V, mA T/C, RTD | 225 Hz |

of the pressure and temperature response. In general 7 to 8 channels were allocated to pressure measurements with the rest assigned to thermocouple stations. When all 16 channels were in use the lowest effective sampling rate was about $20 - 25$ Hz.

A quick-log PC acquisition interface software was used to design the measurement system and the data acquisition parameters for each test. A graphical output of the system was configured to permit on-line monitoring of the sensors in charts and tables. The output from the sensors were also logged into files for post processing of the data.

### Input devices

The input devices were used to implement the desired form and level of input during a test scheme. Hydraulic gradients in variable frequencies and rates were applied and maintained by use of pressure regulators transmitting air pressure to a water column with a very finite diameter (ID=1 $cm^2$, item 6 in Figure 2.4).

The temperature increase was achieved using 1 in immersible electric rod type heaters (Watlow Firerod cartridge heaters) located inside the soil sample and in the reservoirs. The heater used in the reservoirs were larger in diameter (1/2 in), while the others inserted in the soil were 1/8 in in diameter to act as point sources. The characteristics of the heaters are listed in Table 2.2.

### Control and power sources

The hydraulic pressure was maintained by means of pressure regulators. The heat was applied via the rod heaters. The control of these potentials were most critical at the boundaries.

Table 2.2: Heater characteristics

| **Diam. inch** | **Length inch** | **Volts Max.** | **Amp Max.** | **Min. Watts at** 120 V | **Max. Watts at** 120 V |
|---|---|---|---|---|---|
| 1/8 | $1-1/4$ | 240 | 3.1 | – | 360 |
| 1/4 | 1 | 240 | 4.4 | 100 | 525 |

The pressure was maintained via a pressure regulator and monitored with a transducer and a digital readout. These measurements were later integrated to the post processing of the data. The system heat loss required an automated control system to regulate the power input to the heater and maintain the desired temperature increase within a given bandwidth. Figure 2.8 shows the two separate units for heater control (Figure 2.8a), and the close-up (Figure 2.8b) of the power unit and the controller. The power unit is capable of applying variable voltage input to the heater and the controller (CN310-JC) is attached to a thermocouple. This creates a closed-loop control environment by setting the desired value of temperature and a lower and upper limit of variation, such that the voltage input from power source can easily be controlled for particular requirements of a test. The controller's digital read out, and a hand held digital thermometer readout (HH-81) attached to the same thermocouple were used for system check and confirmation.

### 2.3.2 Triaxial set-up

The original experimental study was intended to use a triaxial set-up. The one-dimensional test equipment was designed and constructed to reduce the number of test parameters for closer simulation of the system. Therefore, the triaxial set-up although constructed, was not verified in this work. Nevertheless, a brief discussion of the system is provided here for future reference.

The triaxial set-up was designed to be compatible with thermal requirements of the system: including minimizing heat loss and accommodating a number of sensoral and input devices within its components. The sample caps for the top and bottom of the sample are shown in Figure 2.9. The bottom cap (Figure 2.9a) accommodates

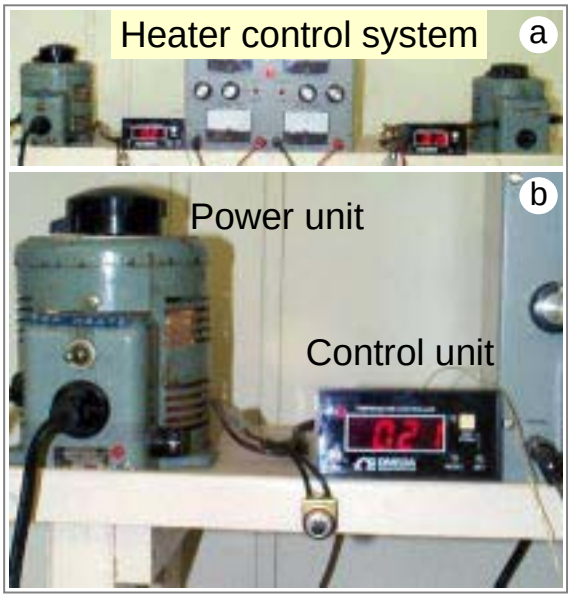


Figure 2.8: Heater control and power source units.

two pressure transducer connections for the bottom and mid height of the sample. Connections for several thermocouples, a heater and in flow and de-aeration are included in the cap housing also. The segments a.1 to a.4 in Figure 2.9a, illustrate various dimensions and views for the bottom cap. Similar notations are used for the top cap where only one pressure transducer and heater with several thermocouples, and fluid out flow connections are shown. Figure 2.9c illustrates the assembled soil sample and the caps. The caps were constructed from Micarta$^R$ a Nema grade C, cloth based material from Westinghouse Electric Corporation, Micarta division, Hampton, S.C. 29924. The physical properties of the material are listed in Table 2.3. A gas impermeable membrane was selected to embody the soil specimen such

Table 2.3: Physical properties for Micarta$^R$

| **Thermal** | | **Strength (psi)** | | | |
|---|---|---|---|---|---|
| **Conduct.** $^\circ$F / in | **Expansion** in / (in $^\circ$C) | **Tensile** | **Compress.** | **Flex.** | **Shear** |
| $7.0E-04$ | $3.95E-05$ | $11,000$ | $40,000$ | $19,000$ | $11,000$ |

that the confining fluid (water) could be replaced with air to minimize the heat loss through the sample surface and the membrane to the surrounding. Figure 2.10 shows the actual caps and platens made for the triaxial coupled flow test set-up. A control panel capable of handling two cells simultaneously is also constructed. This panel supports two test set-ups and allows consolidation of one sample while test may progress for the other. The panel is designed to measure inflow-outflow, controlled application of confining pressure, the top and bottom internal pressures and vacuum (Figure 2.11).

## 2.4 One-dimensional coupled flow test procedure

One-dimensional test set-up and components are all described with the particular specifications and utilization. The general protocol for the transient state coupled flow testing is described here. Discussion of testing under particular boundary conditions will follow in the next section.

### 2.4.1 Test procedure

The sample tube mounted between the reservoirs is equipped with the thermocouples, heaters and quick connects to the pressure transducer. The pressure block, shown in Figure 2.6b, is now connected to the de-aired water chamber and the block is de-aired. This is done by flushing each channel through the teflon tube the top of which is capped by the male end of a quick connect itself. The male end is then connected with the matching female pressure station along the sample tube. The flushing of each channel with de-aired water is performed once again between the pressure block and the T-shaped connection at the sample tube, resulting in full de-aeration of each measurement channel.

The sample is then oriented vertically and submitted to initial pressure gradient to assure high degree of saturation prior to testing. The inflow and outflow measurements are taken during this period and the process is terminated at equilibrium. This method was initially applied to every sample to assure saturation,

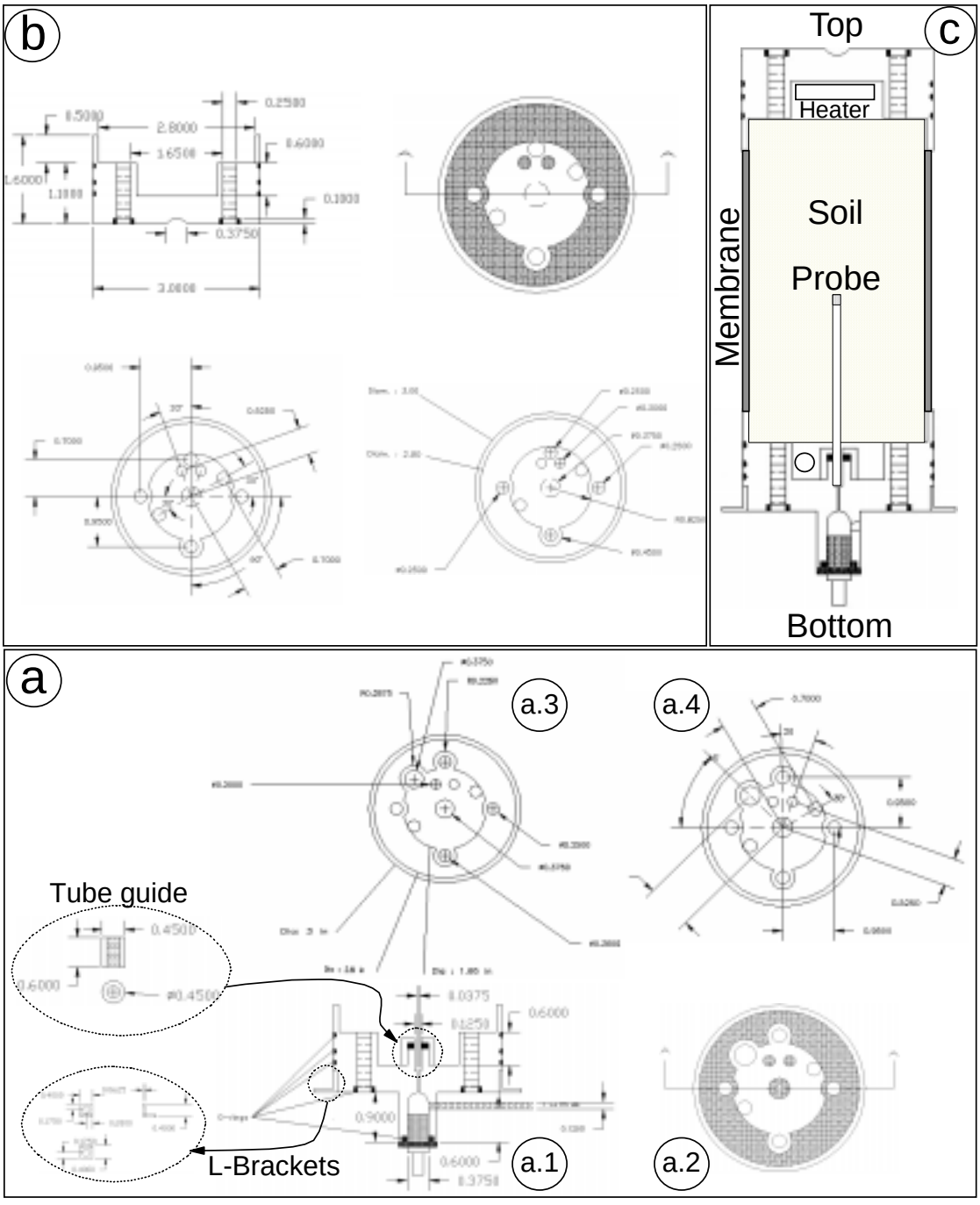


Figure 2.9: Triaxial cap design, a) bottom, b) top, c) assemby.

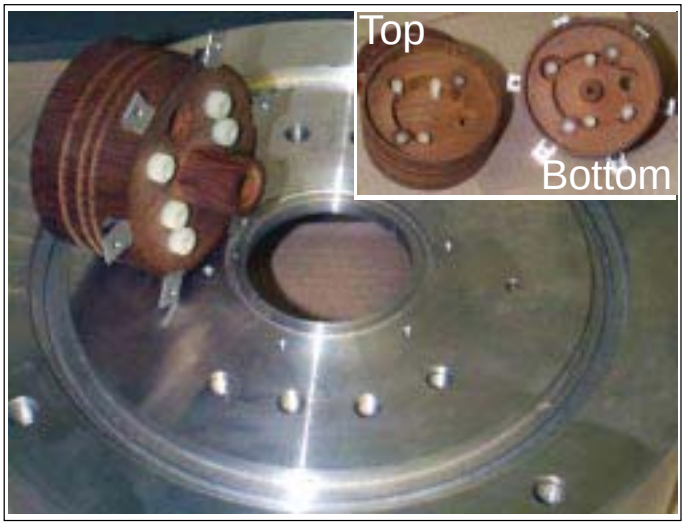


Figure 2.10: Traixial caps (Micarta) and bottom platen.

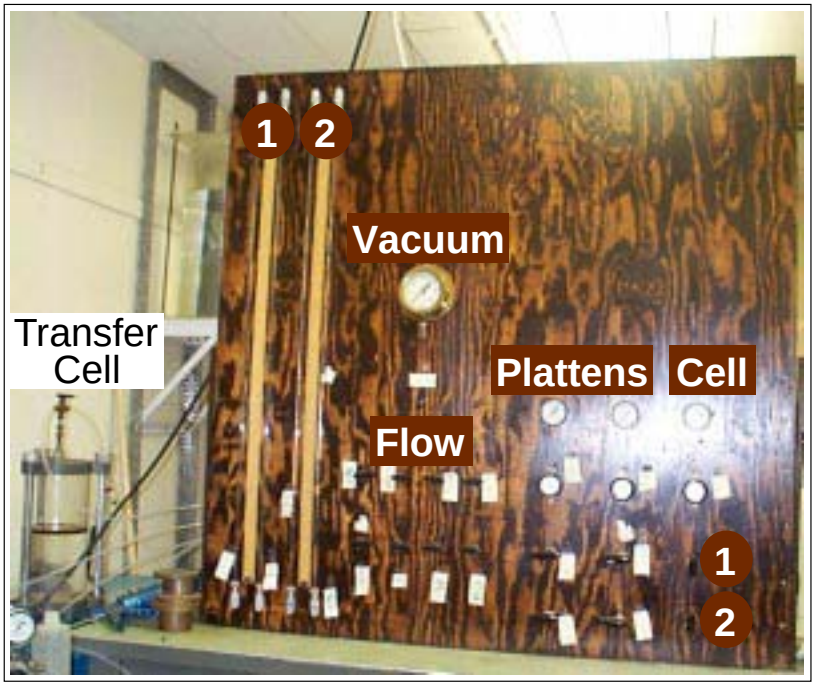


Figure 2.11: System, fluid and pressure control panel.

however was not carried on after it was determined that the initial saturation process in the consolidometer and the following consolidation was sufficient to achieve fluid phase continuity within the interconnected pores.

The near fully saturated sample is then tested under the desired hydraulic and thermal gradients and the transient pressure and temperature response of the system recorded. Prior to the application of the gradients a hydraulic conductivity test is conducted to obtain the coefficient of hydraulic conductivity of the soil specimen. This determination is used to evaluate the degree of disturbance that might occur due to repeated testing under various gradient applications. The initial conductivity is compared to final conductivity determined after the completion of the gradient tests. The hydraulic conductivity tests require in-flow and out-flow measurements along with the applied gradient measurement.

### 2.4.2 Data processing

The transient pressure and temperature response of the system can be recorded in a file either as the raw sensor output (voltage) or converted to desired units (i.e. pressure units). The experimental data collected in this study was recorded in raw sensor signal output and post processed later to handle the drift and other possible causes of variations. Several post processing codes were developed in Fortran90, and combined to form the two final programs, one for each output type; pressure and temperature.

The raw experimental data is first processed to convert to the desired units of the physical phenomena measured (Figure 2.12b). This conversion is performed by a single file that contains the latest calibration factors for each pressure sensor. Figure 2.12, presents a series of graphical outputs at different stages of the data processing subject to the "*loading stage of step-function*" gradient application.

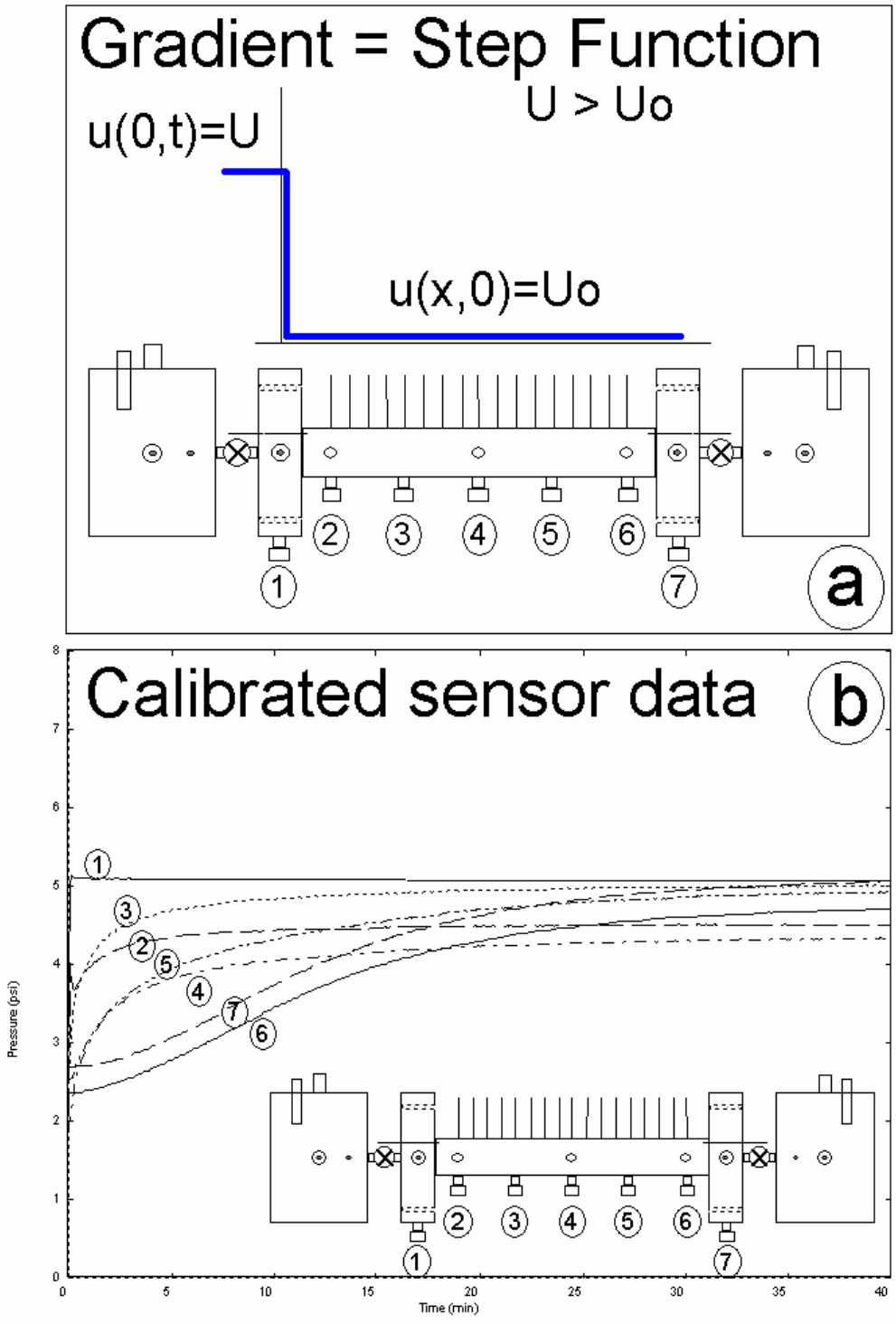


Figure 2.12: Step-wise data conversion and post-processing.

Figure 2.12a shows the set-up and the initial distribution of water pressure: $u(x,0) = U_0$, and the applied constant value at one boundary $u(0,t) = U$, while $U > U_0$ and the other boundary is kept under no flow (closed) conditions ($\partial u/\partial x = 0$). Figure 2.12b is the plot of transient pressure distribution ($U = 5$psi and $U_0 = 2.5$psi) at consecutive stations adjusted for initial point variation and converted to pressure units using the most recent calibration data. However, it was observed that the behavior of the pressure under this conversion did not properly handle the variations in sensors, and the particular drifts that could have occurred during the test period. The data plotted in Figure 2.12b is the adjusted data for the drift with respect to the measured and recorded signal at the original input. The entire post processing is carried out with two separate files, designed to handle pressure and temperature separately.

The calibrated sensor data for sensor $i$ in Figure 2.12b is first reduced by $U_0^i$ (initial pressure value for sensor or station $i$), and then normalized with respect to $(U^i - U_0^i)$ and the final time. The resulting normalized distribution is given in Figure 2.12c.

The normalized experimental data can be used for comparison to the numerical response of a non-dimensional system in parameter estimation routines. The numerical solution of a non-dimensional (normalized) set of governing equations is relatively simple owing to the control of numerical stability and better understanding of the error magnitude. These issues are discussed in detail in Chapter 4. However, any system non-linearity or dependence might easily be lost and overlooked in a non-dimensional normalized system analysis. Therefore original experimental and governing equations are preferred rather than their normalized forms.

Consequently, the corrected normalized data format (Figure 2.12c), which describes the initial segment in post processing for *loading stage of step-function* is converted back to give the appropriate response of $U_0, U$, and the final time distribution. This next stage of post processing is carried out by multiplying each pressure value with $U_0, U$, which results in the final form of the output shown in Figure 2.12d.

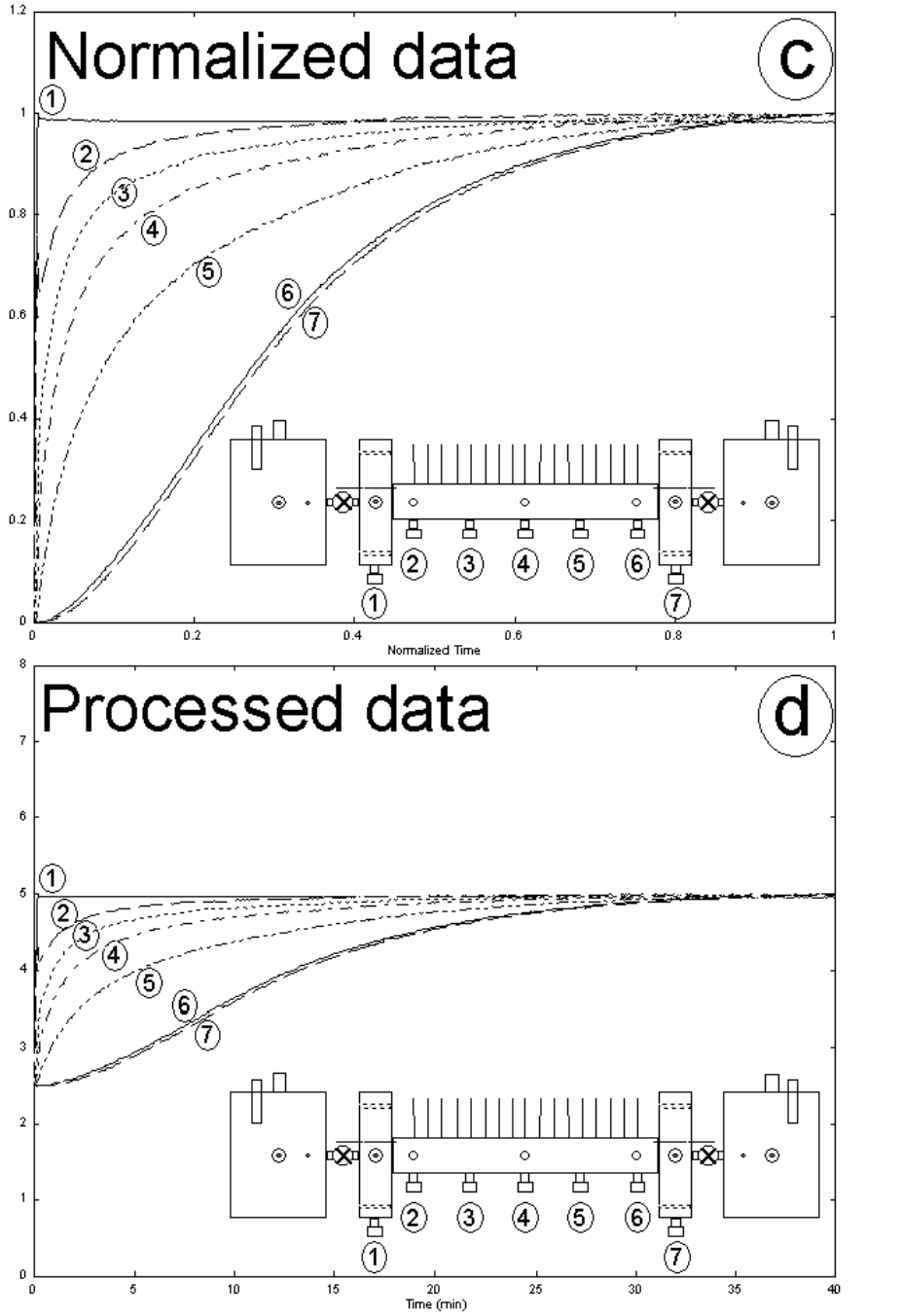


Figure 2.12: (continuing) Step-wise data conversion and post-processing.

## 2.5 Boundary conditions and system response

Different forms of gradients are applied by controlling the pressure and temperature at the boundaries. Hydraulic gradient tests, for instance, are conducted under closed and open boundaries at various pressure levels. Thermal gradients are also applied initially at the boundaries by using the heaters located in the reservoirs. However, for a given power (wattage) of the heater, the temperature increase takes a long time due to the large water volume in the reservoir and its heat capacity. It is therefore preferred to use the heat sources within the soil sample. This arrangement also permits testing under completely closed material boundary conditions. The disadvantage of the arrangement is that it results in lengthy and complicated numerical manipulation of the experimental data, simulation and the parameter identification of the system.

Various forms of gradients such as; constant, transient or step-function type with closed or open material boundaries are considered. Thermal gradient is controlled by the heater power therefore does not lend to variations easily. This lack of flexibility limits the testing schemes and the possibility of different scenarios. However, still various configurations are considered to aid the verification of the experimental-numerical-optimization system. Some of these are based on the responses obtained for such cases as: changing the location of the heater within the sample, the insulated sample as opposed to the default case of un-insulated sample, and also opening and closing the material boundaries.

### 2.5.1 Hydraulic gradient application

The hydraulic gradients include use of closed and open boundaries, and load-unload stages of a transient gradient in the form of a step-function.

#### Open material boundary

Open material boundary conditions are those when the flow through boundaries are permitted and various flux and pressure measurements are recorded. A constant

gradient is maintained across the boundaries during the test. This is similar to a conventional constant-head hydraulic conductivity test of soils, with the additional recording of the transient pressure distribution.

Two types of open boundary tests are described here: loading and unloading. The loading case is when the applied gradient at the boundary ($U$) is larger than the initial condition ($U_0$), and in reverse, the initial state is greater than the applied boundary for the unloading case. Note that other variations are also possible, depending on the initial state distribution along the sample and the applied form of the gradient. Some examples of possible variations are also briefly illustrated.

Typically, the loading stage for an open boundary is applied at the beginning of a test, while the unloading stage is conducted at the end. These two tests are also considered as means to help identify any possible changes in the soil structure due to the gradient applications.

**Pressure increase - loading** A loading stage for an open material type boundary condition can be represented by a step function as the combination of the initial state of uniform pressure distribution in soil, and the pressure at increase of one of its boundaries:

$$\begin{aligned} &u\left(x,0\right)=U_0 \\ &u\left(0,t\right)=U \qquad U>U_0 \\ &u(L,t)=U_0 \end{aligned} \tag{2.1}$$

The graphical representation of the loading stage of step-function pressure distribution is shown in Figure 2.13:

The actual system response under the loading stage is given for a typical soil sample in Figure 2.14. The transient pressure distribution for $U_0 = 0$ and $U = 5$psi are illustrated. An intermediate state of water pressure profile for the given pressure gradient above is shown in Figure 2.15.

The resulting hydraulic conductivity of the system is obtained from the in and out-flow measurements taken under the loading stage for the open system, as shown in Figure 2.16.

It is observed that the loading stage under the open boundary conditions results

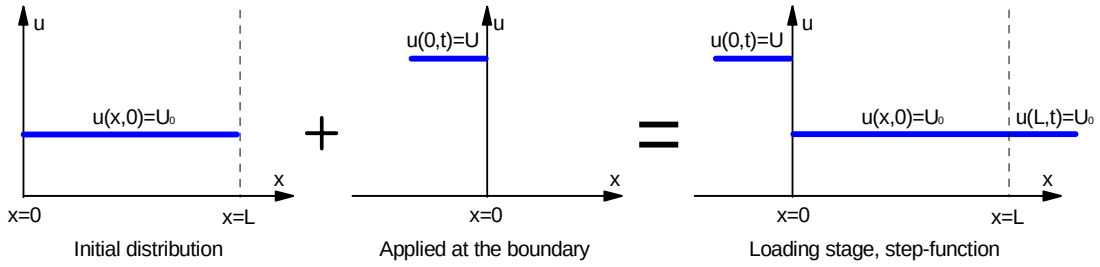


Figure 2.13: Loading stage of step-function type gradient application

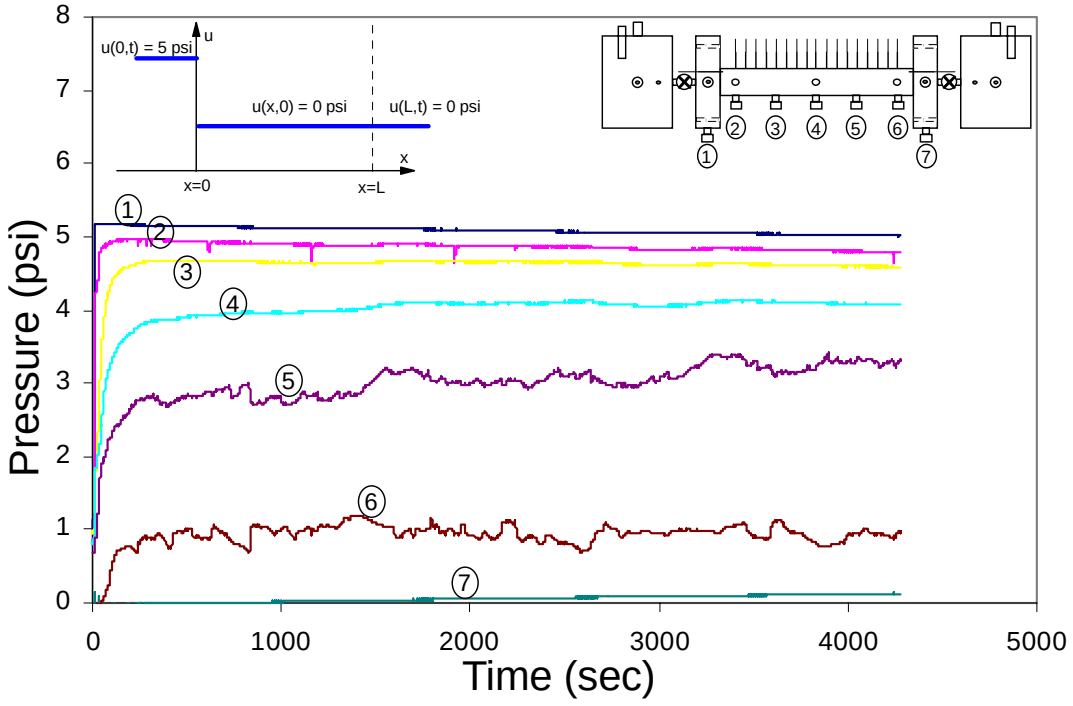


Figure 2.14: Pressure response of an open system for loading stage of a step-function.

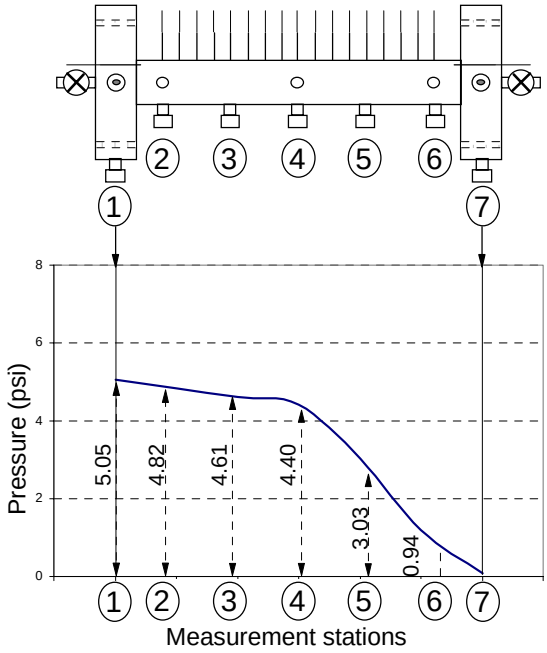


Figure 2.15: Pressure distribution at t = 3000 sec (assumed to be at steady state).

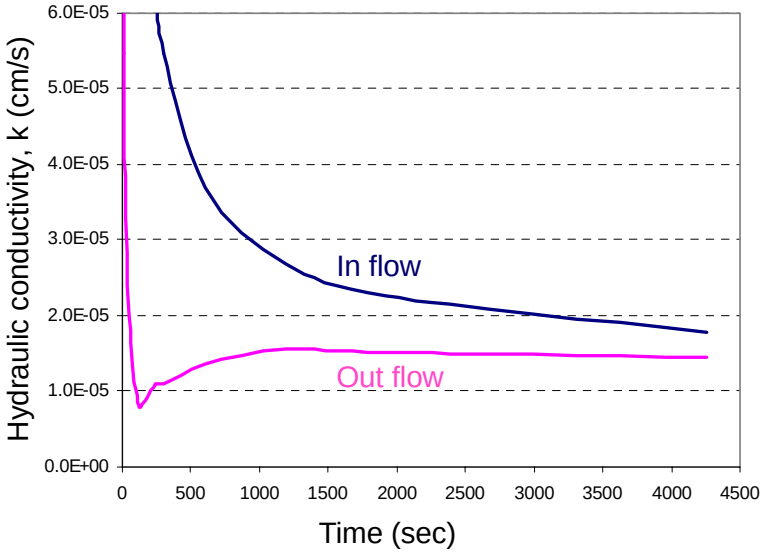


Figure 2.16: Hydraulic conductivity for the same open system at loading stage.

in an almost linear pressure distribution close to steady state (Figure 2.15). The non-uniform pressure drop along the soil sample is due to the internal resistance to the flow under open boundary conditions. Later on, it is shown that under closed boundary conditions the response becomes completely reversible with no loss such that pressure equilibrium is reached faster for all stations.

**Pressure drop - unloading** The unloading stage of a step-function type pressure can be expressed as:

$$\begin{aligned} u\left(x,0\right) &= U_0 \\ u\left(0,t\right) &= U_0 \qquad U < U_0 \\ u(L,t) &= U \end{aligned} \tag{2.2}$$

which can be shown graphically as in Figure 2.17.

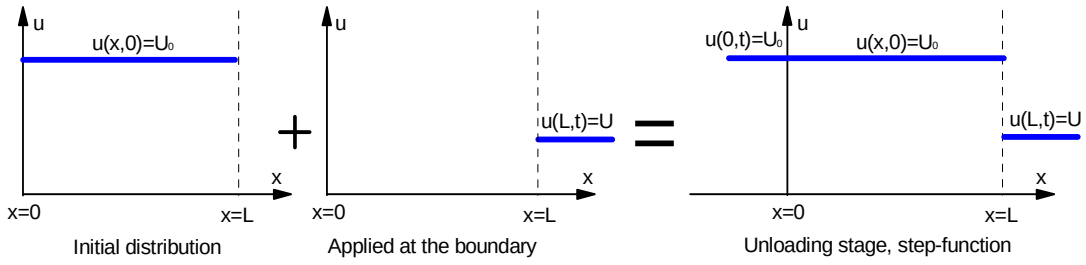


Figure 2.17: Unloading stage of step-function type gradient application.

The transient pressure distribution under the applied unloading stage, with $U_0 =$ 5psi and $U =$ 0psi is shown in Figure 2.18. Similarly, the pressure profile along the length of the specimen near steady state is shown in Figure 2.19. The unloading segment of the open boundary test is conducted after all the other nondestructive gradient tests were completed. This information was used as a check to verify the constancy of the hydraulic conductivity of the media. The hydraulic conductivity variation during the unloading stage is presented in Figure 2.20.

Comparison of the Figures 2.15 and 2.19, shows similar patterns and magnitudes for the final pressure distribution of each case. The Figures 2.16 and 2.19

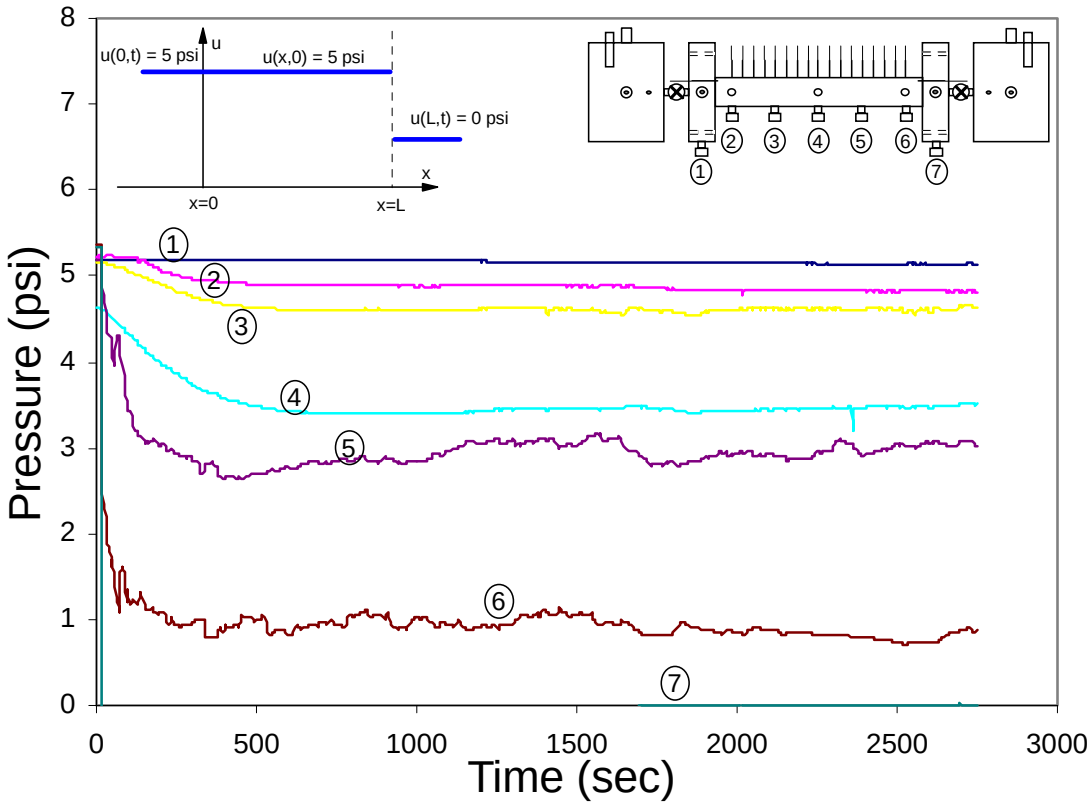


Figure 2.18: Pressure response of an open system for unloading stage of a step-function.

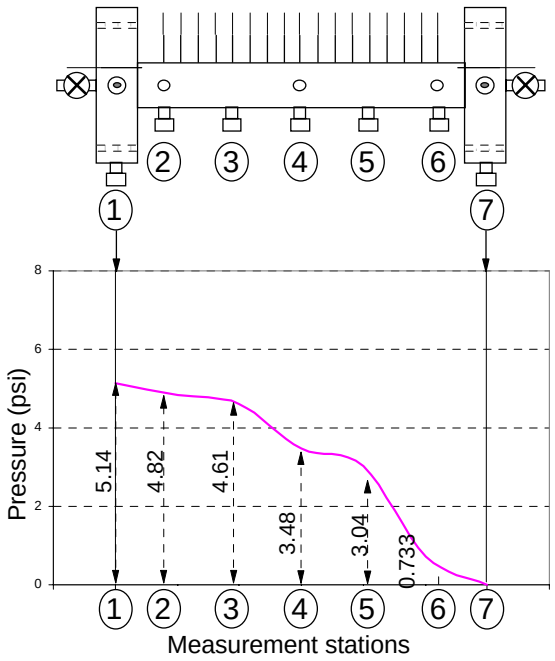


Figure 2.19: Pressure distribution at t = 2500 sec (assumed to be at steady state).

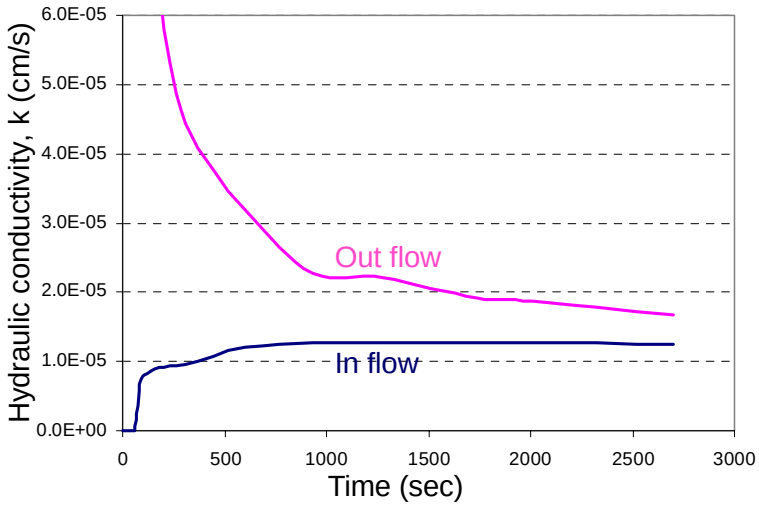


Figure 2.20: Hydraulic conductivity for the same open system at unloading stage.

represent the pre- and post-test hydraulic conductivity behavior and its magnitude. As observed, the hydraulic conductivity of the media was preserved at about $K = 1.5 \times 10^{-5}\,\mathrm{cm\,/\,s}$.

### Closed material boundary

A set of closed-boundary (no-flow allowed) test results for the same soil sample is described here. The pressure loading and unloading stages of were again applied in the form of step-function at the boundaries.

**Pressure increase - loading** Conditions as stated in the expressions for an open system (2.1) are valid for the closed system as well, except where no flow conditions $\left(\frac{\partial u}{\partial x}|_{x=L} = 0\right)$ are maintained at the boundaries. The loading stage response is shown in Figure 2.21. This figure illustrates a relatively well behaved response compared to the pressure responses observed in Figures 2.14 and 2.18 for the open system. It is also observed that pressure equilibrium is reached at every station values at steady state due to absence of irreversible losses. As observed in Figure 2.21, the pressure response at stations 6 and 7 are very close, almost identical in value. This validates that no flow boundary condition was maintained at the far end $\left(\frac{\partial u}{\partial x}|_{x=L} = 0\right)$, requiring the variation of the pressure along the soil at that neighborhood to be minimum. The variation of the pressure profile at selected times of Figure 2.21 is shown as snap shots in Figure 2.22. The time to reach steady state is observed from Figure 2.21 as, $t_f = 1000\,\mathrm{s}$. The pressure profile shown as snap shots were selected for time steps of $t = 0, 0.1t_f, 0.2t_f, 0.4t_f$ and $t_f$.

As observed, the initial pressure distribution along the sample is uniform at 5psi. The sample is then loaded at a constant 8psi on one boundary (1) under closed boundary conditions.

The slope of the pressure profile curves at the $x = L$ are all zero $\left(\frac{\partial u}{\partial x}|_{x=L} = 0\right)$, as expected for closed boundary conditions. It is also observed that the majority of change (increase) in pressure values occur at a time period less than the first half of the time required for steady state conditions and equilibrium to be reached.

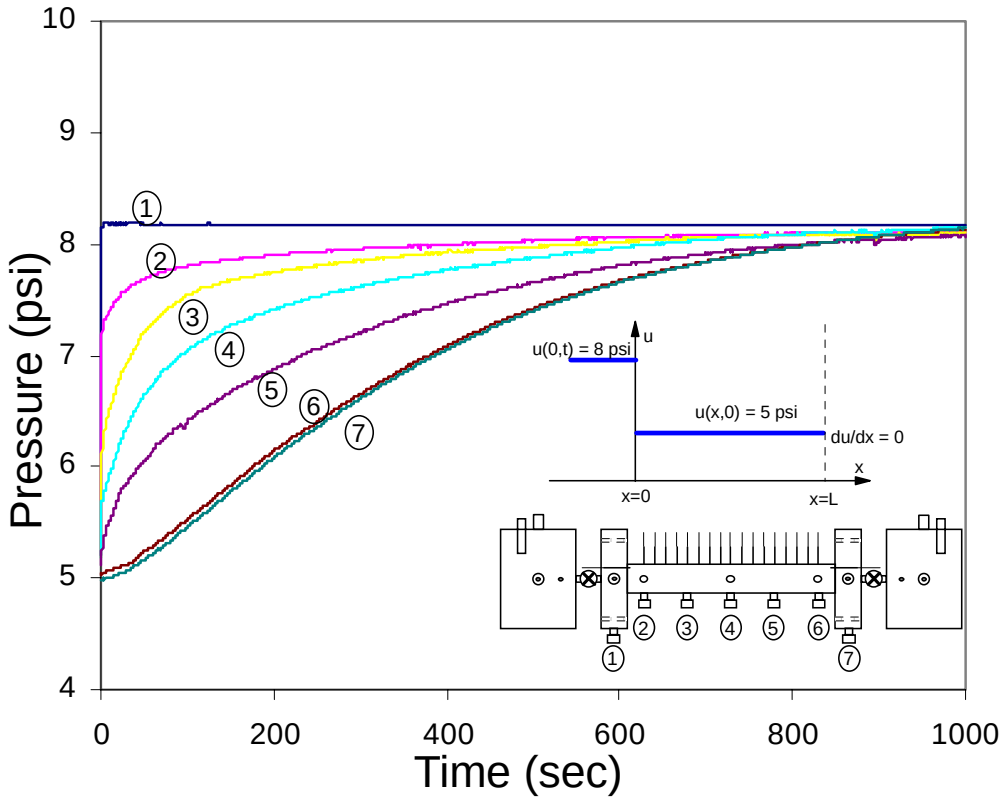


Figure 2.21: Closed system pressure response under loading stage.

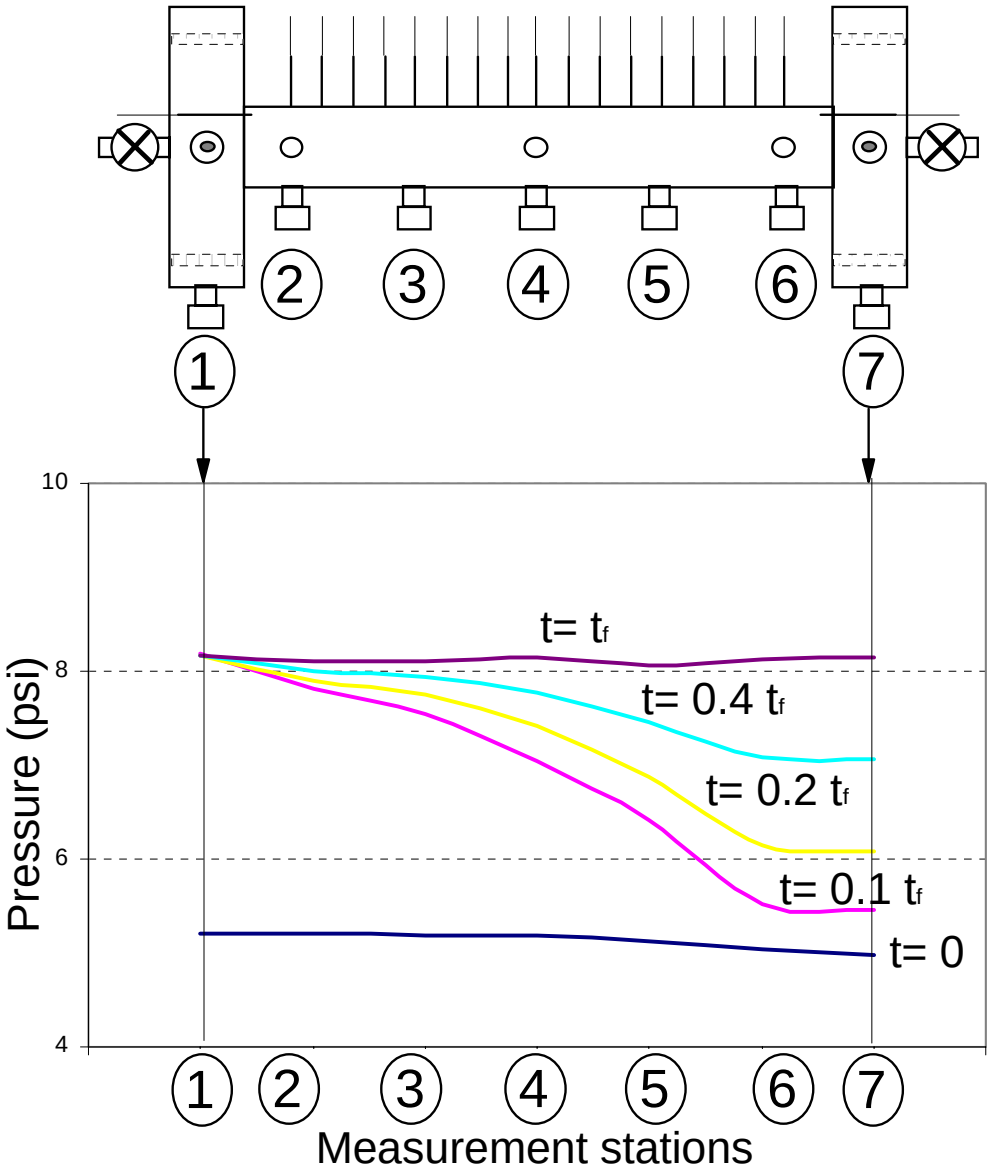


Figure 2.22: Pressure profile across the sample at various time steps.

**Pressure drop - unloading** The unloading stage expressions stated in the relationship (2.2) are also valid under closed boundary conditions. The system is initially at equilibrium with uniform pressure distribution of $U_0 = 8$psi.

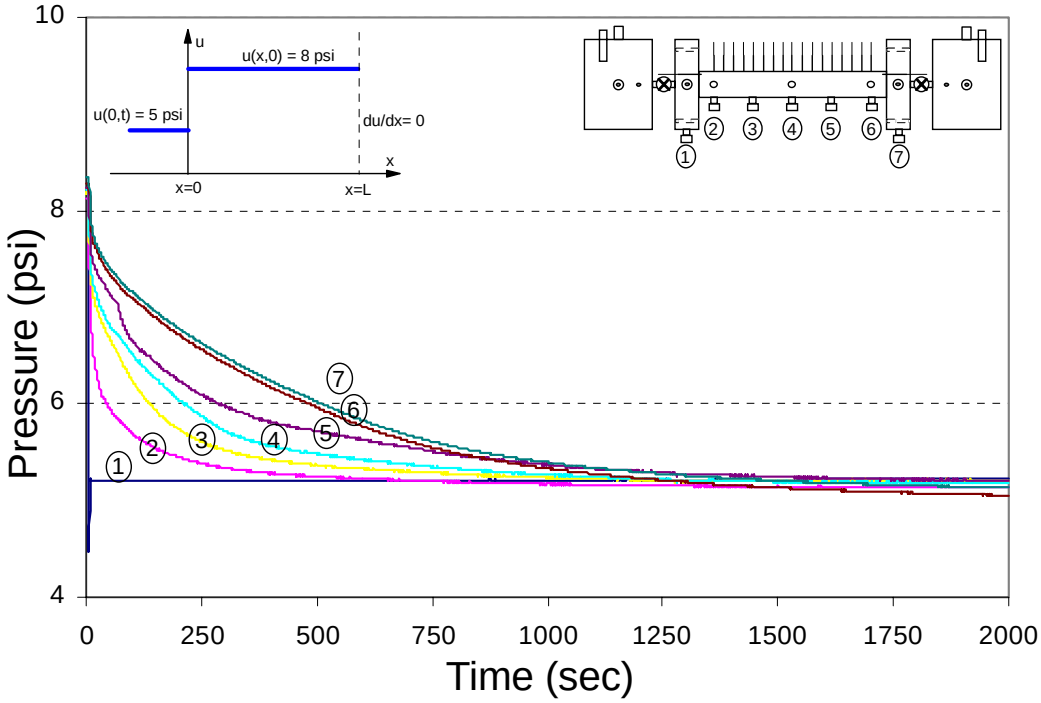


Figure 2.23: Closed system pressure response at unloading stage.

To unload the pressure at $x = 0$ boundary is set to $U = 5$psi and the pressure response is recorded as shown in Figure 2.23. The snap shots of the pressure profiles are given in Figure 2.24 at the similar time steps as before. It is again observed that majority of the pressure variation occurs before the first half of the time period required to achieve steady state and equilibrium.

The tests described above were conducted using the same soil sample. It should be noted that numerous tests similar to these were conducted on dissimilar soil samples to fine tune the experimental procedure. The experimental responses for various soil samples are then used in conjunction with the simulated response to

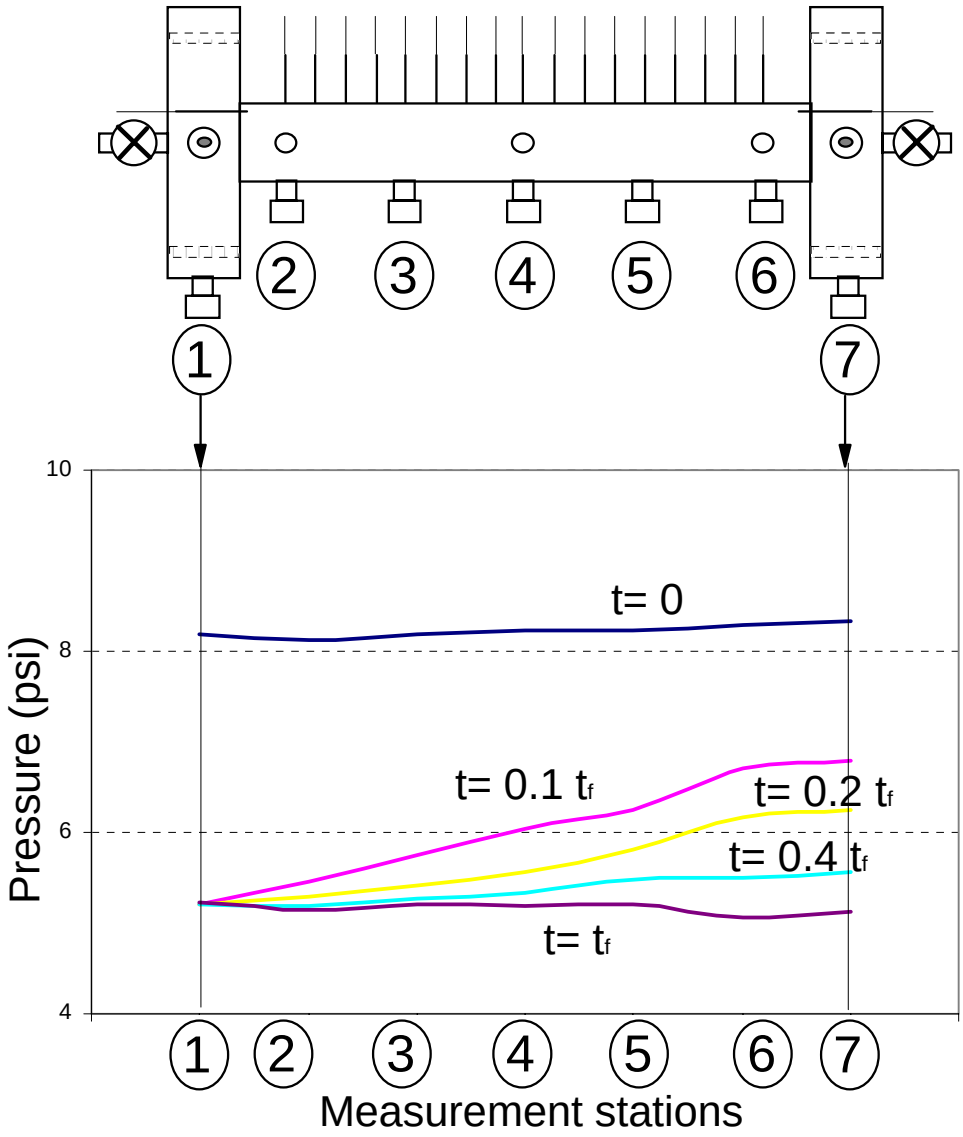


Figure 2.24: Pressure profile for unloading stage under closed boundaries.

obtain the desired soil parameters as described in the following chapters. The transient response of the system is used in this manner to compensate for the lack of ability to measure flux measurements under the closed boundary conditions.

### 2.5.2 Temperature gradient application

The transient distribution of the temperature in soil under the applied thermal gradients is discussed and typical behaviors are demonstrated. These experimental data are also used in conjunction with the numerical simulation to obtain the desired soil properties.

#### Temperature increase - loading

Temperature increase is applied by means of rod type electrical heaters as discussed previously in this chapter. The heat controller and the power units are calibrated to achieve consistent and smooth rise with little fluctuation about the target temperature. The temperature profiles presented in this section are obtained with heat sources embedded in the soil specimen. The power input is calibrated to obtain $30\,^{\circ}\mathrm{C}$ at $20\,\mathrm{V}$ input. Larger voltages, shorten the temperature rise time but result in an oscillation about the target temperature within the set bounds.

The embedded Firerod heaters are the smaller in diameter ($1/8\,\mathrm{in}$) than the reservoir heaters. They are rated at $120\,\mathrm{V}$ for $W_{120\,\mathrm{V}} = 25\,\mathrm{W}$. Using the relationship between the powers and the applied voltages, as shown in equation (2.3) below:

$$W_2 = W_1 \left( \frac{E_2}{E_1} \right)^2 \tag{2.3}$$

the corresponding power for the applied $20\,\mathrm{V}$ is obtained as $W_{20\,\mathrm{V}} = 0.6944\,\mathrm{W}$. This corresponds to a Watt density of approximately $3.4532\,\mathrm{W}\,/\,\mathrm{cm}^3$ using the effective dimensions of the heater (the watt density of the heater at $120\,\mathrm{V}$ is $13\,\mathrm{W}\,/\,\mathrm{cm}^2$). The applied Watt density or total wattage has no particular significance in the experimental stage except to obtain a stable temperature control with minimal oscillations. Recording steady temperature data is important since it is collocated

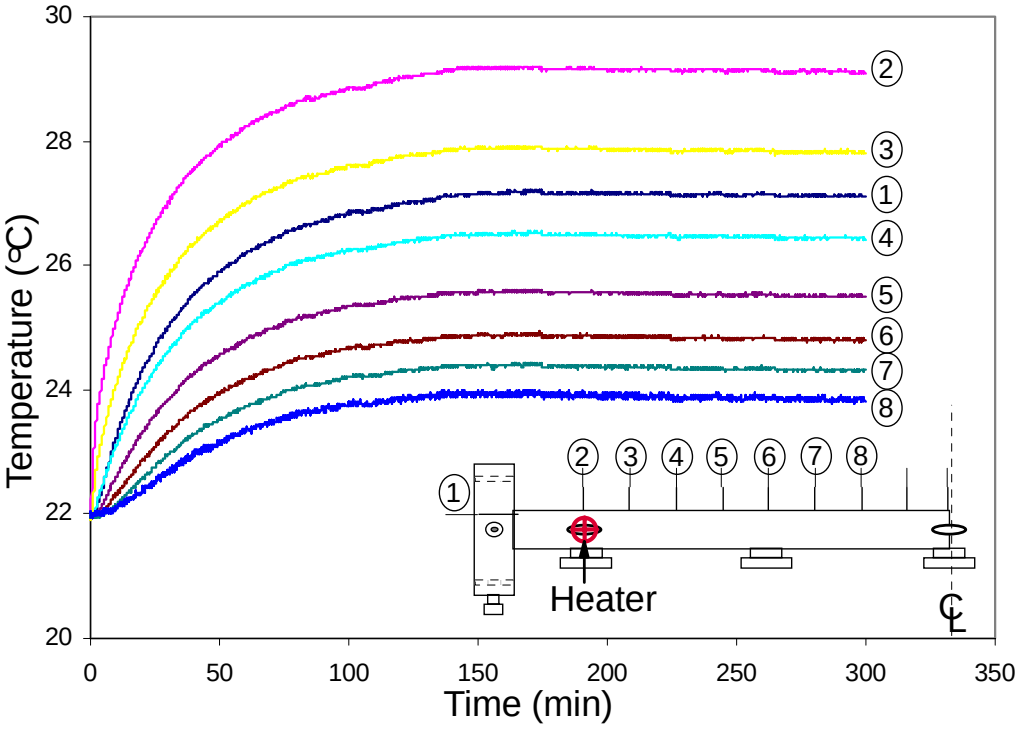


Figure 2.25: Closed system temperature response for applied 20 V.

with the numerical solution and undesired oscillations can affect the subsequent analysis.

The typical response from loading stage tests of soil samples with two different heater locations are presented. The location of heater and the orientation and numbering of measurement stations (thermocouples) for each test are provided on each graph.

The number of available data acquisition channels limited the number of temperature measurements along a sample, resulting in 8 to 9 thermocouple measurement locations. These locations were strategically selected and placed to obtain continuous temperature profiles with the available number of measurement channels for each test.

One of the heater locations was selected as the left end of the soil specimen coinciding with the first pressure station along the sample (Figure 2.25). The 8 thermocouples are placed as shown in Figure 2.25. The number 2 thermocouple coincides with the heater location and measures the heater temperature and also provides feedback for the closed loop control of the heater.

The second internal heat source location is shown to be at the center of the soil sample to take advantage of the symmetry and the relative ease in numerical discretization and collocation of the experimental and numerical responses.

The thermocouple locations with the heat source placed at the center of the specimen are illustrated in Figure 2.27. The temperature distributions with time under the loading stage of the heater are shown in this figure also.

Figure 2.26 shows the temperature profile along the soil sample (measurement stations) at the same time intervals used previously in the hydraulic gradient applications. Since the sample is un-insulated, convective heat loss on the surface does not allow uniform distribution of the temperature. The steady state is approximated as the time when little or no changes occurs in the temperature at a given point. It is estimated around 200 min as observed in Figure 2.25.

Figure 2.27 shows the transient temperature profiles of the soil, where the heater is located at the center of the sample and the thermocouples cover only the left half portion starting from the heater location. The temperature profile along the left

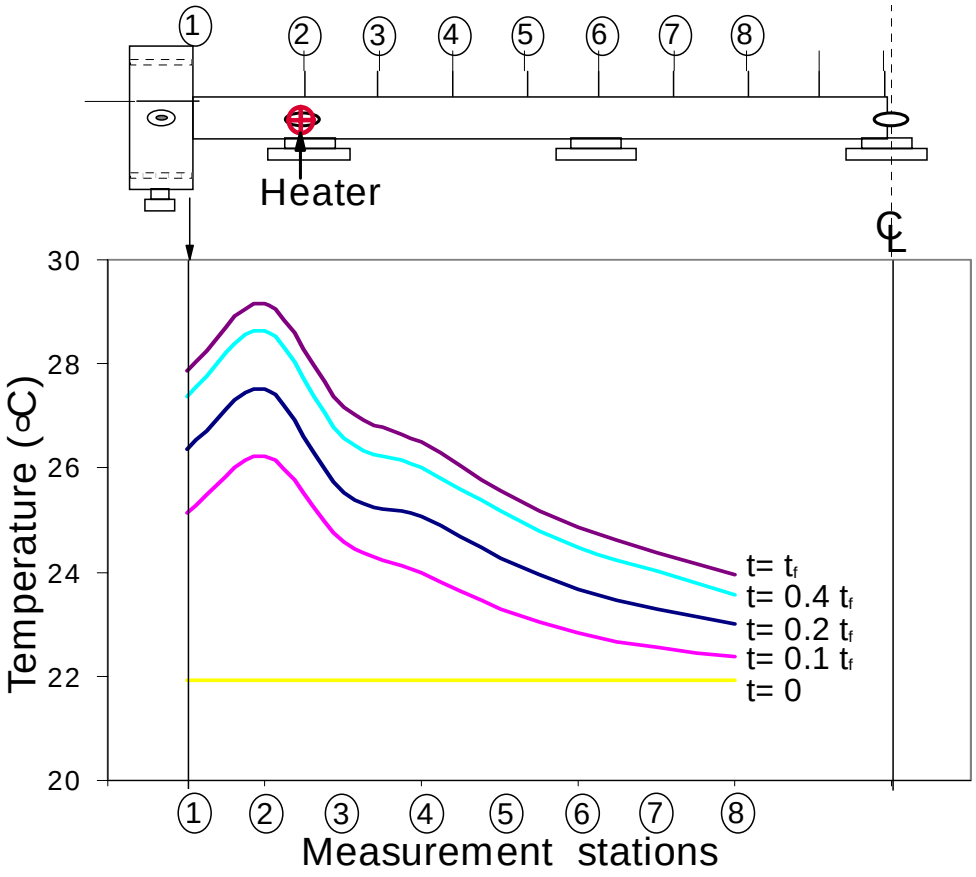


Figure 2.26: Temperature profile for $t_f$ = 200 min, loading stage under closed boundaries.

half of the sample is shown in Figure 2.28. The time steps are selected again as $t = 0, 0.1t_f, 0.2t_f, 0.4t_f$ and $t_f$ are used as the rest of the cases shown before. Steady state is observed at approximately $t_f = 150\,\text{min}$.

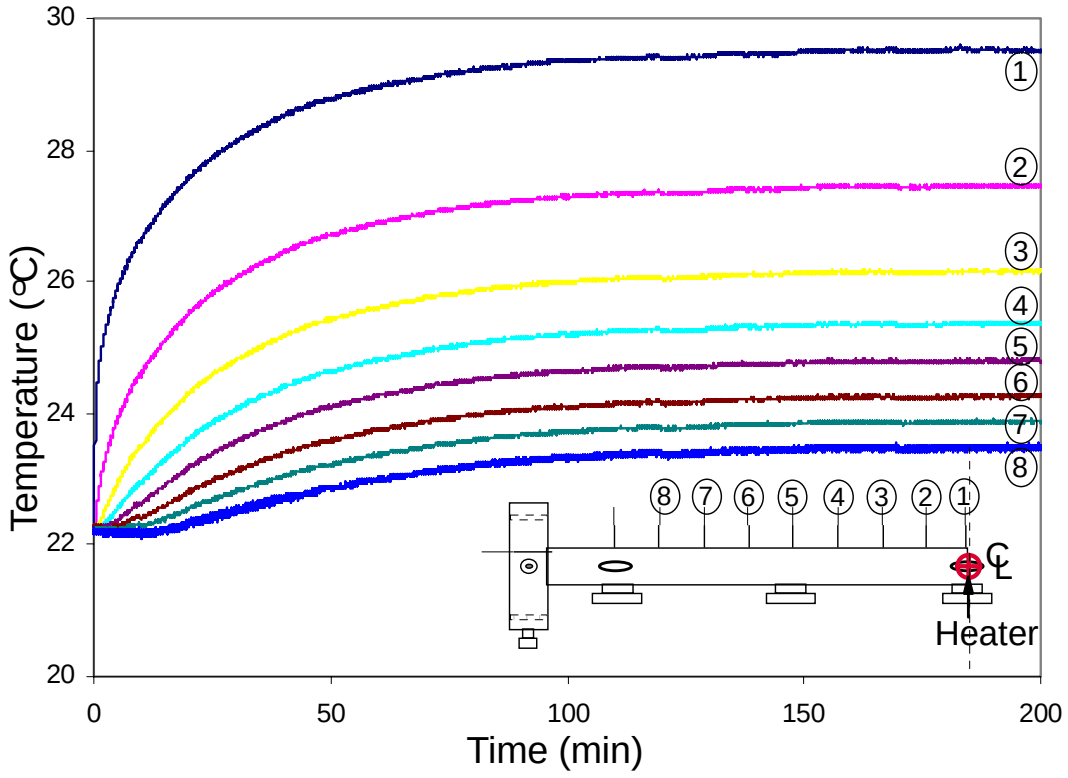


Figure 2.27: Closed system temperature response for heater located at center.

The two test cases above demonstrated the robustness of the system to changing initial conditions. The following section provides typical responses for the cool-down (unloading) stage of temperature gradient.

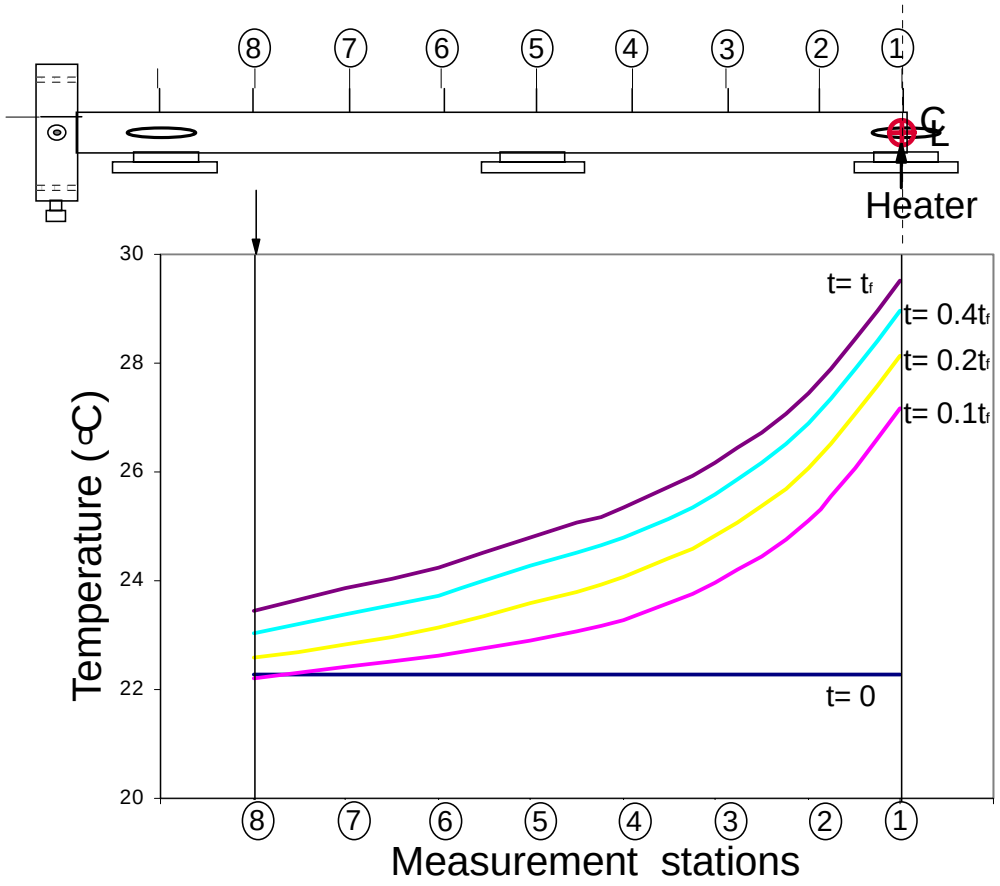


Figure 2.28: Temperature profile for tf=150 min, loading stage with heater located at center under closed boundary conditions.

### Temperature decrease - unloading

The cool-down period is initiated by turning off the heater after a uniform distribution of temperature along the sample is obtained. The transient temperature distribution with the case of heater close to left end of the sample is recorded as shown in Figure 2.29. Free convection over the un-insulated cylindrical surface causes the soil

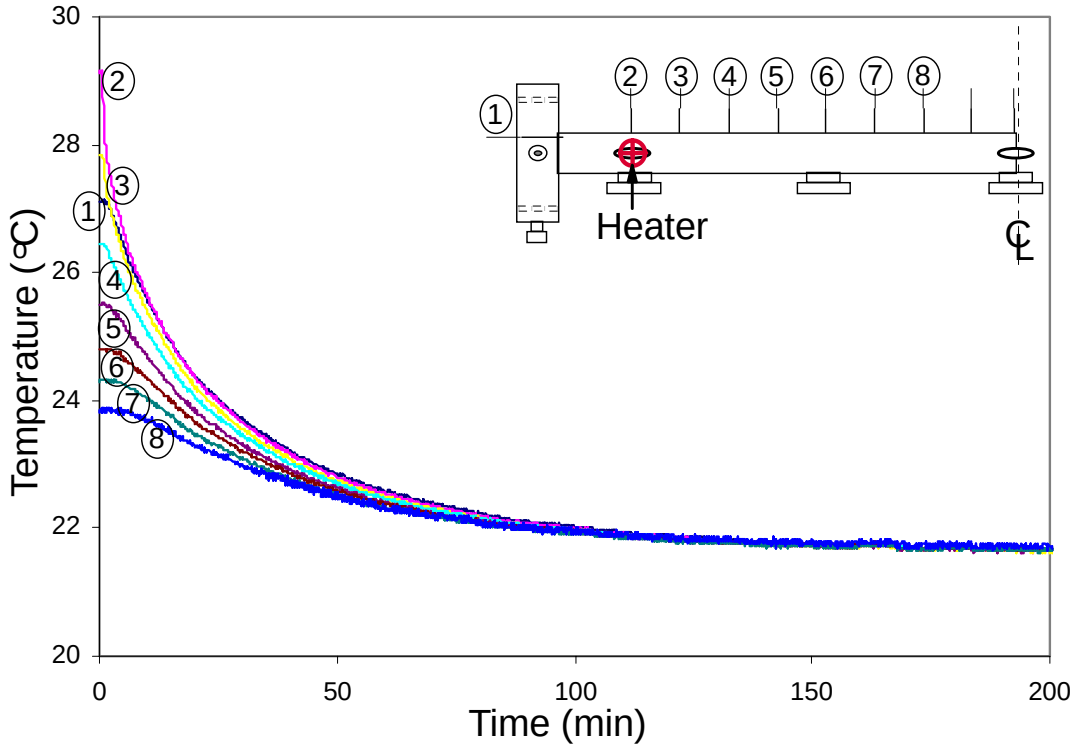


Figure 2.29: Closed system temperature response for cool-down (unloading) stage.

system to come to equilibrium with room temperature at approximately 200 min. The corresponding temperature decay profile along the sample for the stated time steps is shown in Figure 2.30. Figure 2.31 represents the cool-down period of the sample with the heater located at the center. The corresponding profiles at selected time steps is shown in Figure 2.32.

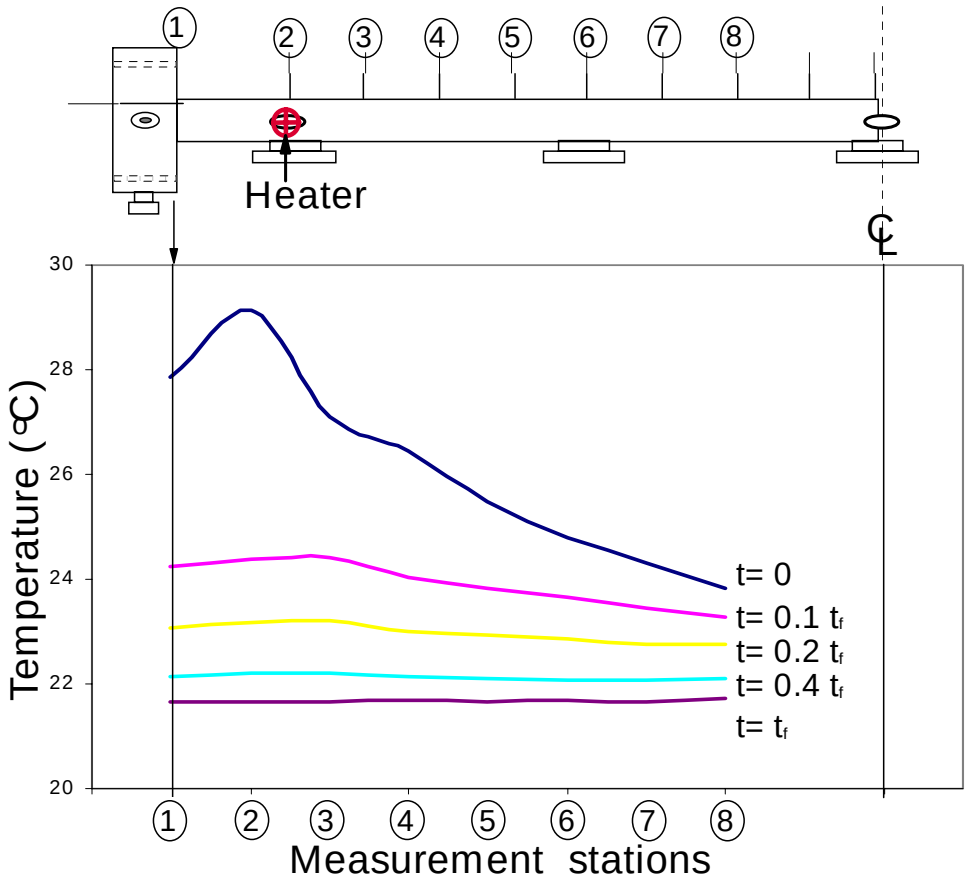


Figure 2.30: Temperature profile for $t_f$=200 min, cool-down stage with heater located at the left end under closed boundary conditions.

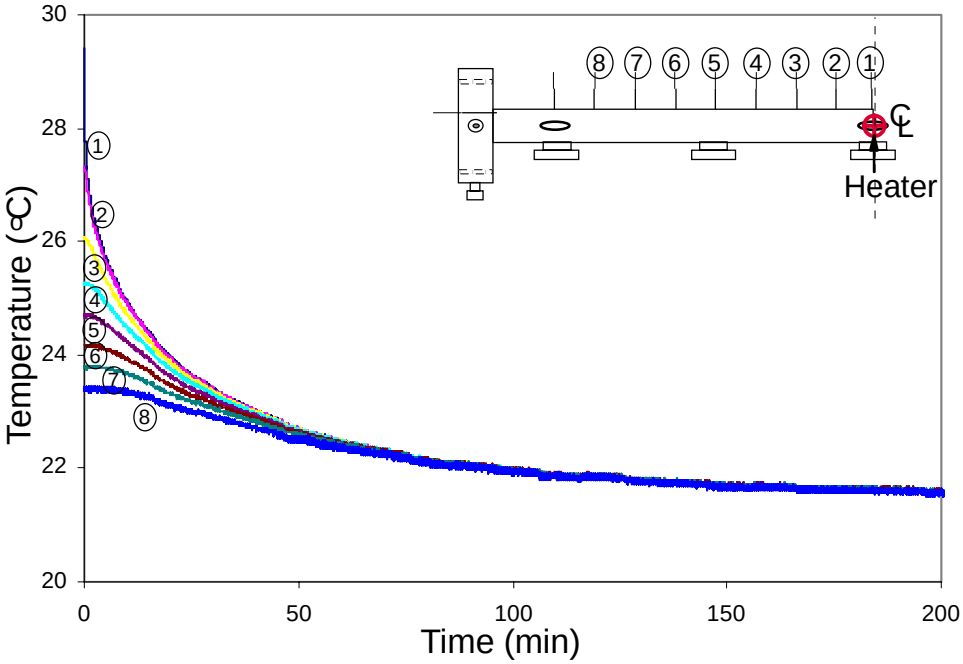


Figure 2.31: Closed system temperature response for cool-down stage with heater located at center.

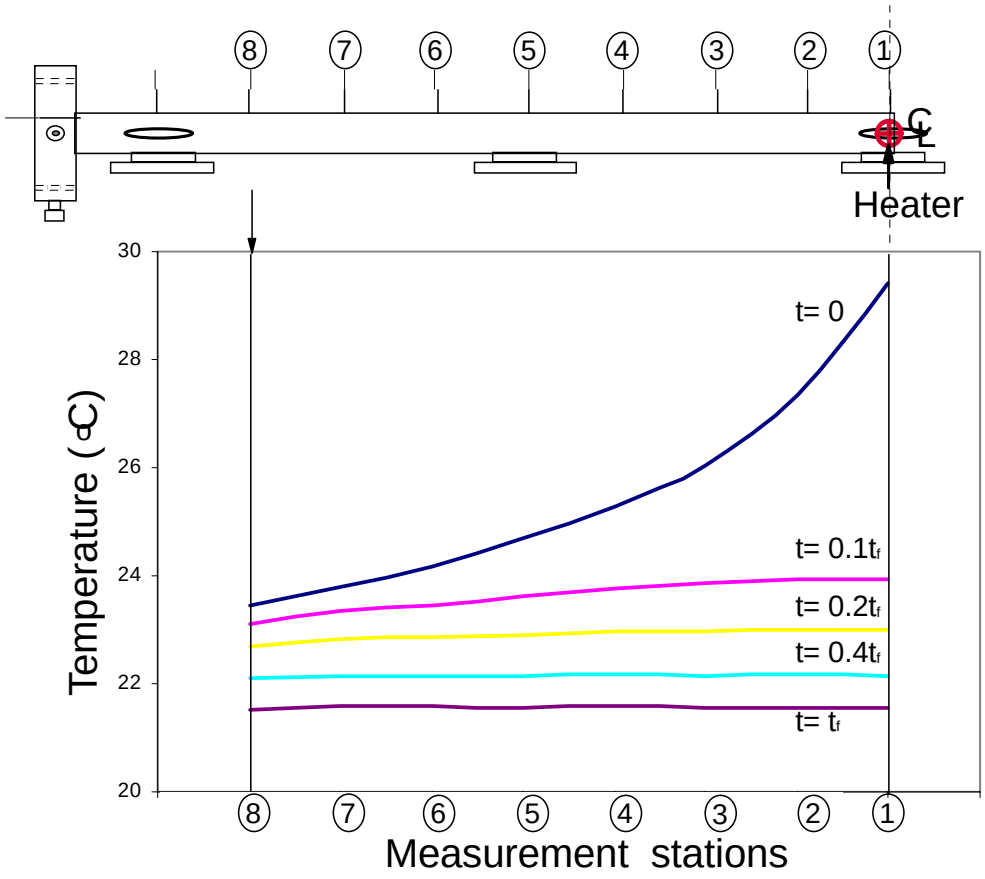


Figure 2.32: Temperature profile for $t_f$=200 min, cool-down stage with heater located at center under closed boundary conditions.

## 2.6 Concluding remarks

The experimental set-up and components are described in this chapter. The various test types and their relevance are mentioned. Other non-destructive tests are conducted under various boundary conditions. The experimental measurements are used in conjunction with the numerical results for the parameter identification purposes in the coming chapters.

# Chapter 3

# Analytical Formulations and Model

The conservation equations for the transient response and the coupled flow under thermal and hydraulic gradients are derived. In this chapter the conservation equations are obtained for a two-phase porous medium. They include mass, linear and angular momentum, and energy conservation of the system.

First, the thermodynamics expressions such as the Gibbs and Helmholtz free energy are used to obtain the relationships between the entropy, internal energy, work, and the other conservation expressions. The entropy conservation equation together with the internal energy equation is used to separate the rate of entropy change and the entropy flux, which typically allows expressing the fluxes and gradients (forces) of coupled flow components in an open system. This method of determining fluxes and forces by the use of the entropy source term generates a set of coupled flow expressions where the coupled coefficient matrix is symmetric.

The remainder of the chapter states the constitutive laws governing the stress-strain relationships for the porous media and the fluid flux expressions for a Newtonian fluid. Finally, a simplified set of governing equations based on a list of stated assumptions are obtained. The boundary conditions are discussed briefly and left for further discussion in the numerical methods section. Following is a list of the

notations used in the analytical equations (table 3.1).

Table 3.1: List of notations

| | | | |
|---|---|---|---|
| $\beta_p$ | Isothermal compressibility | $p$ | Fluid hydrostatic pressure |
| $\beta_T$ | Thermal expansion | $\vec{q}_f$ | Fluid flux $\left(n\vec{V}_f\right)$ |
| $\epsilon$ | Volumetric strain | $r^E$ | Energy production rate per volume |
| $\mu$ | Chemical potential | $S, s$ | Entropy, specific entropy |
| $\overline{\rho}_\alpha, \vec{V}_\alpha$ | Component density, velocity | $T_i, T_f, T_s,$ | Phase temperature |
| $\rho, \vec{V}$ | Total density, Velocity | $u_i$ | Specific internal energy |
| $\overline{\rho}_i, \overline{\rho}_f, \overline{\rho}_s$ | Partial phase density, $\overline{\rho}_i = n_i\rho_i$ | $\vec{V}_i, \vec{V}_f, \vec{V}_s$ | Phase mass avg velocity |
| $\rho_i, \rho_f, \rho_s$ | Material density, fluid, solid | $\vec{V}_r, \vec{q}_r$ | Relative velocity, flux |
| $\overline{\overline{\sigma}}^i, \overline{\overline{\sigma}}^f, \overline{\overline{\sigma}}^s$ | Phase stress components | $\vec{w}_s$ | Solid displacement vector |
| $\overline{\overline{\sigma}}^{s'}$ | Effective stress | $\vec{X}_k$ | Coupled forces, gradients |
| $\overline{\overline{\tau}}^f$ | Fluid phase shear stress | | |
| $\overline{\overline{\Phi}}_s$ | Dissipation function | | |
| $a_v$ | Soil skeleton compressibilty | | |
| $c_v$ | Volumetric heat capacity | | |
| $e$ | Void ratio | | |
| $\vec{F}_i$ | External body force/mass | | |
| $g$ | Gravitational constant | | |
| $\vec{j}_\alpha$ | Component flux in a phase | | |
| $\vec{j}_i, \vec{j}_f, \vec{j}_s$ | Diffusive phase flux | | |
| $\vec{j}_i^E$ | Conductive energy flux | | |
| $\vec{j}_q$ | Heat Flux | | |
| $K$ | Hydraulic conductivity | | |
| $n_i, n, (1-n)$ | Phase porosity, fluid, solid | | |

## 3.1 General form of conservation equations

The general form of conservation equations are presented below. These equations are later used in formulating the pertinent conservation equations for the two-phase deformable porous media. The general conservation forms for a scalar ($a$) and a

vector quantity $\left(\vec{A}\right)$, are used to describe the governing processes.

General form of the conservation law (Figure 3.1) for a scalar density $(a)$ of a quantity per unit volume is [13]:

$$\int_V \frac{\partial a}{\partial t} dV = -\int_A a\vec{V}_a \cdot d\vec{A} + \int_V I_a dV \tag{3.1.1}$$

where $I_a$, is the source term per unit volume per unit time. Applying Green's transformation to the surface integral term in equation (3.1.1):

$$\int_V \frac{\partial a}{\partial t} dV = \int_V \left[-\nabla \cdot (a\vec{V}_a) + I_a\right] dV \tag{3.1.2}$$

For the arbitrary volume the local form becomes:

$$\frac{\partial a}{\partial t} = -\nabla \cdot (a\vec{V}_a) + I_a \tag{3.1.3}$$

The substantial derivative of $(a)$ in terms of the time derivative at a fixed point is expressed as:

$$\frac{da}{dt} = \frac{\partial a}{\partial t} + \vec{V} \cdot \nabla a \tag{3.1.4}$$

The flux term (divergence term on the RHS) in equation (3.1.3) can be separated in to its conductive (diffusion) and convective terms, so that:

$$\frac{\partial a}{\partial t} = -\nabla \cdot (a\vec{V}) - \nabla \cdot \vec{j}_a + I_a \tag{3.1.5}$$

or

$$\frac{da}{dt} = -a\nabla \cdot \vec{V} - \nabla \cdot \vec{j}_a + I_a \tag{3.1.6}$$

Where the diffusive flux for component $a$, $\vec{j}_a = a(\vec{V}_a - \vec{V})$, can be expressed relative to the velocity of the center of mass $\left(\vec{V} = \frac{\sum_i a_i \overrightarrow{V_{ai}}}{\sum_i a_i}\right)$.

Similarly, the conservation equation for a vector quantity $\vec{A}$, takes the following form:

$$\frac{\partial \vec{A}}{\partial t} = -\nabla \cdot (\vec{A}\vec{V}) - \nabla \cdot \underset{=A}{j} + \overrightarrow{I}_A \tag{3.1.7}$$

or

$$\frac{d\vec{A}}{dt} = -\vec{A} \cdot \left(\nabla \vec{V}\right) - \nabla \cdot \underset{=A}{j} + \overrightarrow{I}_A \tag{3.1.8}$$

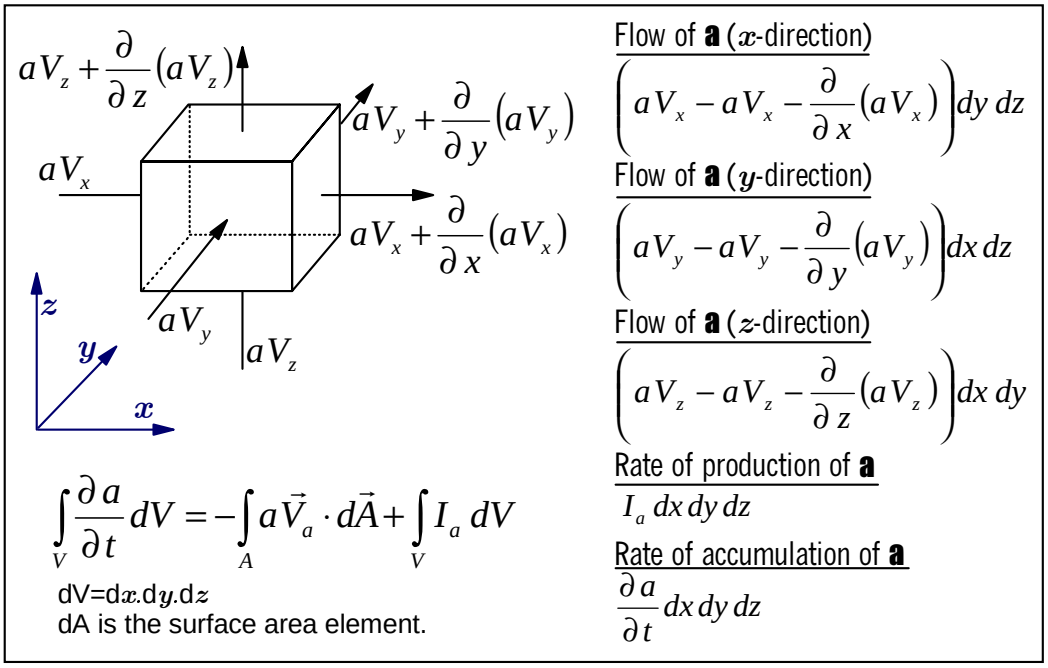


Figure 3.1: Elemental control volume for conservation of a scalar quantity "a".

## 3.2 Conservation of mass

General form for the conservation of mass of a multi-phase system, where the production term for the phases ($I_i = 0$, for solid and fluid phases) is neglected, can be expressed similar to equation (3.1.3) [11]:

$$\frac{\partial \overline{\rho}_i}{\partial t} = -\nabla \cdot (\overline{\rho}_i \vec{V}_i) \tag{3.2.1}$$

where $\overline{\rho}_i$ is the mass of a phase in a given volume, expressed as: $\overline{\rho}_i = \rho_i n_i$, and $n_i$ is the ratio of the phase volume to total volume (i.e. porosity of solid phase). The following volumetric relationships valid for the saturated two-phase porous system are considered:

| | |
|---|---|
| $n_f = n = V_f/V_T$ | Fluid phase fraction |
| $n_s = V_s/V_T = (1-n)$ | Solid phase fraction (porosity) |
| $\sum_{i=f,s} n_i = 1$ | Phase fractions, summed over the multi-phase system |

A continuity equation for a component ($\alpha$) that might be present in the phase $i$:

$$\frac{\partial \overline{\rho}_\alpha}{\partial t} = -\nabla \cdot (\overline{\rho}_\alpha \vec{V}_i) - \nabla \cdot \vec{j}_\alpha + I_{\alpha i} \tag{3.2.2}$$

where $I_{\alpha i}$, is the production rate of the component ($\alpha$) in phase $i$ which may be due to its interaction with the rest of the mixture. Equation (3.2.2) can be expressed in terms of the substantial derivatives:

$$\frac{d\overline{\rho}_\alpha}{dt} = -\overline{\rho}_\alpha \nabla \cdot \vec{V}_i - \nabla \cdot \vec{j}_\alpha + I_{\alpha i} \tag{3.2.3}$$

The $\overline{\rho}_\alpha$ is the mass density of a component ($\alpha$) that may be present in phase $i$, $\vec{j}_\alpha = \overline{\rho}_\alpha(\vec{V}_\alpha - \vec{V}_i)$ is the diffusive flux for component $\alpha$ in phase $i$, where $\vec{V}_\alpha$ is the velocity of component ($\alpha$) in phase $i$.

### 3.2.1 Conservation of mass for solid and fluid phases

The continuity equations for solid and the fluid phases are expressed as follows, where $\overline{\rho}_s = \rho_s(1-n)$ and $\overline{\rho}_f = \rho_f n$ are the partial masses for each phase.

$$\frac{\partial \left[\rho_s(1-n)\right]}{\partial t} = -\nabla \cdot \left[\rho_s(1-n)\vec{V}_s\right] \tag{3.2.4}$$

$$\frac{\partial(\rho_f n)}{\partial t} = -\nabla \cdot (\rho_f n \vec{V}_f) \tag{3.2.5}$$

The balance of mass for the entire system $\left(\rho = \sum \overline{\rho}_i = \sum \rho_i n_i \text{ and } \rho\vec{V} = \sum \overline{\rho}_i \vec{V}_i\right)$ can be obtained by summing the equations (3.2.4) and (3.2.5):

$$\frac{\partial \rho}{\partial t} + \nabla \cdot (\rho \vec{V}) = 0 \tag{3.2.6}$$

The solid phase conservation equation (3.2.4) can be further simplified if the solid phase density ($\rho_s$) is assumed to be a constant. This is based on the assumption that the changes in density of the solid particles subject to stresses and temperature fields are negligible compared to the changes realized by the overall soil skeleton. Then:

$$\frac{\partial \left(1-n\right)}{\partial t} = -\nabla \cdot \left[(1-n)\,\vec{V}_s\right] \tag{3.2.7}$$

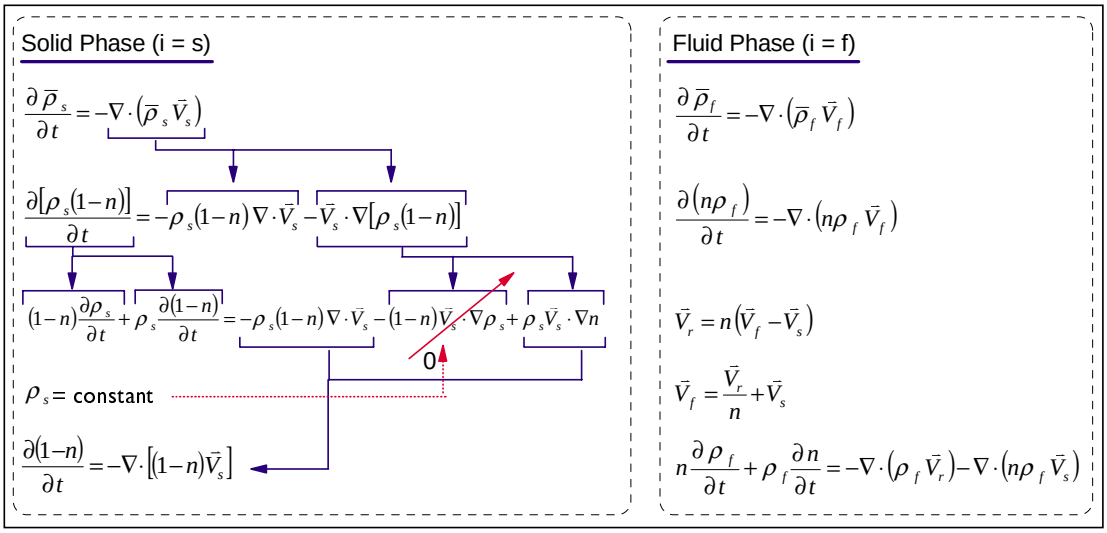


Figure 3.2: Balance of mass diagram for fluid and solid phase.

The balance equation for fluid phase can also be modified in terms of relative velocity $\vec{V_r} = n(\vec{V_f} - \vec{V_s})$, which is identical to Darcy's flux term as shown in Figure 3.2 and the equation below:

$$n\frac{\partial \rho_f}{\partial t} = -\rho_f \frac{\partial n}{\partial t} - \nabla \cdot (\rho_f \vec{V_r}) - \nabla \cdot (n\rho_f \vec{V_s}) \tag{3.2.8}$$

Solid phase mass balance equation (3.2.7) also represents the porous medium's rate of dilatation. A typical form of the mass conservation equation for all the components (which will be referenced later in the entropy equations) is in terms of the mass fraction of a component ($\alpha$): $w_\alpha = \frac{\overline{\rho}_\alpha}{\rho}$, where $\overline{\rho}_\alpha$ is the mass of component $\alpha$ per unit volume and $\sum_\alpha w_\alpha = 1$ for all the components present:

$$\rho\frac{dw_\alpha}{dt} = -\nabla \cdot \vec{j}_\alpha \tag{3.2.9}$$

## 3.3 Conservation of linear momentum

Conservation of the linear momentum describes the forces acting on a body which cause it to accelerate. Under the equilibrium conditions, the acceleration of the

body will be zero. Using equation (3.1.7), where the vector quantities are $\vec{A}_i = \bar{\rho}_i \vec{V}_i$, $\vec{I}_i = \bar{\rho}_i \vec{F}_{\ i}$ and $\vec{F}_i$ is the resultant external body force per unit mass of the phase, the conservation for the multi-phase system can be written as follows [13]:

$$\frac{\partial(\overline{\rho}_i \vec{V}_i)}{\partial t} = -\nabla \cdot (\overline{\rho}_i \vec{V}_i \vec{V}_i^m) + \overline{\rho}_i \vec{F}_i + Internal\ Forces \tag{3.3.1}$$

$$\frac{\partial(\overline{\rho}_i \vec{V}_i)}{\partial t} = -\nabla \cdot \left[\overline{\rho}_i \vec{V}_i \vec{V}_i - \overline{\rho}_i \vec{V}_i \left(\vec{V}_i - \vec{V}_i^m\right)\right] + \overline{\rho}_i \vec{F}_i + Int.Forces \tag{3.3.2}$$

$$\frac{\partial(\overline{\rho}_i \vec{V}_i)}{\partial t} = -\nabla \cdot (\overline{\rho}_i \vec{V}_i \vec{V}_i - n_i \underline{\underline{\sigma}}^i) + \overline{\rho}_i \vec{F}_i + Int.\ Forces \tag{3.3.3}$$

where "$\underline{\underline{\sigma}}^i$" is used to represent the diffusive flux of a phase $i$ and, $\vec{j}_i^m = \rho \vec{V}_i (\vec{V}_i - \vec{V}_i^m)$ of the momentum equation . The internal forces between the phases per unit volume are $\int_A \underline{\underline{\sigma}}^i \cdot d\vec{A} + \overline{\rho}_i \vec{F}_i^{ji}$ .

The use of mass balance equation (3.2.1) in reducing the momentum balance equation (3.3.3) is shown in Figure 3.3.

$$\frac{\partial(\overline{\rho}_i \vec{V}_i)}{\partial t} = -\nabla \cdot \left(\overline{\rho}_i \vec{V}_i \vec{V}_i - n_i \underline{\underline{\sigma}}^i\right) + \overline{\rho}_i \vec{F}_i + Int.Forces$$

$$\overline{\rho}_i \frac{\partial \vec{V}_i}{\partial t} + \vec{V}_i \frac{\partial \overline{\rho}_i}{\partial t} = -\vec{V}_i \cdot \nabla(\overline{\rho}_i \vec{V}_i) - \overline{\rho}_i \vec{V}_i \cdot (\nabla \vec{V}_i) + \nabla \cdot \left(n_i \underline{\underline{\sigma}}^i\right) + \overline{\rho}_i \vec{F}_i + Int.Forces$$

$$\overline{\rho}_i \frac{\partial \vec{V}_i}{\partial t} = -\vec{V}_i \left(\frac{\partial \overline{\rho}_i}{\partial t} + \nabla \cdot (\overline{\rho}_i \vec{V}_i)\right) - \overline{\rho}_i \vec{V}_i \cdot (\nabla \vec{V}_i) + \nabla \cdot \left(n_i \underline{\underline{\sigma}}^i\right) + \overline{\rho}_i \vec{F}_i + Int.Forces$$

$$\frac{\partial \overline{\rho}_i}{\partial t} + \nabla \cdot (\overline{\rho}_i \vec{V}_i) = 0 \quad \text{Mass conservation equation for phase i}$$

$$\overline{\rho}_i \frac{\partial \vec{V}_i}{\partial t} = -\overline{\rho}_i \vec{V}_i \cdot (\nabla \vec{V}_i) + \nabla \cdot \left(n_i \underline{\underline{\sigma}}^i\right) + \overline{\rho}_i \vec{F}_i + Int.Forces$$

Figure 3.3: Linear momentum conservation for phase i.

$$\overline{\rho}_i \frac{\partial \vec{V}_i}{\partial t} = -\overline{\rho}_i \vec{V}_i \cdot \nabla \vec{V}_i + \overline{\rho}_i \vec{F}_i + \nabla \cdot (n_i \underline{\underline{\sigma}}^i) + Int.Forces \tag{3.3.4}$$

The equation (3.3.4) is expressed in terms of the indical notation as below by neglecting the internal forces between the two phases:

$$\overline{\rho}_k \frac{\partial \left(V_k\right)_j}{\partial t} = \frac{\partial \left(n_k \sigma_{ij}^k\right)}{\partial x_i} - \overline{\rho}_k \left(V_k\right)_i \frac{\partial \left(V_k\right)_j}{\partial x_i} + \overline{\rho}_k \left(F_k\right)_j \tag{3.3.5}$$

where the index $k$ represents the $k^{th}$ phase, (k=1,2).

The conservation of linear momentum, equation (3.3.5), can be expressed as the total derivative given below:

$$\overline{\rho}_i \frac{d\vec{V}_i}{dt} = \overline{\rho}_i \vec{F}_i + \nabla \cdot \left(n_i \underline{\underline{\sigma}}^i\right) \tag{3.3.6}$$

As a result, the linear momentum equation for each phase becomes:

$$\overline{\rho}_s \frac{d\vec{V}_s}{dt} = \overline{\rho}_s \vec{F}_s + \nabla \cdot \left((1-n)\, \underline{\underline{\sigma}}^s\right) \tag{3.3.7}$$

$$\overline{\rho}_f \frac{d\vec{V}_f}{dt} = \overline{\rho}_f \vec{F}_f + \nabla \cdot \left(n\, \underline{\underline{\sigma}}^f\right) \tag{3.3.8}$$

It is more appropriate to obtain the conservation of momentum equations based on the average motion of each phase, as in equations (3.3.7) and (3.3.8), rather than the constituents (components) in each phase. In general, identifiable interfaces between different phases do exist, but seldom such a physical interface is present under miscible conditions for the components in each phase. Furthermore, the dynamics of component motion is primarily influenced by the bulk phase kinematics and not the motion of different components relative to one another within each phase. Also, components in a phase are assumed to exist only in trace quantities and the constitutive rate laws relating the diffusion of the components with respect to the average motion of each phase are often used to express their transfer. This justifies the expression of the linear momentum equation in terms of the phase velocities alone.

## 3.4 Conservation of angular momentum

The conservation of the angular momentum is a measure of unbalanced forces and couples which cause the body to rotate. This representation for simple bodies without couples reduces to a statement of a symmetric stress tensor at a point. In the two- and three-dimensional analysis of mixtures, interaction of phases within an element may result in the development of unbalanced stress tensors and vorticity for each phase [11]. However, a macroscopic one-dimensional flow does not account specifically for vorticity. The effects may still exist as a microscopic phenomenon but will not effect the symmetric nature of the stress sensor at the macroscopic level. Therefore the angular momentum conservation expressions will not be developed in here.

## 3.5 Conservation of energy

The heat energy is associated with the temperature and it is distinct from the kinetic or the potential energies. Heat energy flows from one neighboring element to another when the temperatures are different. Internal energy expressions in terms of local thermodynamics state are used to express the heat energy of the medium. The energy conservation and the corresponding components of internal energy are obtained for a representative unit volume.

The specific energy density per unit volume of a phase $i$ comprises of two parts: the specific internal energy and the specific kinetic energy. The total energy balance equation [39], [25], [32] for an arbitrary volume are derived using equation (3.1.3) in terms of partial specific quantities:

$$\frac{\partial}{\partial t}\left\{\overline{\rho}_i\left(u_i+\frac{\vec{V}_i^2}{2}\right)\right\}=-\nabla\cdot\left\{\overline{\rho}_i\left(u_i+\frac{\vec{V}_i^2}{2}\right)\vec{V}_i+\vec{j}_i^{E}\right\}$$
$$+\left\{\vec{V}_i\cdot\left(\overline{\rho}_i\vec{F}_i\right)+\nabla\cdot\left(\underline{\underline{\bar{\sigma}}}^{i}\cdot\vec{V}_i\right)+\overline{\rho}_i r^{E}\right\} \tag{3.5.1}$$

where the components are:

$\vec{j}_i^E$ : conductive energy flux (due to heat conduction and molecular diffusion) $\overline{\rho}_i \left(u_i + \frac{\vec{V}_i^2}{2}\right)\left(\vec{V}_i^E - \vec{V}_i\right)$

$r^E$ : rate of energy production per unit volume.

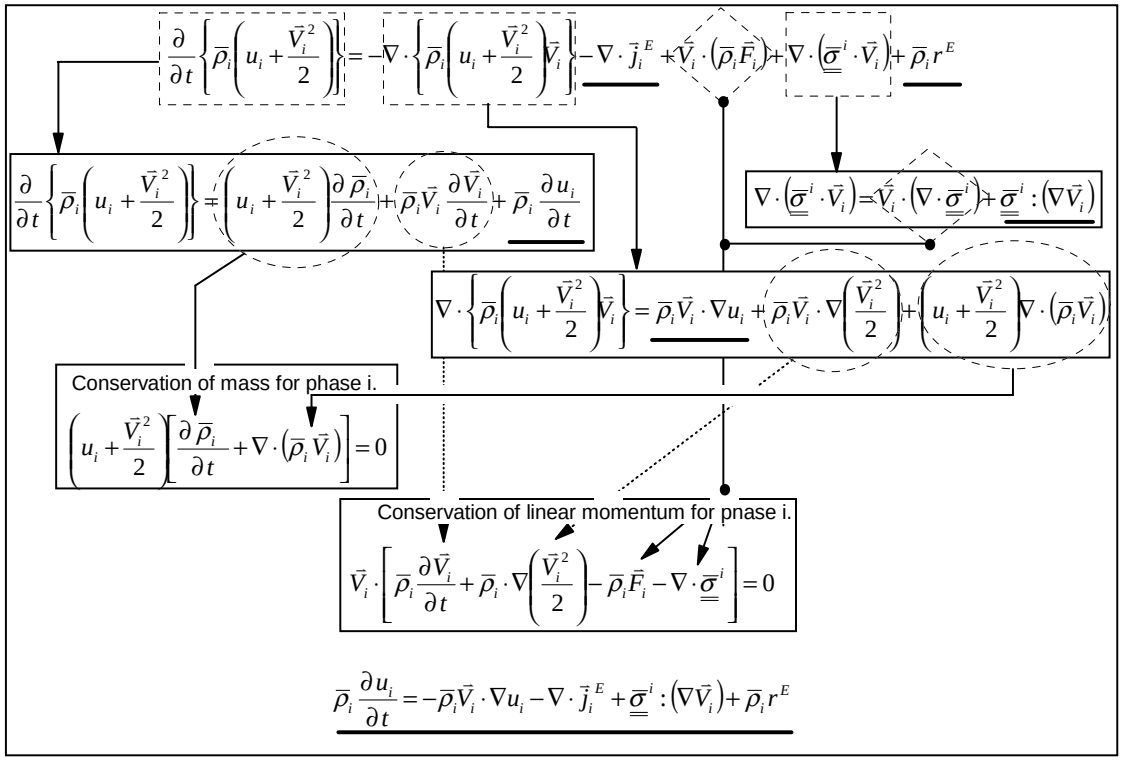


Figure 3.4: Conservation of internal energy diagram for phase i.

The conservation of energy equation (3.5.1) is reduced by combining it with the mass balance (3.2.1) and the momentum balance (3.3.6) equations as shown in Figure 3.4.

$$\overline{\rho}_i \frac{\partial u_i}{\partial t} = -\overline{\rho}_i \vec{V}_i \cdot \nabla u_i - \nabla \cdot \vec{j}_i^E + \underline{\overline{\sigma}}^i : \left(\nabla \vec{V}_i\right) + \overline{\rho}_i r^E \tag{3.5.2}$$

The rate of change of internal energy of the phase can also be expressed in terms of the total derivatives as shown below:

$$\overline{\rho}_i \frac{du_i}{dt} = -\nabla \cdot \vec{j}_i^E + \underline{\overline{\sigma}}^i : \left(\nabla \vec{V}_i\right) + \overline{\rho}_i r^E \tag{3.5.3}$$

Furthermore, if desired, the $\bar{\underline{\sigma}}^i$ term for the fluid phase can be broken down into shear and hydrostatic terms and expressed as $\bar{\underline{\sigma}}^f = \bar{\underline{\tau}}^f - \bar{p}\,\underline{\delta}$. Then the internal energy equation for the fluid phase can be rewritten as:

$$\overline{\rho}_f \frac{du_f}{dt} = -\nabla \cdot \vec{j}_f^E + \bar{\underline{\tau}}^f : \nabla \vec{V}_f - \bar{p} \nabla \cdot \vec{V}_f + \overline{\rho}_f r^E \tag{3.5.4}$$

The advantage of representing the rate of internal energy as in equation (3.5.4) is the separation of its two components; the irreversible rate of internal energy gain by shear, and the reversible rate of gain by compression.

The total internal energy balance of the system is obtained in equation (3.5.5) by summing the energy terms for each phase (solid and fluid):

$$\rho \frac{du}{dt} = -\nabla \cdot \vec{j}^E + \underline{\sigma} : \nabla \vec{V} + \rho r^E \tag{3.5.5}$$

## 3.6 Thermodynamical properties

The basic concepts of the theory of irreversible thermodynamics, as they apply to the problem at hand, are outlined in this section. The coupled flow laws in the form of proportionalities that describe the irreversible processes are also discussed. When two or more of these irreversible processes occur simultaneously within the same system they lead to coupled effects. The following sections will illustrate the use of the irreversible thermodynamics laws in expressing these coupled processes in porous media.

### 3.6.1 Thermodynamic potentials and internal energy

Gibbs, Helmholtz free energy and Gibbs-Duhem equations [35], [9], [24], [13], [36] are the main relations used in obtaining the final form of the governing equations. The Gibbs equation stated here represents the internal energy in terms of changes in total entropy, volume and mass of an open system:

$$dU = TdS + \bar{\sigma} dV + \sum \mu_i dm_i \tag{3.6.1}$$

The specific quantities (per unit mass) can be obtained for each of the variables in equation (3.6.1). These can then be used to express the Gibbs equation in terms of the specific quantities, as follows:

$$\begin{array}{ll} U = mu & \frac{U}{V} = \frac{mu}{V} = \rho u \\ S = ms & \frac{S}{V} = \frac{su}{V} = \rho s \\ m_i = mw_i & \frac{m_i}{V} = \frac{mw_i}{V} = \rho w_i \end{array}$$

$$\rho du = \rho T ds + \frac{\bar{\sigma}}{V} dV + \rho \sum \mu_i dw_i \tag{3.6.2}$$

Figure 3.5 shows the relationship between the volume ratio change and the void ratio change, which are used in replacing the volume terms on right hand side (RHS) of the equation (3.6.2):

$$\rho du = \rho T ds + \frac{\bar{\sigma}}{(1+e_0)} de + \rho \sum \mu_i dw_i \tag{3.6.3}$$

or, re-expressing the equation (3.6.3) per unit mass of an open system:

$$du = T ds + \frac{1}{\rho} \frac{\bar{\sigma}}{(1+e_0)} de + \sum \mu_i dw_i \tag{3.6.4}$$

The Helmholtz free energy is expressed in terms of the specific quantities as following:

$$F = u - sT \tag{3.6.5}$$

The differential form of equation (3.6.5) is used to express the cross relations between the partial derivatives with respect to the independent variables $(s, e, w_j)$, often referred to as the Maxwell's relations [8]:

$$dF = du - sdT - Tds \tag{3.6.6}$$

Another representation for the Helmholtz free energy is obtained by substituting equations (3.6.4) in equation (3.6.6):

$$dF = -sdT + \frac{1}{\rho} \frac{\bar{\sigma}}{(1+e_0)} de + \sum \mu_i dw_i \tag{3.6.7}$$

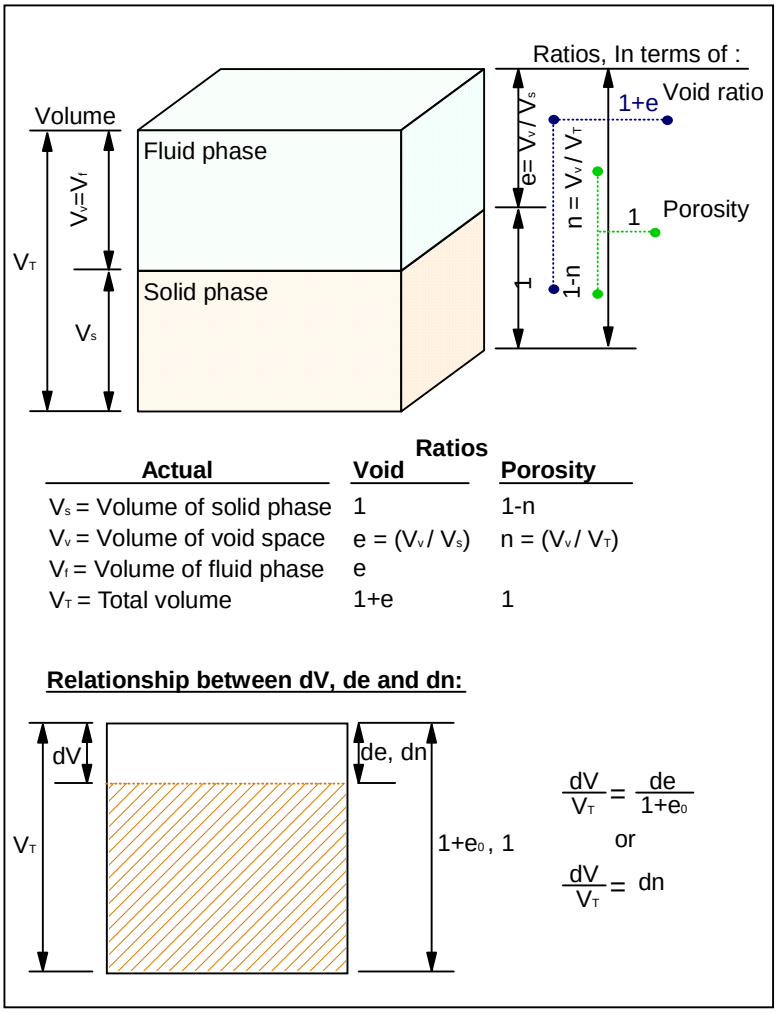


Figure 3.5: Two phase, saturated porous media volume change diagram.

The differential forms of the $F = F(T, e, w_i)$, $u = u(s, e, w_j)$ and $s = s(T, e)$ terms are expressed as:

$$du = \frac{\partial u}{\partial s}|_{e,w_i} ds + \frac{\partial u}{\partial e}|_{s,w_i} de + \sum_j \frac{\partial u}{\partial w_j}|_{s,e,w_k,k\neq j} dw_j \tag{3.6.8}$$

$$dF = \frac{\partial F}{\partial T}|_{e,w_i} dT + \frac{\partial F}{\partial e}|_{T,w_i} de + \sum_j \frac{\partial F}{\partial w_j}|_{s,e,w_k,k\neq j} dw_j \tag{3.6.9}$$

$$ds = \frac{\partial s}{\partial T}|_e dT + \frac{\partial s}{\partial e}|_T de \tag{3.6.10}$$

Note that the contribution of the component fractions $(\partial s/\partial w_j)$ to the entropy change are neglected in equation (3.6.10). The following relationships are obtained by combining the equations (3.6.7) and (3.6.9):

$$\frac{\partial F}{\partial T}|_{e,w_i} = -s \qquad \frac{\partial F}{\partial e}|_{T,w_i} = \frac{1}{\rho}\frac{\bar{\sigma}}{(1+e_0)} \qquad \frac{\partial F}{\partial w_j}|_{s,e,w_k,k\neq j} = \mu_i \tag{3.6.11}$$

The first term on the RHS of the equation (3.6.10), which is the expression for the variation of entropy with respect to temperature, can be re-written following the chain rule:

$$\frac{\partial s}{\partial \bar{\sigma}}|_e = \left(\frac{\partial s}{\partial T}|_e\right)\left(\frac{\partial T}{\partial \bar{\sigma}}|_e\right) \tag{3.6.12}$$

Equation (3.6.12) can be used here to introduce the two coefficients for isothermal compressibility ($\beta$) and thermal expansion ($\kappa$) [13], where $\bar{\sigma}$ is positive in tension:

$$\beta = \frac{1}{V}\left(\frac{\partial V}{\partial T}|_{\bar{\sigma}}\right) = \frac{1}{(1+e_0)}\left(\frac{\partial e}{\partial T}|_{\bar{\sigma}}\right) \tag{3.6.13}$$

$$\kappa = \frac{1}{V}\left(\frac{\partial V}{\partial \bar{\sigma}}|_T\right) = \frac{1}{(1+e_0)}\left(\frac{\partial e}{\partial \bar{\sigma}}|_T\right) \tag{3.6.14}$$

The property of the exact differentials is used to combine equations (3.6.10) and (3.6.11) to obtain the cross (Maxwell) relationships:

$$\frac{\partial^2 F}{\partial T \partial e}|_{w_i} = -\frac{\partial s}{\partial e} = \frac{1}{(1+e_0)}\frac{\partial\left(\bar{\sigma}/\rho\right)}{\partial T} \tag{3.6.15}$$

The variation of the internal energy with change in temperature can also be expressed in terms of the specific heat ($c_v$) [13]:

$$\frac{\partial u}{\partial T} = T\frac{\partial s}{\partial T} = c_v \tag{3.6.16}$$

The Maxwell relationships in equations (3.6.15) and (3.6.16) are used in the differential form of entropy equation (3.6.10) to obtain the following:

$$Tds = c_v dT - T\frac{1}{(1+e_0)}\frac{\partial(\bar{\sigma}/\rho)}{\partial T}de \tag{3.6.17}$$

Introducing the expression obtained for $Tds$ in equation (3.6.17), into the internal energy expression for an open system, (equation 3.6.3):

$$\rho du = \rho c_v dT + \left[\frac{\bar{\sigma}}{(1+e_0)} - \frac{\rho T}{(1+e_0)}\frac{\partial(\bar{\sigma}/\rho)}{\partial T}\right]de + \rho\sum_i \mu_i dw_i \tag{3.6.18}$$

The time derivative of the equation (3.6.18) is:

$$\rho\frac{du}{dt} = \rho c_v\frac{dT}{dt} + \left[\frac{\bar{\sigma}}{(1+e_0)} - \frac{\rho T}{(1+e_0)}\frac{\partial(\bar{\sigma}/\rho)}{\partial T}\right]\frac{de}{dt} + \rho\sum_i \mu_i\frac{dw_i}{dt} \tag{3.6.19}$$

Another form of expression for rate of change of internal energy for a porous system was given in equation (3.5.5):

$$\rho\frac{du}{dt} = -\nabla\cdot\vec{j}^E + \underline{\underline{\bar{\sigma}}}\colon\nabla\vec{V} + \rho r^E$$

Combining equations (3.5.5) and (3.6.19) and rearranging:

$$-\nabla\cdot\vec{j}^E + \underline{\underline{\bar{\sigma}}}\colon\nabla\vec{V} + \rho r^E =$$

$$\rho c_v\frac{dT}{dt} + \left[\frac{\bar{\sigma}}{(1+e_0)} - \frac{\rho T}{(1+e_0)}\frac{\partial(\bar{\sigma}/\rho)}{\partial T}\right]\frac{de}{dt} + \rho\sum_i \mu_i\frac{dw_i}{dt} \tag{3.6.20}$$

Then:

$$\rho c_v\frac{dT}{dt} =$$

$$-\nabla\cdot\vec{j}^E + \underline{\underline{\bar{\sigma}}}\colon\nabla\vec{V} + \rho r^E - \left[\frac{\bar{\sigma}}{(1+e_0)} - \frac{\rho T}{(1+e_0)}\frac{\partial(\bar{\sigma}/\rho)}{\partial T}\right]\frac{de}{dt} - \rho\sum_i \mu_i\frac{dw_i}{dt} \tag{3.6.21}$$

The equation (3.6.21) can be further reduced to equation (3.6.22) by taking advantage of the nature of the symmetry of the stress term $\left(\underline{\underline{\bar{\sigma}}}\right)$, and the replacement of the divergence $\nabla\vec{V}$ term as shown in the diagram in Figure 3.6:

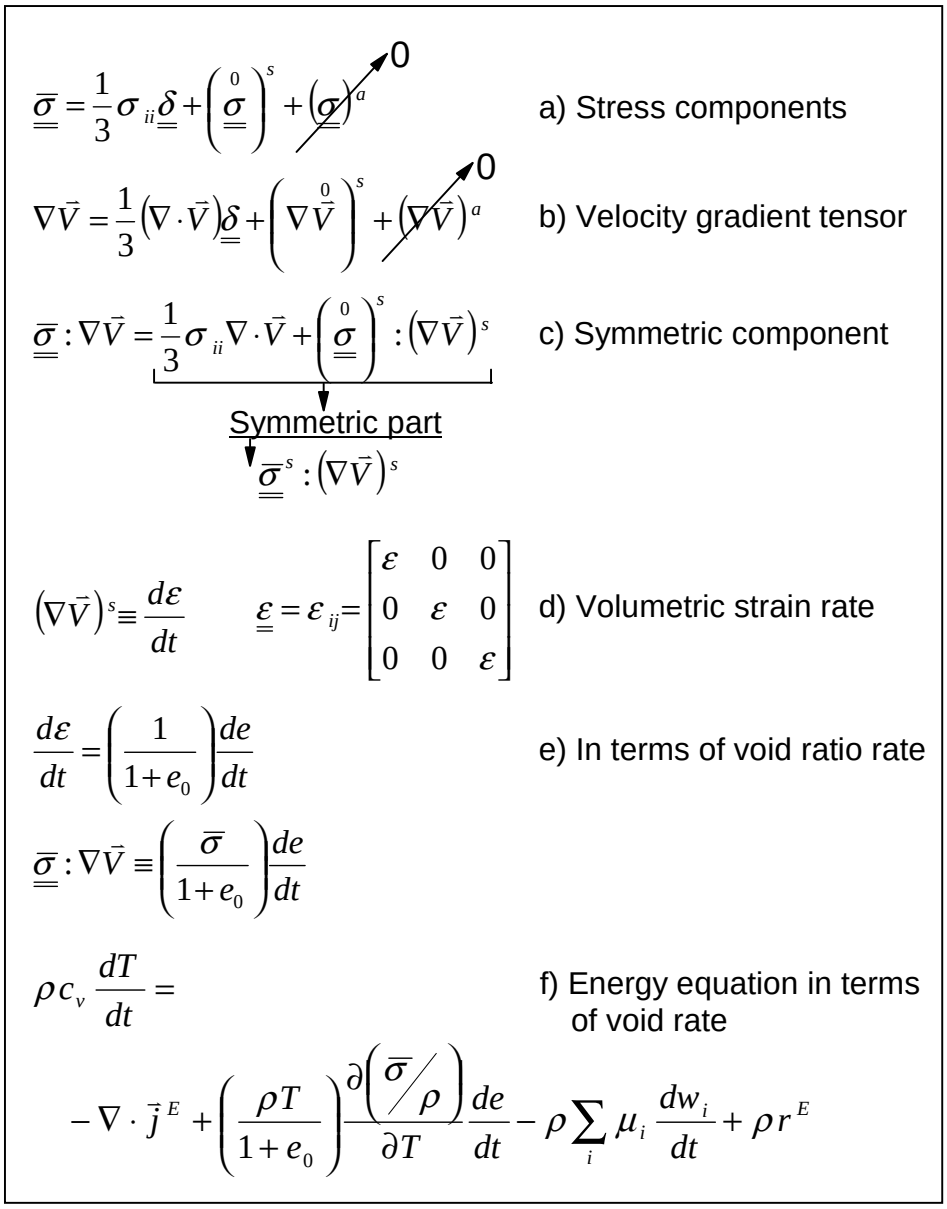


Figure 3.6: A void ratio change diagram obtained from the symmetrical stress tensor and volumetric strain rate of porous media.

$$\rho c_v \frac{dT}{dt} = -\nabla \cdot \vec{j}^E + \left(\frac{\rho T}{(1+e_0)}\right) \frac{\partial\left(\bar{\sigma}/\rho\right)}{\partial T} \frac{de}{dt} + \rho r^E - \rho \sum_i \mu_i \frac{dw_i}{dt} \tag{3.6.22}$$

Equation (3.6.22) is the heat balance equation. The last term on the RHS can be replaced with $\nabla \cdot \vec{j}_i$ using the conservation of mass of a component (equation 3.2.9), resulting in $\sum \mu_i \nabla \cdot \vec{j}_i$. The subscripts $k$ and $\alpha$ are added to the heat balance equation above representing a particular phase, and the components within that phase, respectively, so that:

$$\overline{\rho}_k \left(c_v\right)_k \frac{dT_k}{dt} = -\nabla \cdot \vec{j}_k^E + \left(\frac{\overline{\rho}_k T_k}{(1+e_0)}\right) \frac{\partial\left(\bar{\sigma}_{ii}^k/\overline{\rho}_k\right)}{\partial T} \frac{de}{dt} + \overline{\rho}_k r^E - \overline{\rho}_k \sum_\alpha \mu_\alpha \frac{dw_\alpha}{dt} \tag{3.6.23}$$

Note that the interphase conduction of heat is neglected in equation (3.6.23). It is also assumed that the solid and the fluid phases are at the same temperature at the same time and location, $T_s = T_f = T$ . The assumption of equilibrium for the temperature of the two phases at a given time and space results in a heat balance equation for the entire system, (equation 3.6.22). The lumped parameters (averaged coefficients); $\rho = \sum \bar{\rho}_i = n\rho_f + (1-n)\rho_s$ or $\rho c_v = \sum \bar{\rho}_i \left(c_v\right)_i = n\rho_f c_{v_f} + (1-n)\rho_s c_{v_s}$, are used to characterize the medium.

### 3.6.2 Entropy balance

The balance equation for the total entropy in an arbitrary volume is:

$$\int_V \frac{\partial\left(\rho s\right)}{\partial t} dV = -\int_A \vec{j}_s \cdot d\vec{A} + \int_V \phi_s dV \quad \text{and} \quad \frac{\partial\left(\rho s\right)}{\partial t} = -\nabla \cdot \vec{j}_s + \phi_s \tag{3.6.24}$$

where $\vec{j}_s$ is the entropy flux and $\phi_s$ is the entropy production rate term for an arbitrary volume. The partial derivative on the LHS of equation (3.6.24) can be reduced to the following expression, as shown in the diagram in Figure 3.7, as well:

$$\frac{\partial\left(\rho s\right)}{\partial t} = \rho \frac{ds}{dt} - \nabla \cdot \left(\rho s \vec{V}\right) \tag{3.6.25}$$

Equation (3.6.25) is obtained from $d(\rho s)/dt = \rho ds/dt + s d\rho/dt$ and by replacing the second term on the RHS of equation (3.6.24) by the RHS term in the conservation of mass equation to obtain $-\nabla \cdot \left(\rho s \vec{V}\right)$.

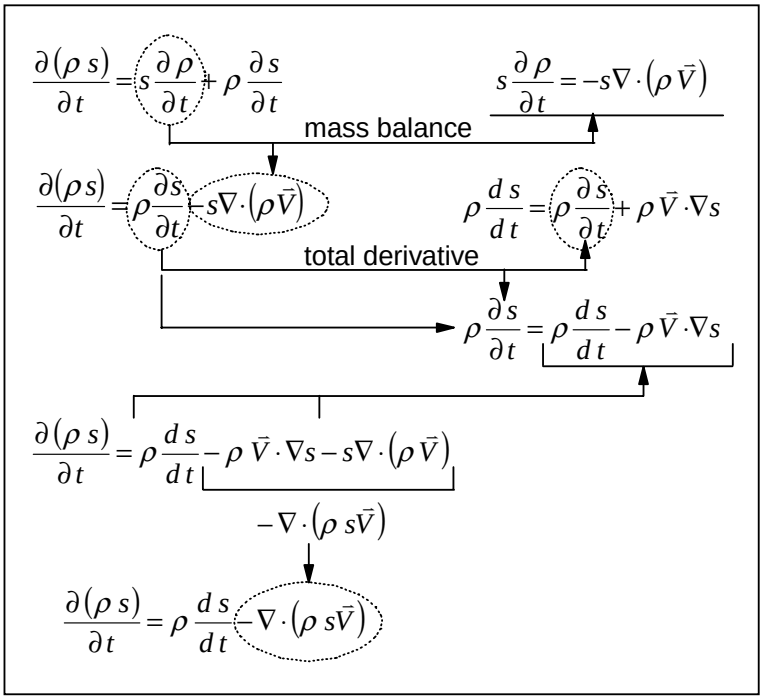


Figure 3.7: Entropy balance diagram

The time derivative of the Gibbs equation (3.6.2) for an open system is expressed as:

$$\rho T\frac{ds}{dt} = \rho\frac{du}{dt} - \frac{\bar{\sigma}}{V}\frac{dV}{dt} - \rho\sum_i \mu_i\frac{dw_i}{dt} \tag{3.6.26}$$

$$\rho T\frac{ds}{dt} = \rho\frac{du}{dt} - \frac{\bar{\sigma}}{(1+e_0)}\frac{de}{dt} - \rho\sum_i \mu_i\frac{dw_i}{dt} \tag{3.6.27}$$

The $\nabla\vec{V}$ term in the internal energy balance equation (3.5.5): $\rho du/dt = -\nabla\cdot\vec{j}^E + \rho r^E + \underline{\underline{\bar{\sigma}}}\colon\nabla\vec{V}$ , represents the symmetric part of the time derivative of the strain tensor $\left(d\underline{\underline{\epsilon}}/dt\right)$, as was given in the Figure 3.6 earlier. The expression of the rate of entropy change is obtained by incorporating equations (3.6.27) and (3.5.5) in to equation (3.6.28) and using the property illustrated in Figure 3.6, so that:

$$\rho T\frac{ds}{dt} = -\nabla\cdot\vec{j}^E + \rho r^E + \underline{\underline{\bar{\sigma}}}\colon\nabla\vec{V} - \frac{\bar{\sigma}}{(1+e_0)}\frac{de}{dt} - \rho\sum_i \mu_i\frac{dw_i}{dt} \tag{3.6.28}$$

$$\rho T\frac{ds}{dt} = -\nabla\cdot\vec{j}^{E} + \rho r^{E} - \rho\sum_{i}\mu_{i}\frac{dw_{i}}{dt} \tag{3.6.29}$$

The separation of the entropy equation and the flux components enables a clear definition and determination of the valid forms of the flux and the corresponding gradients (forces) for an open system. Such a separation becomes possible when the expression for $\rho ds/dT$ by equation (3.6.25) is replaced in equation (3.6.29):

$$\frac{\partial(\rho s)}{\partial t} + \nabla\cdot\left(\rho s\vec{V}\right) = \frac{1}{T}\left[-\nabla\cdot\vec{j}^{E} + \rho r^{E} - \rho\sum_{i}\mu_{i}\frac{dw_{i}}{dt}\right] \tag{3.6.30}$$

The last term in equation (3.6.30) is replaced by the conservation of mass expression (equation 3.2.9):

$$\frac{\partial(\rho s)}{\partial t} = -\nabla\cdot\left(\rho s\vec{V}\right) + \frac{1}{T}\left[-\nabla\cdot\vec{j}^{E} + \rho r^{E} - \sum_{i}\mu_{i}\left(-\nabla\cdot\vec{j}_{i}\right)\right] \tag{3.6.31}$$

Equation (3.6.31) can be rearranged to take the form of the entropy balance equation (3.6.24). The RHS terms are rearranged such that they can be expressed in terms of the divergence of a flux and the rate of entropy production term.

$$-\frac{\nabla\cdot\vec{j}^{E}}{T} = -\nabla\cdot\left(\frac{\vec{j}^{E}}{T}\right) - \frac{\vec{j}^{E}}{T^{2}}\cdot(\nabla T) \tag{3.6.32}$$

$$\frac{\mu_{i}}{T}\left(-\nabla\cdot\vec{j}_{i}\right) = -\nabla\cdot\left(\frac{\mu_{i}\vec{j}_{i}}{T}\right) + \vec{j}_{i}\cdot\nabla\left(\frac{\mu_{i}}{T}\right) \tag{3.6.33}$$

Replacing the expressions (3.6.32) and (3.6.33) in the entropy equation (3.6.31) and rearranging:

$$\frac{\partial(\rho s)}{\partial t} = -\nabla\cdot\left[\rho s\vec{V} + \frac{\vec{j}^{E}}{T} - \sum_{i}\frac{\mu_{i}\vec{j}_{i}}{T}\right] - \frac{\vec{j}^{E}}{T^{2}}\cdot(\nabla T) - \sum_{i}\vec{j}_{i}\cdot\nabla\left(\frac{\mu_{i}}{T}\right) + \frac{\rho r^{E}}{T} \tag{3.6.34}$$

This form of the equation helps to define the entropy flux, $\vec{j}_{s}$ and the rate of entropy production $\phi_{s}$ for an open system (neglecting the internal rate of energy production

term $\rho r^E/T$) as follows:

$$\vec{j}_s = \rho s\vec{V} + \frac{\vec{j}^E}{T} - \sum_i \frac{\mu_i \vec{j}_i}{T} \tag{3.6.35}$$

The dissipation function $\Phi_s = T\phi_s$, has the dimensions of free energy per unit time and is the measure of the rate of local dissipation of free energy by the irreversible processes. The dissipation function can also be used to express the sum of the products of flows (fluxes) and forces (gradients), $\left(\Phi_s = \sum_k \vec{j}_k \cdot \vec{X}_k\right)$.

$$\phi_s = \frac{1}{T}\sum_k \vec{j}_k \cdot \vec{X}_k = -\frac{\vec{j}^E}{T^2} \cdot (\nabla T) - \sum_i \vec{j}_i \cdot \nabla\left(\frac{\mu_i}{T}\right) \tag{3.6.36}$$

and

$$\Phi_s = T\phi_s = \sum_k \vec{j}_k \cdot \vec{X}_k = -\frac{\vec{j}^E}{T} \cdot (\nabla T) - \sum_i \vec{j}_i \cdot T\nabla\left(\frac{\mu_i}{T}\right) \tag{3.6.37}$$

## 3.7 Phenomenological relations

The dissipation function, or as stated previously, the rate of entropy generation equation (3.6.37), obtained for an open system, provides the proper form of the flux and the corresponding forces. This is the basic requirement for validity of Onsager's reciprocal relationships in expressing the phenomenological relationships for a two-phase multi-component system [29], [31], [36], [19], [24]. In here, linear relationships between fluxes and forces are assumed and they are illustrated by a symmetric coupled coefficient matrix.

The flux and force terms for an open, two-phase, multi-component system are:

$$\vec{j}_i = \sum_{k=1}^{n} L_{ik}\vec{X}_k + L_{iE}\vec{X}_E$$

$$\vec{j}_E = \sum_{k=1}^{n} L_{Ek}\vec{X}_k + L_{EE}\vec{X}_E \tag{3.7.1}$$

where the fluxes are:

$\vec{j}_i =$ material fluxes of the species

$\vec{j}_E =$ energy flux

and the force terms ($\vec{X}_i$) are obtained from the dissipation function equation (3.6.37).

$$\vec{X}_k = -T\nabla\left(\frac{\mu_k}{T}\right) \qquad \text{and} \qquad \vec{X}_E = -\frac{\nabla T}{T} \tag{3.7.2}$$

The material fluxes for species can be expressed in terms of $n-1$ independent flows:

$$\vec{j}_i = \sum_{k=1}^{n-1} L_{ik}\left(\vec{X}_k - \vec{X}_n\right) + L_{iE}\vec{X}_E$$

$$\vec{j}_E = \sum_{k=1}^{n-1} L_{Ek}\left(\vec{X}_k - \vec{X}_n\right) + L_{EE}\vec{X}_E \tag{3.7.3}$$

where $\vec{j}_n = -\sum_{i=1}^{n-1}\vec{j}_i$ is the expression for the $n^{th}$ flux term.

The two-phase multi-component flux and force relationships can be reduced further to obtain the relationships in terms of the fluid and energy flux. This process of heat and fluid flow in a two phase system is called "*thermo-osmosis*", which is a special case of thermal diffusion. The dissipation function for a single component system, indicating that no species are present in the fluid phase (two phase system):

$$\Phi_s = \vec{j}_E \cdot \vec{X}_E + \vec{j}_f \cdot \vec{X}_f$$

$$\Phi_s = \vec{j}_E \cdot \left(-\frac{\nabla T}{T}\right) + \vec{j}_f \cdot \left(-T\nabla\left(\frac{\mu_f}{T}\right)\right) \tag{3.7.4}$$

The thermodynamic energy flux $\vec{j}_E$ can be replaced with the calorimetric heat flow [31]:

$$\vec{j}_q = \vec{j}_E - h_f\vec{j}_f \tag{3.7.5}$$

where

$\vec{j}_q =$ the heat flux
$\vec{j}_E =$ the energy flux
$h_f =$ the specific enthalpy of fluid (water)
$\vec{j}_f =$ the fluid flux

The transformation presented above requires the gradients (forces) also be changed since the dissipation must remain invariant in the transformation. The substitution required in this case [19] is:

$$\Phi_s = \vec{j}_q \cdot \left(-\frac{\nabla T}{T}\right) + h_f\vec{j}_f \cdot \left(-\frac{\nabla T}{T}\right) + \vec{j}_f \cdot \left(-T\nabla\left(\frac{\mu_f}{T}\right)\right) \tag{3.7.6}$$

Expanding the fluid chemical potential term $\left(\mu_f\right)$ [8]:

$$\vec{X}_f = \left(-T\nabla\left(\frac{\mu_f}{T}\right)\right) = h_f\left(\frac{\nabla T}{T}\right) - \nabla\mu_f|_T \tag{3.7.7}$$

where the subscript $T$ indicates constant temperature conditions. The dissipation function for the fluid and heat flux reduces to its final form as follows:

$$\Phi_s = \vec{j}_q \cdot \left(-\frac{\nabla T}{T}\right) + \vec{j}_f \cdot \left(-\nabla\mu_f|_T\right) \tag{3.7.8}$$

The resulting fluid and heat flow equations are then obtained in the form of coupled flow expressions:

$$\begin{aligned} \vec{j}_f &= -L_{ff} \cdot \nabla\mu_f|_T - L_{fq} \cdot \left(\frac{\nabla T}{T}\right) \\ \vec{j}_q &= -L_{qf} \cdot \nabla\mu_f|_T - L_{qq} \cdot \left(\frac{\nabla T}{T}\right) \end{aligned} \tag{3.7.9}$$

The change in chemical potential of fluid (water) at constant temperature can be evaluated from the Gibbs equation. The transfer of a single component, fluid, is equivalent to:

$$\nabla\mu_f|_T = \nu_f \nabla p \tag{3.7.10}$$

The substitution of the equation (3.7.10) for the chemical potential of fluid in the coupled flow expressions (3.7.9) results in the following set of equations:

$$\begin{aligned} \vec{j}_f &= L_{ff} \cdot \left(-\nu_f \nabla p\right) + L_{fq} \cdot \left(-\frac{\nabla T}{T}\right) \\ \vec{j}_q &= L_{qf} \cdot \left(-\nu_f \nabla p\right) + L_{qq} \cdot \left(-\frac{\nabla T}{T}\right) \end{aligned} \tag{3.7.11}$$

where

$\nu_f =$ specific volume of the soil fluid (water at saturation is $\frac{1}{\rho_f}$)

$p =$ soil fluid (water) pressure resulting in fluid flow

$T =$ absolute temperature value

The coefficient $(L_{qq}/T)$ is equivalent to the Fourier thermal conductivity $(\lambda)$ and $L_{qf} = L_{fq}$ is the coupling coefficient between fluid and heat flow. The term on the LHS of the fluid flux equation (3.7.11) is the relative fluid flux due to the

application of hydraulic gradient, (identical to $\vec{q}_r$ of equation 3.9.8, $\vec{q}_r = -\underline{\underline{K}} \cdot\nabla\left(\frac{p\,\underline{\underline{\delta}}}{\rho_f g}\right)$). Equating the expressions for the fluid flux under hydraulic gradient for a homogeneous isotropic medium will result in:

$$L_{ff}\nu_f = \frac{K}{\rho_f g} \quad \text{or} \quad L_{ff}\nu_f = \frac{k}{\mu_f}$$

where $K$ is the hydraulic conductivity, $k$ the permeability coefficient of the porous media $\left(K = k\frac{\rho_f g}{\mu_f}\right)$, and $\mu_f$ is the viscosity of the fluid.

The coupling coefficient $L_{fq}$ can be expressed as [12]:

$$L_{fq} = -DT^2\left(\frac{\partial n}{\partial T}\right) \tag{3.7.12}$$

where $D$ is the isothermal soil water diffusivity and $n$ represents the volumetric moisture content (identical to porosity for a saturated two-phase system). At normal temperature levels the term $\left(\frac{\partial n}{\partial T}\right)$ is negative, thus making $L_{fq}$ positive. This indicates the presence of positive coupling where, the contributions of two gradients are added causing an increased fluid and heat flux.

The *potential* fluid flux can also be expressed for hydraulic flow in terms of transient pressure distribution (and hydraulic conductivity) in a deformable porous media via the mass and linear momentum conservation equations. However, it is more appropriate to first define the stress components of the two-phase system, followed by the pertinent assumptions and simplifications made in expressing the potential fluid flux term.

## 3.8 Stresses in porous media

The stress components of a deformable two-phase porous medium are derived for each phase using the strain producing effective stress.

The stress $\underline{\underline{\sigma}}$ (macroscopic total stress) used in the conservation of linear momentum can be expressed in terms of the contribution of each phase stress[2]:

$$\underline{\underline{\sigma}} = \sum_i n_i\,\underline{\underline{\sigma}}^i = n\,\underline{\underline{\sigma}}^f + (1-n)\,\underline{\underline{\sigma}}^s \tag{3.8.1}$$

where $\underline{\underline{\sigma}}^f$ and $\underline{\underline{\sigma}}^s$ are the stresses in the fluid and the solid phase. For the fluid phase:

$$\underline{\underline{\sigma}}^f = \underline{\underline{\tau}}^f - p_f \, \underline{\underline{\delta}} \tag{3.8.2}$$

$\underline{\underline{\tau}}^f$ represents the viscous stress, and $p_f$ the compressive pressure. Note that the stresses in both phases are expressed as positive for tension and the fluid pressure term positive for compression.

In the mechanics of a porous media of particulate matter, the stress in solids $\left(\underline{\underline{\sigma}}^s\right)$, is not the strain producing stress based on the assumption that the deformation is produced by the rearrangement of grains, due to slipping or rolling which is much larger than the compression of the solid material itself. The intergranular, or effective stress is introduced by subtracting the pressure in fluid from the stress in solid (neglecting $\underline{\underline{\tau}}^f$).

$$\begin{aligned} \underline{\underline{\sigma}} &= (1-n)\, \underline{\underline{\sigma}}^s - n p_f \, \underline{\underline{\delta}} \\ \underline{\underline{\sigma}} &= (1-n) \left[\underline{\underline{\sigma}}^s + p_f \, \underline{\underline{\delta}}\right] - p_f \, \underline{\underline{\delta}} \\ \underline{\underline{\sigma}} &= \underline{\underline{\sigma}}^{s'} - p_f \, \underline{\underline{\delta}} \end{aligned} \tag{3.8.3}$$

and the effective stress is obtained:

$$\underline{\underline{\sigma}}^{s'} = (1-n) \left[\underline{\underline{\sigma}}^s + p_f \, \underline{\underline{\delta}}\right] \tag{3.8.4}$$

where again, the stresses are positive in tension and the pressure is positive in compression. In here, the conventional soil mechanics notation will be used for stress terms where both are taken as positive in compression, and the negative sign before the pressure term in equation (3.8.3) is replaced as:

$$\underline{\underline{\sigma}} = \underline{\underline{\sigma}}^{s'} + p_f \, \underline{\underline{\delta}} \tag{3.8.5}$$

A two phase (saturated) deformable porous system under constant applied total stress, $\underline{\underline{\sigma}}$, requires that the change in the fluid phase pressure is equal in magnitude to the change in effective stress of the porous skeleton. One-dimensional consolidation theory takes advantage of this by replacing the change in effective stress term by the equivalent change in fluid phase hydrostatic pressure term.

## 3.9 Constitutive relations

Constitutive relationships for the stress-strain and the relative fluid flux are derived for a deformable porous media.

### 3.9.1 Compressibility

The deformation in porous media is due to the realized effective stress and the change in the porosity of the medium due to this stress value:

$$n = n\left(\underset{=}{\sigma}^{s'}\right) \tag{3.9.1}$$

The macroscopic displacement vector for solids $\vec{w}_s$, and the non-zero velocity of the soil particles $\vec{V}_s$ for a deformable medium are related as:

$$\vec{V}_s = \frac{d\vec{w}_s}{dt} \tag{3.9.2}$$

The solid phase mass balance equation (3.2.7) obtained earlier can be rearranged as:

$$\nabla \cdot \vec{V}_s = -\frac{1}{(1-n)} \frac{d_s\,(1-n)}{dt} \tag{3.9.3}$$

where $\dfrac{d_s}{dt}(...) = \dfrac{\partial}{\partial t}(...) + \vec{V}_s \cdot \nabla(...)$.

The $\nabla \cdot \vec{V}_s$ term is equivalent to the volumetric rate of strain ($\epsilon^s = \epsilon^s_x + \epsilon^s_y + \epsilon^s_z$ and $\dot{\underset{=}{\epsilon}}^s = \frac{d\underset{=}{\varepsilon}^s}{dt}$), which is equivalent to that of the soil skeleton $\left(\dot{\underset{=}{\epsilon}} = \frac{d\underset{=}{\varepsilon}}{dt}\right)$, since the deformation of the skeleton is considered as the re-arrangement of the solid particles:

$$\nabla \cdot \vec{V}_s = \frac{d\varepsilon}{dt} = -\frac{1}{(1-n)} \frac{d_s\,(1-n)}{dt} \tag{3.9.4}$$

The mass balance equation (3.2.8) for the fluid phase is also re-arranged in five steps as shown in Figure 3.8. As a result of this re-arrangement, the fluid phase balance equation takes the following form:

$$n\frac{d_s\rho_f}{dt} + \left[\frac{\rho_f}{1+e_0}\right]\frac{de}{dt} + \nabla \cdot \left(\rho_f \vec{V}_r\right) = 0 \tag{3.9.5}$$

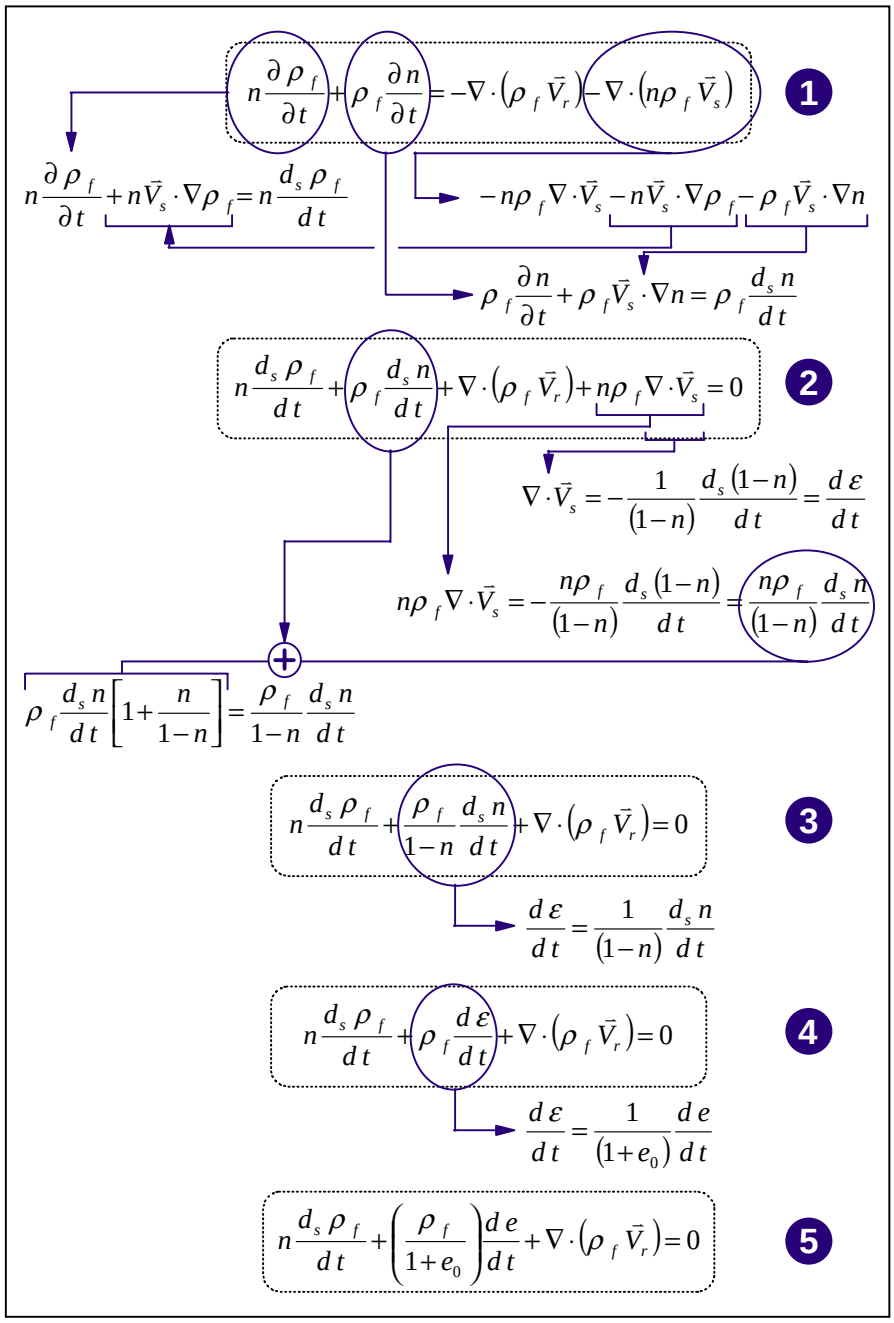


Figure 3.8: Step-by-step reduction of the fluid phase mass conservation equation diagram.

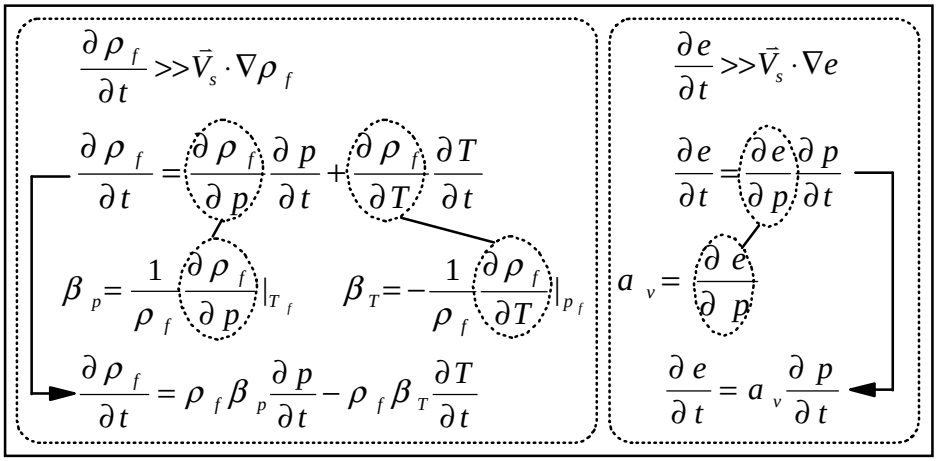


Figure 3.9: Fluid phase density and skeleton deformation dependence on pressure and temperature diagram.

Equation (3.9.5) can further be simplified when it is reorganized as shown in Figure 3.9.The coefficients $\beta_p$, $\beta_T$ and $a_v$ used in Figure 3.9 are the isothermal compressibility and the thermal expansion coefficient of the fluid phase, and the coefficient of compressibility of the porous medium, respectively. The effect of thermal expansion of the solid skeleton (void space) is not included in this derivation. The typical values of compressibility and expansion coefficients for water at 20 °C and atmospheric pressure are, $\beta_p = 4.6 \times 10^{-10}\,\mathrm{Pa}^{-1}$ and $\beta_T = 2.1 \times 10^{-4}\,\mathrm{K}^{-1}$ [17]. Using the relations shown in Figure 3.9, the equation (3.9.5) can be expressed in terms of the coefficients above, where the fluid phase density, $\rho_f$, is replaced as follows:

$$\left(n\beta_p + \frac{a_v}{1+e_0}\right)\frac{\partial p}{\partial t} - n\beta_T \frac{\partial T}{\partial t} + \nabla \cdot \vec{V}_r = 0 \tag{3.9.6}$$

### 3.9.2 Advective flux

The expression for the advective flux within the porous medium is derived. The relative flux in the two phase fluid saturated porous media is:

$$\vec{q}_r = \vec{V}_r = n\left(\vec{V}_f - \vec{V}_s\right) \tag{3.9.7}$$

The expressions for fluxes are used in the conservation of linear momentum equation to obtain the dominating components of the potential flow regime. The momentum conservation equations (3.3.4) and (3.3.6) show the momentum transfer in each phase. The external force contribution to momentum of each phase can be neglected since the porous medium orientation is horizontal assumed to span the same elevation. A Newtonian fluid phase is considered where the shear terms in the fluid phase are related to the gradient of the velocity components. The rate of change of momentum for fluid phase is expressed in terms of the momentum transfer due to the pressure gradient, and the resistance to flow within the fluid and porous medium.

There are two particular cases of simplified momentum equations. The first case results in the typical form of the Darcy's law by neglecting the inertial effects and the viscous resistance in the fluid phase itself [2]:

$$\vec{q_r} = \vec{V_r} = - \underline{\underline{K}} \cdot \nabla \left( \frac{p \ \underline{\underline{\delta}}}{\rho_f g} \right) \tag{3.9.8}$$

where the coefficient $\underline{\underline{K}}$ is the hydraulic conductivity, a second rank symmetrical tensor, and the RHS term in the parenthesis represents the required pressure head ($\varphi$) to drive the fluid with a specified relative flux.

The other case represents the flow regime following the immediate onset of the flow, where the inertial effects are larger than the viscous effects at fluid-solid interface and inside the fluid, resulting in:

$$\overline{\rho}_f \frac{d\vec{V}_f}{dt} = -\nabla \cdot \left( np \ \underline{\underline{\delta}} \right) \tag{3.9.9}$$

The particular form of equation representing the physical state of the phenomena, either at the onset or afterwards, is to be adapted in the final form of the fluid phase mass balance equation as stated in equation (3.9.6). A summary of constitutive equations are listed in Table 3.2.

Table 3.2: A set of system governing equations

| **Balance** | **Phase** | **Equation** |
|---|---|---|
| Mass | Solid (3.2.7) | $\frac{\partial(1-n)}{\partial t} = -\nabla \cdot \left[(1-n)\,\vec{V}_s\right]$ |
| | Fluid (3.9.6) | $\left(n\beta_p + \frac{a_v}{1+e_0}\right)\frac{\partial p}{\partial t} - n\beta_T \frac{\partial T}{\partial t} + \nabla \cdot \vec{V}_r = 0$ |
| Momentum | Solid (3.3.7) | $\overline{\rho}_s \frac{d\vec{V}_s}{dt} = \overline{\rho}_s \vec{F}_s + \nabla \cdot \left((1-n)\,\underline{\underline{\sigma}}^s\right)$ |
| | Fluid (3.9.8) | $\vec{V}_r = -K\nabla\left(\frac{p}{\rho_f g}\right)$ |
| Energy | System (3.6.22) | $\rho c_v \frac{dT}{dt} = -\nabla \cdot \vec{j}^E + \left(\frac{\rho T}{(1+e_0)}\right)\frac{\partial(\bar{\sigma}/\rho)}{\partial T}\frac{de}{dt} + \rho r^E$ |
| **Fluxes** | | |
| Open | Component | $\vec{j}_i = \sum_{k=1}^{n-1} L_{ik}\left(\vec{X}_k - \vec{X}_n\right) + L_{iq}\vec{X}_q$ |
| | Heat (3.7.3) | $\vec{j}_q = \sum_{k=1}^{n-1} L_{qk}\left(\vec{X}_k - \vec{X}_n\right) + L_{qq}\vec{X}_q$ |
| Single component | Fluid | $\vec{j}_f = L_{ff}\cdot(-\nu_f \nabla p) + L_{fq}\cdot\left(-\frac{\nabla T}{T}\right)$ |
| | Heat (3.7.11) | $\vec{j}_q = L_{qf}\cdot(-\nu_f \nabla p) + L_{qq}\cdot\left(-\frac{\nabla T}{T}\right)$ |
| **Constitutive** | | |
| Effective Stress | (3.8.5) | $\underline{\underline{\sigma}}^{s'} = \underline{\underline{\sigma}} - p_f\,\underline{\underline{\delta}}$ |
| Volumetric Strain rate | Figures 3.4 & 3.5 | $\frac{d\epsilon}{dt} = \frac{1}{1+e_0}\frac{de}{dt}$ |
| Compressibility of Soil Skeleton | Figure 3.8 | $a_v = -\frac{\partial e}{\partial p}$ |
| | Equation of State | $\rho_f = \rho_f(p,T)$ |

## 3.10 Simplified model

The governing equations listed above represent the physical processes in the porous media due to the application of hydraulic and thermal gradients. The simplified forms of these relations are used in the numerical simulations to obtain the numerical thermal and hydraulic response of a physical system.

The simplifying assumptions were selected so that the experimental verification of the processes were possible which included the measurement of a number of these desired responses. These assumptions were selected to minimize the number of unknown parameters required by the parameter identification process.

### 3.10.1 Simplifying assumptions

A number of simplifying assumptions pertinent to the system in hand were required to allow for a realistic modeling and simulation of the processes. The variation of some parameters were negligible compared to others in terms of their contribution to the overall magnitude of the responses. In some cases individual parameters were combined, to be represented in a compound form under a single parameter, which provided a better control on the entire simulation and the subsequent parameter identification process.

#### Assumptions

**A.1** The solid phase particles are assumed to be incompressible, $\rho_s$ is constant.

**A.2** The effect of $\nabla\rho_f$ is assumed to be much smaller than the time rate of change of the fluid density.

**A.3** The compressibility of the porous skeleton is much larger that the compressibility of the fluid phase due to pressure $\left(\beta_p\right)$ and temperature $(\beta_T)$ in ground-water problems.

**A.4** The two phase porous media under constant applied total stress requires that the incremental change in the effective stress be identical to the change in the hydrostatic pressure term in the fluid phase.

**A.5** The inertial effects in the equation of motion (momentum balance) are neglected compared to the viscous resistance for the cases with advective flow components.

**A.6** The viscosity effects within the fluid itself in the equation of motion are neglected.

**A.7** The hydraulic conductivity coefficient ($K$) is assumed to be independent of location and is assumed constant for a homogeneous isotropic porous media.

**A.8** The heat flux term $\vec{j}_q$ is placed in the energy flux term (molecular) $\vec{j}^E$, neglecting the energy transfer due to local molecular activities.

**A.9** The conductive heat flux term for a closed system is represented by Fourier's law: $\vec{j}_q = L_{qq}\vec{X}_q$, where $\vec{X}_q$ is the temperature gradient and the coefficient $L_{qq}/T = \lambda$ for the thermal conductivity of the system.

**A.10** The temperature values for both phases in one location are assumed to be identical $T_s = T_f = T$. This is based on the assumption of the relatively small granular solid particles having high thermal conductivity and the fluid phase velocity being relatively small, which causes the averaged temperature of the two phases to be equivalent.

**A.11** The single energy equation representing the energy balance for both phases is expressed in terms of lumped parameters: $\rho = n\rho_f + (1-n)\,\rho_s$, $\lambda = n\lambda_f + (1-n)\,\lambda_s$, and $\rho c_v = n\rho_f c_{vf} + (1-n)\,\rho_s c_{vs}$.

**A.12** One dimensional system along the long dimension of the physical set-up and the direction of the applied gradients.

### 3.10.2 A simplified system

The simplified system of the governing equations is presented. As was discussed previously, in the experimental methodology segment, the elimination of material fluxes under the closed boundaries minimized the disturbance to the original structure of the soil skeleton.

In the following set of equations, the assumption number (A.3) is already applied, where the deformation of the two phase porous system is only due to the potential compressibility of the soil skeleton, which is used to obtain the strain inducing (effective) stress. The assumptions number (A.1) and (A.2) are also in effect in the current form of the equation (3.9.6). The compressibility of the fluid phase itself can be ignored from the same equation under assumption number (A.3). The advective fluid flux equation (3.9.8) is a simplified form of the momentum balance of the fluid phase in the light of the assumptions number (A.5) and (A.6).

#### Uncoupled expressions

The fluid phase mass balance equation (3.9.6) for hydraulic flux case makes use of the relative advective flux representation in equation (3.9.8) and the assumptions number (A.7) and (A.2):

$$\left(\frac{a_v}{1+e_0}\right)\frac{\partial p}{\partial t} = K\nabla^2\left(\frac{p}{\rho_f g}\right)$$

$$\frac{\partial p}{\partial t} = \left(\frac{K\left(1+e_0\right)}{a_v \rho_f g}\right)\nabla^2 p \tag{3.10.1}$$

The energy balance equation (3.6.22) is reduced to the form below by using the compressibility coefficients for the fluid phase and the assumption number (A.1):

$$\rho c_v \frac{dT}{dt} = -\nabla\cdot\vec{j}^E - \frac{T}{(1+e_0)}\left(\frac{\beta_T}{\beta_p}\right)\frac{de}{dt} + \rho r^E \tag{3.10.2}$$

The volumetric compressibility of the soil skeleton used in the above equation is replaced by the pressure term, so that:

$$\rho c_v \frac{dT}{dt} = -\nabla \cdot \vec{j}^E - T\left(\frac{\beta_T}{\beta_p}\right)\frac{a_v}{(1+e_0)}\frac{dp}{dt} + \rho r^E \tag{3.10.3}$$

Introduction of the heat flux expression for the energy flux term (assumption number A.8) results in:

$$\rho c_v \frac{dT}{dt} = -\nabla \cdot \vec{j}_q - T\left(\frac{\beta_T}{\beta_p}\right)\frac{a_v}{(1+e_0)}\frac{dp}{dt} + \rho r^E \tag{3.10.4}$$

Substituting the Fourier heat flux expression, and neglecting the contribution of the fluid expansion term for an uncoupled expression, the energy balance equation takes the following form:

$$\rho c_v \frac{dT}{dt} = -\nabla \cdot \left(L_{qq}\vec{X}_q\right) + \rho r^E$$

or

$$\rho c_v \frac{dT}{dt} = \nabla \cdot \left(\lambda T \left(\nabla T/T\right)\right) + \rho r^E \tag{3.10.5}$$

**Coupled expressions**

The coupled form for the simultaneous flow of fluid and heat in porous media is obtained by substituting the coupled flux equations (3.7.11) in the mass and the energy balance equations. Then the fluid phase mass balance equation (3.9.6) can be written as, with assumption number (A.3):

$$\left(\frac{a_v}{1+e_0}\right)\frac{\partial p}{\partial t} = \nabla \cdot \left[L_{ff} \cdot \left(\nu_f \nabla p\right) + L_{fq} \cdot \left(\frac{\nabla T}{T}\right)\right] \tag{3.10.6}$$

and, using the hydraulic conductivity coefficient $K$ for a homogeneous isotropic porous medium, and assuming a constant coupling coefficient $L_{fq}$:

$$\left(\frac{a_v}{1+e_0}\right)\frac{\partial p}{\partial t} = \left(\frac{K}{\rho_f g}\right)\nabla^2 p + L_{fq}\nabla\left(\frac{\nabla T}{T}\right) \tag{3.10.7}$$

Similarly, the energy balance equation (3.10.4) is reduced using the coupled heat flux expression in equation (3.7.11):

$$\rho c_v \frac{dT}{dt} = \nabla \cdot \left[L_{qf} \cdot \left(\nu_f \nabla p\right) + L_{qq} \cdot \left(\frac{\nabla T}{T}\right)\right] - T\left(\frac{\beta_T}{\beta_p}\right)\frac{a_v}{(1+e_0)}\frac{dp}{dt} + \rho r^E \tag{3.10.8}$$

By assuming constant values of $L_{qf}$ and $L_{qq}$, and replacing $L_{qq}$ with the conduction coefficient $\lambda$:

$$\rho c_v \frac{dT}{dt} = (L_{qf}\nu_f)\,\nabla^2 p + \lambda T \nabla\left(\frac{\nabla T}{T}\right) - T\left(\frac{\beta_T}{\beta_p}\right)\frac{a_v}{(1+e_0)}\frac{dp}{dt} + \rho r^E \qquad (3.10.9)$$

The above two equations (3.10.7) and (3.10.9), integrated with the expression for the coupled fluxes (equation 3.7.11) form the simplified set of governing equations for the porous system.

### 3.10.3 Boundary conditions

The boundary conditions are considered in terms of the material and heat fluxes. The control of these are achieved by the manipulation of the pressure and temperature values, at the boundaries, as discussed in Chapter 2.

The material boundaries can either be closed or open. The value of pressure or its gradient can either be set to a constant, or varied as required. The temperature values are controlled at the boundaries by application of the heat sources at these locations. The surface heat loss can be allowed or minimized by use of a thermal insulation. Heat sources within the body of the sample may also be permitted. As a result, various combinations of boundary conditions were considered in this study.

The actual boundary conditions applied on experimental and numerical simulations are discussed in the experimental and numerical sections of this dissertation.

### 3.10.4 Concluding remarks

The pertinent analytical background and the derivation of the governing equations of a multi-phase multi-component deformable open porous system were presented. The coupled flow equations representing the irreversible fluxes and their corresponding gradients are obtained from the entropy production rate which preserves the symmetry of the coefficient matrix indicated in Onsager's reciprocal theorem [8]. The governing equations representing a closed system were then obtained from these generic forms. The numerical solution of the equations generated the transient pressure and temperature distributions due to the applied boundary and initial conditions.

The numerical simulations were carried out mostly for the closed system where no material flux was allowed through the boundaries. A simulation model could also be generated easily for an open multi-phase, multi-component system using the following set of governing equations: (3.2.7), (3.2.9), (3.3.7), (3.7.3), (3.9.6), (3.9.9), (3.6.22), and (3.8.5). In this work, however, the development of the closed boundary experimental procedure dictated the final simplified form of the model. The experiments were intended to address two basic issues:

- To develop a non-destructive approach achieved under no material flux and small stress increments to minimize disturbance to the soil structure.
- To develop a simple experimental system that would allow accurate transient measurements of the desired responses along the specimen.

The issue of accurate real-time experimental measurements were crucial to validate the simulation and parameter identification approaches for the model. As a result of these considerations, an inert closed two-phase system was selected. This selection eliminated the inclusion of chemical components within each phase and subsequently the need for the non-trivial measurement of the transient values of the chemical concentrations.

However, the governing equations are derived to handle multi-component cases of as well as open boundary conditions, as discussed in the earlier sections of this chapter. Validation of these equations were not included with in the scope of this dissertation.

# Chapter 4

# Numerical Solution of Partial Differential Equations

## 4.1 Numerical Engine

Mathematical formulations that represent a physical phenomena are often in the form of partial differential equations (PDEs). The analytical solutions for the formulated PDEs are often not possible, and except for a few known forms, the solution of the PDEs are presented in the numerical form. One common numerical solution technique of PDEs is the "Method of Lines" (MOL). In application of MOL, the PDEs are converted to Ordinary Differential Equations (ODEs) or Differential Algebraic Equations (DAEs) by approximating the spatial derivatives with algebraic approximations. This results in equations with derivatives with respect to the initial value variable, $t$, which are then integrated over time.

The MOL approach is used in formulating a simulation environment for the PDEs representing the coupled flow in porous media derived in the previous chapter. The purpose of such simulation is to permit a dynamic environment for parameter identification and implement the estimator tool. The requirements considered for such a simulation is modularity, flexibility, ease of use and modification, stability and computational quality. The computational speed of the numerical construct

will highly depend on the size and the properties of the initial value problem, the spatial discretization and the efficiency of the time integrators.

Available quality mathematical software (routines) are utilized whenever applicable. The numerical methods and schemes involved in the design of the simulation program and their implementation to the PDEs representing the coupled flow in porous media will be described in this chapter.

## 4.2 Method of lines (MOL)

The method of lines is a well recognized generic procedure for solving partial differential equations [33]. A typical application of MOL to the well known second-order PDEs in terms of dependent variable $\overline{w}(\overline{x},t)$ is considered below for illustration purposes, where $\overline{x} = [x,y,z]^T$. A system of $n$-degree PDEs with corresponding boundary and initial conditions are shown here:

$$\overline{w}_t = \overline{f}(\overline{x},t,\overline{w},\overline{w}_x,\overline{w}_{xx}) \qquad t>0, \overline{x}\in(0,L) \tag{4.1}$$

applicable boundary condition functions (BCs)

$$g_0(\overline{x},t,\overline{w},\overline{w}_x,\overline{w}_{xx}) = 0 \qquad t>0, \overline{x}=0 \tag{4.2}$$

$$g_L(\overline{x},t,\overline{w},\overline{w}_x,\overline{w}_{xx}) = 0 \qquad t>0, \overline{x}=L \tag{4.3}$$

with given initial condition functions (ICs)

$$\overline{w}(\overline{x},0) = \overline{w}_0(\overline{x}) \qquad x\in[0,L] \tag{4.4}$$

where

$\overline{w} = [w_1,.....,w_n]^T$ is the dependent variable vector for the system of PDEs,

$\overline{w}_0 = [w_{1,0},.....,w_{n,0}]^T$ is the initial condition vector,

$\overline{w}_t = \partial\overline{w}/\partial t = [\partial w_1/\partial t,.....,\partial w_n/\partial t]$ is the time derivative vector,

$\overline{w}_x = \partial\overline{w}/\partial\overline{x} = [\partial w_1/\partial\overline{x},....,\partial w_n/\partial\overline{x}]$ is the spatial first derivative vector,

$\overline{f} = [f_1,....,f_n]^T$, $g_0$ and $g_L$ denote the linear or nonlinear functions.

As a first step in the numerical solution with MOL, the spatial derivatives are replaced with their algebraic approximations, which results in a set of ordinary

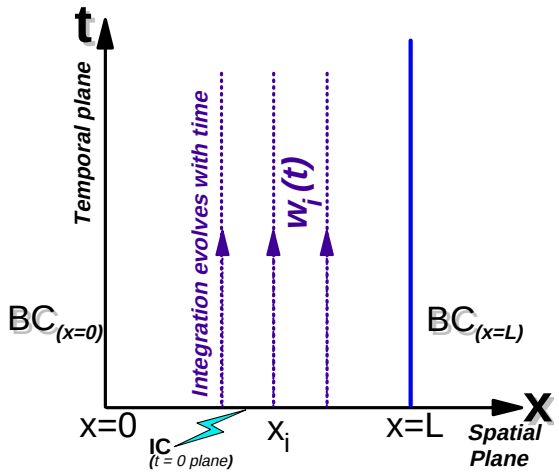


Figure 4.1: The Numerical Method of Lines (NUMOL)

differential equations (ODEs) or differential-algebraic equations (DAEs). The PDEs may reduce to DAEs if the derivatives with respect to $t$ are zero. A typical set of explicit ODEs is shown below:

$$\overline{w}_t = \overline{h}(\overline{w}, t) \qquad\qquad t > 0 \tag{4.5}$$

where the $\overline{h}(\overline{w}, t)$ are the derivative vectors of the resulting set of ODEs. The above set of ODEs are only subject to the initial condition vector:

$$\overline{w}(\overline{x}, 0) = \overline{w}_0(\overline{x}) \tag{4.6}$$

The second part of MOL implementation is the time integration of the resulting set of ODEs (initial-value problem). The boundary value, independent variable $\overline{x}$ is defined between the boundaries on a spatial grid. The ODEs (approximating the PDEs) are defined at each point in the spatial grid. The second stage of the MOL method is then implemented and the ODEs are integrated simultaneously along the spatial grid, "numerical method of lines", Figure 4.1.

The two step approach of MOL provides flexibility in order to handle different classes of PDEs: elliptic, parabolic, hyperbolic, or a combination, linear and nonlinear, in one or multi-dimensional coordinate system.

The efficiency of the MOL is a function of the spatial discretization and use of quality DAE or ODE solvers. Variety of methods (finite elements and finite difference) are available for spatial discretization, some are briefly described and the implementation of finite difference discretization based on Taylor series expansion is discussed in this chapter. The time integration, selection of appropriate algorithm, time steps, order of the method which directly effect the accuracy and the stability issues that determine the attainability of a solution are discussed and the automatic implementation in the solvers are illustrated.

## 4.3 Spatial approximation

The approximation of the spatial derivatives is the first step in implementation of the MOL method for solution of the PDEs. This can be carried out using several methods; splines, finite element methods, weighted residuals and polynomial approximations. The accuracy of the MOL solution is highly dependent on the accuracy of the spatial approximations [33]. The implementation of the algorithm should also be reasonably flexible to allow straight forward modifications to accommodate various orders and attributes of the spatial derivative terms in the PDEs.

The accuracy of each approximation method is based on the order and degree of the algorithm and the number of terms used to approximate a given spatial derivative. The flexibility requirement can be easily geared into the algorithm of the method by envisioning possible creative manners that the code might be used in the future.

### 4.3.1 Use of splines for spatial discretization

Splines can be used as a form of functional approximation method to approximate the spatial derivatives. Use of splines to establish functional approximation to the

spatial terms offers several advantages; a) splines allow nonuniform grid approximation in $x$, b) use of spline of degree $n$ assures continuity to the $n-1$ order derivative terms (based on selection of the spline coefficients), c) splines are well established functional approximations, therefore library subroutines are readily available to compute the spline coefficients. A cubic spline is considered below to illustrate the application to the spatial (one-dimensional) PDE derivatives:

$$w(x,t) \approx w(x_i,t) + a_1(t)(x-x_i) + a_2(t)(x-x_i)^2 + a_3(t)(x-x_i)^3 \tag{4.7}$$

where $a_1, a_2$ and $a_3$ are the cubic spline coefficients and $w(x_i,t)$ is the dependent variable at grid point $x = x_i$. The approximations to the spatial partial derivatives for the first and second-order derivatives can be expressed as:

$$\frac{\partial w(x,t)}{\partial x} \approx a_1(t) + 2a_2(t)(x-x_i) + 3a_3(t)(x-x_i)^2 \tag{4.8}$$

$$\frac{\partial^2 w(x,t)}{\partial x^2} \approx 2a_2(t) + 6a_3(t)(x-x_i) \tag{4.9}$$

The goal in use of a cubic spline is to obtain a smooth first derivative term, and a continuous second derivative term within and at the boundaries. The spline coefficients above can be determined easily from the $w(x,t)$ values at some time $t$. The $w(x,t)$ values are obtained from MOL solutions and are also used for calculation of spatial derivatives which, are used for the next step of MOL application.

Fortran and C++ codes for determination of spline coefficients are available in IMSL or math libraries or Numerical Recipes [1].

### 4.3.2 Use of weighted residuals for spatial discretization

The weighted residuals method is a procedural approach that approximates the exact solution by a set of $N$ basis functions and progresses by minimizing the residuals resulting from this approximation. The $N$ basis functions $\varphi_i(x)$ are selected such that the approximation (trial solution) is obtained [34]:

$$\widehat{w}(x,t) = \sum_{i=1}^{N} c_i(t)\,\varphi_i(x) \tag{4.10}$$

The expression of the approximation in terms of two functions dependent on time $c_i(t)$, and space $\varphi_i(x)$ is preferred separately since it eases certain mathematical manipulations, but at the same time is not the only possibility. The functions are selected priori and should constitute a complete set in a given space $\mathbf{S}$, allowing any non-zero function to be expanded in terms of the basis functions $\varphi_i(x)$. The time and spatial derivatives of the PDEs can be easily obtained using the separated form of the trial solution. The approximations to the time and second-order spatial partial derivatives can be obtained as in the case of discretization with splines:

$$\widehat{w}_t(x,t) = \sum_{i=1}^{N} c_i'(t)\,\varphi_i(x) \tag{4.11}$$

$$\widehat{w}_{xx}(x,t) = \sum_{i=1}^{N} c_i(t)\,\varphi_i''(x) \tag{4.12}$$

The equations above can be put together in demonstration of the application of the method to the one-dimensional parabolic problem (Fourier's second law):

$$\frac{\partial w}{\partial t} = D\frac{\partial^2 w}{\partial x^2} \tag{4.13}$$

with typical initial and boundary conditions:

$$w(x_0,t) = 0 \tag{4.14}$$

$$\frac{\partial w(x_L,t)}{\partial t} = 0 \tag{4.15}$$

$$w(x,0) = 1 \tag{4.16}$$

Using expressions obtained in equations (4.11) and (4.12) for time and second-order spatial derivatives in the Fourier's second law (equation 4.13):

$$\sum_{i=1}^{N} c_i'(t)\,\varphi_i(x) \approx D\sum_{i=1}^{N} c_i(t)\,\varphi_i''(x) \tag{4.17}$$

The approximate relationship in equation (4.17) can be expressed in terms of the residual $R(x,t)$.

$$\sum_{i=1}^{N} c_i'(t)\,\varphi_i(x) - D\sum_{i=1}^{N} c_i(t)\,\varphi_i''(x) = R(x,t) \tag{4.18}$$

The ideal case for the approximation is reached when the residual is zero for all values of $x$ and $t$. The method of weighted residuals forces the $R(x,t)$ to zero to achieve minimization in an integral form making it orthogonal to the weighting function $\omega(x)$:

$$\int_{x_0}^{x_L} \omega(x) R(x,t)\, dx = 0 \tag{4.19}$$

Multiplying the equation (4.18) with a basis function $\varphi_j(x)$, and integrating between the boundaries $(x_0, x_L)$, is the basics of the Galerkin method (making the residual orthogonal to the basis functions). The selection of the basis functions are necessary to evaluate the integral. In general the basis functions are chosen to satisfy the accompanying boundary conditions for convenience (in this case sine and cosine functions satisfy the typical boundary conditions). There after the system is reduced analytically to a set of ODEs and the coefficients, $c_i(t)$, are determined at this point and a solution is obtained. Yet, the described approach to this residual method requires the analytical derivation and integration of components which might indicate some difficulties. Often a semi-analytical solution is preferred, in which the integrals are evaluated numerically, where the weighting function, $w(x,t)$, can be selected as a delta function, resulting in a collocation form $(w_i(x,t) = \delta(x - x_i))$ of residual method, or as the basis functions and result in the Galerkin's method. As indicated earlier, selection of basis function to satisfy the boundary conditions were preferred. Another possibility would be the use of weighting function that has local support (non-zero only over a small interval of $x$). This choice is the basis of the finite elements method.

### 4.3.3 Use of finite elements for spatial discretization

The development of the series solution in terms of sine and cosine basis functions was briefly described in the previous section. The use of a basis function with local support, being non-zero in a given interval $(\Delta x)$ of $x$, is the fundamental of the finite element method. Various forms of elements (splines, polynomials etc.) are available for discretization of different PDEs. A linear finite element is illustrated here (Figure

2a). The $\phi_i(x)$ is centered at $x = x_i$ and has two linear segments between $x_i - \Delta x$ and $x_i + \Delta x$, with $\phi_i(x_i) = 1$, and $\phi_i(x_i - \Delta x) = \phi_i(x_i + \Delta x) = 0$.

The differentiation and integration of such a linear element in the weighted residual method is relatively easy, and the differentiation of the linear finite element illustrated in figure 2b, $d\phi_i(x)/dx$, is piecewise constant.

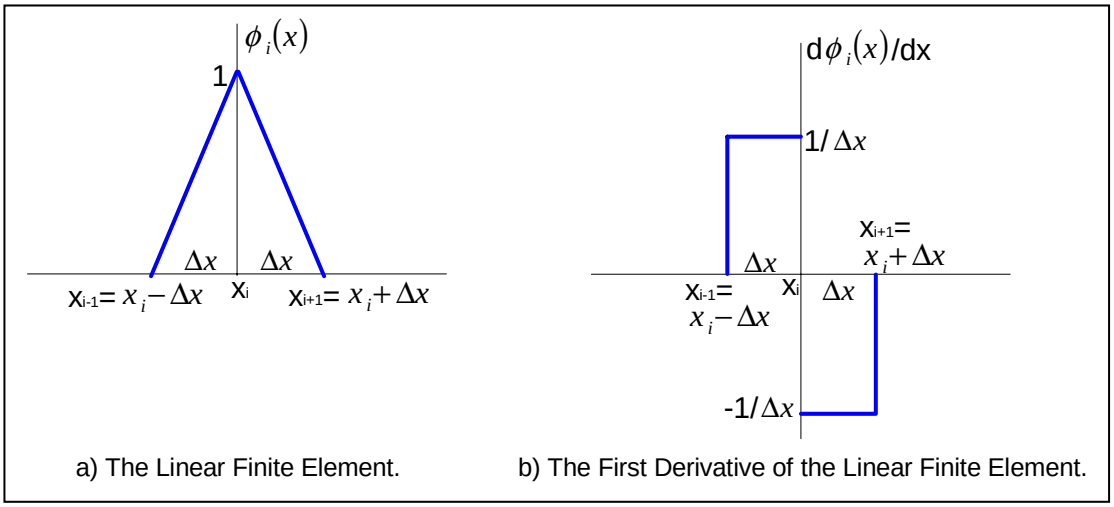


Figure 4.2: The Linear Finite Element Representation.

The basis function in figure 2a is then substituted into the assumed basic series solution, equation (4.10), and from there to generate the terms of PDEs representing the physical system in question. The expression for the residual term $R(x,t)$, is then obtained and the weighted residual method is implemented to obtain the representative ODE form of the equations.

The determination of new integrals is required each time for a new PDE, which can be solved by numerical quadrature. This can be time consuming, especially for cases with complicated basis functions.

### 4.3.4 Use of polynomials for spatial discretization

Typical polynomial expansion and use of Taylor series to obtain the relevant **finite difference** expressions for spatial approximations to convert the system PDEs to the desired ODEs is illustrated in this segment. The widely used polynomial approximations of various orders for the first and second order derivatives, for one or more dimensional expressions are given below [33].

The dependent variable $w(x)$, with respect to the spatial independent variable $x$, discussed earlier is used here (as a function of space alone) to demonstrate the typical polynomial expression and spatial approximation applied to the PDE terms.

$$w(x) = a_0 + a_1(x - x_i) + a_2(x - x_i)^2 + a_3(x - x_i)^3 + ..... \tag{4.20}$$

where $x_i$ is a value of $x$ to be specified and $a_0$, $a_1$, $a_2$, $a_3$, .... are constants to be determined using the Taylor series expansion of $w(x)$ at $x = x_i$. The first constant $a_0$, can be determined by setting $x = x_i$, $a_0 = w(x_i)$. Differentiating equation (4.20) with respect to $x$,

$$dw(x)/dx = a_1 + 2a_2(x - x_i) + 3a_3(x - x_i)^2 + ..... \tag{4.21}$$

and setting $x = x_i$, $a_1 = dw(x_i)/dx$ is obtained. Consecutive differentiations with respect to $x$ at $x = x_i$ gives; $a_2 = (1/2!)\, d^2w(x_i)/dx^2$, $a_3 = (1/3!)\, d^3w(x_i)/dx^3$, ... with a general expression for $i = n^{th}$ term:

$$a_n = (1/n!)\, d^n w(x_i)/dx^n \tag{4.22}$$

**Formulas for first derivatives**

**Second-order approximation** The use of Taylor series is demonstrated with an expression approximating the first derivative $(dw(x_i)/dx)$ of $w(x_i)$[33], which is obtained in terms of values $w(x_{i+1})$, $w(x_i)$ and $w(x_{i-1})$:

$$\begin{aligned} w(x_{i+1}) &= w(x_i) + (dw(x_i)/dx)(x_{i+1} - x_i) \\ &\quad + (1/2!)\left(d^2w(x_i)/dx^2\right)(x_{i+1} - x_i)^2 \end{aligned}$$

$$
\begin{aligned}
& + (1/3!)\left(d^3 w(x_i)/dx^3\right)(x_{i+1} - x_i)^3 + ... \\
= \; & w(x_i) + (dw(x_i)/dx)(\Delta x) \\
& + (1/2!)\left(d^2 w(x_i)/dx^2\right)(\Delta x)^2 \\
& + (1/3!)\left(d^3 w(x_i)/dx^3\right)(\Delta x)^3 + ... \qquad (4.23)
\end{aligned}
$$

$$
\begin{aligned}
w(x_{i-1}) = \; & w(x_i) + (dw(x_i)/dx)(-\Delta x) \\
& + (1/2!)\left(d^2 w(x_i)/dx^2\right)(-\Delta x)^2 \\
& + (1/3!)\left(d^3 w(x_i)/dx^3\right)(-\Delta x)^3 + ... \qquad (4.24)
\end{aligned}
$$

where $\Delta x = (x_{i+1} - x_i)$ and $-\Delta x = (x_{i-1} - x_i)$. The first derivative term is obtained by subtracting equation (4.24) from (4.23)

$$w(x_{i+1}) - w(x_{i-1}) = (2\Delta x)\, dw(x_i)/dx + (2/3!)\left(d^3 w(x_i)/dx^3\right)(-\Delta x)^3 + ...$$

or

$$dw(x_i)/dx = \frac{w(x_{i+1}) - w(x_{i-1})}{2\Delta x} + O(\Delta x)^2 \qquad (4.25)$$

The equation (4.25) is the second order central difference expression for first derivative evaluated at $x_i$ which can be applied to $w(x_i)$ for $i = 2, 3, ..., N-1$ terms on the spatial grid. The boundary terms at $i = 1$ and $N$ need the terms before $i = 0$ and $i = N + 1$ to evaluate the first derivative with respect to $x$.

**Handling boundary conditions** Boundary conditions for finite difference formulation can be dealt with in various ways. The analytical methods for approximating boundary conditions of Dirichlet type ($w(x,t)$ specified) are easily incorporated into the discretization formula. The Neumann ($dw(x,t)/dx$ specified) or combined (Dirichlet and Neumann) type of boundary conditions can also be handled by using the method of fictitious boundaries, which is the introduction of fictitious grid points outside the spatial domain of interest. However, these are mostly problem-specific, which require the mathematical formulation of boundary conditions for every new PDE problem. The problem-specific nature of the analytical approaches above makes it difficult to have a general purpose algorithm capable of handling

any type of boundary condition. Furthermore the method should be robust and straightforward and flexible with minimum amount of effort to allow handling of various PDE problems.

The desired robustness and order of accuracy are achieved by eliminating the fictitious point approach and instead formulating the boundary conditions using biased discretization formulas near the boundaries. This approach expresses the $dw(x_1)/dx$ in terms of $w(x_1)$, $w(x_2)$ and $w(x_3)$, and $dw(x_N)/dx$ in terms of $w(x_{N-2})$, $w(x_{N-1})$ and $w(x_N)$ for a second-order approximation described here. The first derivative term at $x_1$, is obtained by using the Taylor series for $w(x_2)$ and $w(x_3)$:

$$\begin{aligned} w(x_2) &= w(x_1) + (dw(x_1)/dx)(\Delta x) \\ &\quad + (1/2!)\left(d^2w(x_1)/dx^2\right)(\Delta x)^2 \\ &\quad + (1/3!)\left(d^3w(x_1)/dx^3\right)(\Delta x)^3 + ... \end{aligned} \tag{4.26}$$

$$\begin{aligned} w(x_3) &= w(x_1) + (dw(x_1)/dx)(2\Delta x) \\ &\quad + (1/2!)\left(d^2w(x_1)/dx^2\right)(2\Delta x)^2 \\ &\quad + (1/3!)\left(d^3w(x_1)/dx^3\right)(2\Delta x)^3 + ... \end{aligned} \tag{4.27}$$

The maximum accuracy for the first derivative term is obtained by dropping out as many of the higher-order terms as possible. Multiplying equation (4.26) by 4, and subtracting equation (4.27), the second derivative terms are dropped:

$$\begin{aligned} 4w(x_2) - 3w(x_1) - w(x_3) &= (2\Delta x)(dw(x_1)/dx) \\ &\quad - (4/3!)\left(d^3w(x_1)/dx^3\right)(\Delta x)^3 + ... \end{aligned}$$

or

$$dw(x_1)/dx = \frac{-3w(x_1) + 4w(x_2) - w(x_3)}{2\Delta x} + O\left(\Delta x^2\right) \tag{4.28}$$

Similarly, the Taylor series written for $w(x_{N-1})$ and $w(x_{N-2})$ are used to obtain the second-order derivative term, $dw(x_N)/dx$:

$$dw(x_N)/dx = \frac{3w(x_N) - 4w(x_{N-1}) + w(x_{N-2})}{2\Delta x} + O\left(\Delta x^2\right) \tag{4.29}$$

The equations (4.28), (4.25) and (4.29) represent the second-order expressions for the first derivative. The first derivative expression at the boundaries and interior points can be further generalized and expressed in terms of a differential matrix which consists of the weighting coefficients obtained in the above equations[33]:

$$d\overline{w}/dx = [1/(2\Delta x)] \begin{bmatrix} -3 & 4 & -1 \\ -1 & 0 & 1 \\ 1 & -4 & 3 \end{bmatrix} \overline{w} + O\left(\Delta x^2\right) \tag{4.30}$$

The above representation is sufficiently general to be coded in a general purpose subroutine (DSS002). The coefficient matrix has the following properties [33]: 1) the coefficients in a row sum to zero, which is a required in order for the matrix to differentiate a constant to zero, 2) the matrix is antisymmetric, with respect to a line drawn through center which connects members with same magnitude, but opposite signs, which occurs only for the odd-order derivatives, 3) the multiplier $(\frac{1}{2})$ includes the grid spacing, $\Delta x$, in the denominator.

Another typical problem that might occur based on the model assumptions, is the inconsistency in the initial and boundary conditions. This type of problem occurs when there is no smooth transition from one state to the other, meaning that the initial conditions do not satisfy the boundary conditions state for the problem at $t = 0$, for $x_i$ where $i = 1$ and/or $N$. The discontinuity caused is numerically damped out in the parabolic PDEs, but are propagated further in hyperbolic PDEs. Problematic PDEs should be reformulated to assure consistency in these conditions.

**Accuracy of the approximation** The equation (4.30) is implemented in subroutine DSS002 [33]. It can be shown that (4.30) is accurate for differentiating a constant and a first-order polynomial. Furthermore, the accuracy for a second degree polynomial:

$$w(x) = a_0 + a_1 x + a_2 x^2 \tag{4.31}$$

can be shown by substituting into equation (4.25) and illustrate that the expression is accurate for zero-, first-, and second-order polynomials:

$$dw(x_i)/dx = \frac{a_0 + a_1(x_i + \Delta x) + a_2(x_i + \Delta x)^2}{2\Delta x}$$

$$
\begin{aligned}
& -\frac{\left(a_0 + a_1\left(x_i - \Delta x\right) + a_2\left(x_i - \Delta x\right)^2\right)}{2\Delta x} + O\left(\Delta x^2\right) \\
= \; & a_1 + 2a_2 x
\end{aligned} \tag{4.32}
$$

Similar check is performed for a third degree polynomial of the form:

$$w\left(x\right) = a_0 + a_1 x + a_2 x^2 + a_3 x^3 \tag{4.33}$$

by inserting equation (4.33) in (4.25) and repeating a similar calculation performed in equation (4.32). The result obtained from differentiating equation (4.33) with a second-order polynomial is:

$$dw\left(x_i\right)/dx = a_1 + 2a_2 x + 3a_3 x^2 + a_3 \Delta x^2 \tag{4.34}$$

It is clear that the expression is not exact for third and higher order polynomials [33]. The error term involved in equation (4.34) decreases with $\Delta x$. Furthermore, substitution of the third degree polynomial equation (4.33) into first-derivative expressions at the boundaries, equations (4.28) and (4.29), indicates that the error in these equations is larger than the expression for the interior grid points, equation (4.25). The magnitude of the obtained error at the boundaries, $-2a_3\Delta x^2$, is twice of the interior error term, yet it is second-order correct.

The use of polynomials is limited for discretization since spatial variation of PDEs can hardly be duplicated by polynomials. Yet the solution will improve with the decreasing value of $\Delta x$ (use of more grid points). Another approach to improve the accuracy of the application is to use a higher-order differentiation formula [33].

**Fourth-order approximation** The second-order derivation for approximating the first derivative uses three points for differentiation. Approximation of the derivative at point $x_i$, using five grid points $(x_{i-2}, x_{i-1}, x_i, x_{i+1}, x_{i+2})$ in terms of Taylor series will result in a fourth-order approximation. The generic derivation of the required coefficients and the conditions to be satisfied are listed below [33]. The Taylor series at these points:

$$
\begin{aligned}
w\left(x_{i-2}\right) \; = \; & w\left(x_i\right) + \left(dw\left(x_i\right)/dx\right)\left(-2\Delta x\right) \\
& + \left(1/2!\right)\left(d^2 w\left(x_i\right)/dx^2\right)\left(-2\Delta x\right)^2 + ...
\end{aligned} \tag{4.35}
$$

$$\begin{aligned} w(x_{i-1}) &= w(x_i) + (dw(x_i)/dx)(-\Delta x) \\ &\quad + (1/2!)\left(d^2w(x_i)/dx^2\right)(-\Delta x)^2 + ... \end{aligned} \tag{4.36}$$

$$\begin{aligned} w(x_{i+1}) &= w(x_i) + (dw(x_i)/dx)(\Delta x) \\ &\quad + (1/2!)\left(d^2w(x_i)/dx^2\right)(\Delta x)^2 + ... \end{aligned} \tag{4.37}$$

$$\begin{aligned} w(x_{i-2}) &= w(x_i) + (dw(x_i)/dx)(2\Delta x) \\ &\quad + (1/2!)\left(d^2w(x_i)/dx^2\right)(2\Delta x)^2 + ... \end{aligned} \tag{4.38}$$

The derivation of $dw(x_i)/dx$ requires that we take a linear combination of equations (4.35) to (4.38) and drop most of the higher derivative terms. A systematic approach would be multiplying each equation by coefficients $a$, $b$, $c$, and $d$ respectively (from 4.35 to 4.38) and summing the resulting equations. The first derivative term $dw(x_i)/dx$ is to be retained resulting in the following relationship:

$$-2a - b + c + 2d = 1 \tag{4.39}$$

The requirement to eliminate the second derivative terms, $d^2w(x_i)/dx^2$ , the third and the fourth terms results in conditions stated as:

$$4a + b + c + 4d = 0 \tag{4.40}$$

$$-8a - b + c + 8d = 0 \tag{4.41}$$

$$16a + b + c + 16d = 0 \tag{4.42}$$

Solving linear equations (4.39) to (4.42) for the four coefficients gives: $a = 2/4!$, $b = -16/4!$, $c = 16/4!$, $d = -2/4!$, which placed as multipliers of equations (4.35) to (4.38) and summed will result in the expression for the first derivative:

$$\begin{aligned} dw(x_i)/dx &= (1/(4!\Delta x))(2w(x_{i-2}) - 16w(x_{i-1}) + 0w(x_i) \\ &\quad + 16w(x_{i+1}) - 2w(x_{i+2})) + O\left(\Delta x^4\right) \end{aligned} \tag{4.43}$$

The obtained central difference approximation equation is fourth-order correct and sum of its coefficients is zero, indicating that it will differentiate a constant to

zero. However, the central difference equation (4.43) can not be used for grid points $i = 1, 2, N-1, N$. This equation requires information on two grid point values before and after the central grid point. Therefore the Taylor series expansions at the interior points should be used in derivation of the first derivatives for these points. The equation for $dw(x_1)/dx$ requires the Taylor series for $w(x_2)$, $w(x_3)$, $w(x_4)$, and $w(x_5)$ similar to equations (4.35) to (4.38). It then requires to be multiplied by coefficients and to satisfy conditions similar to those stated in equations (4.39) to (4.42) which will result in the values of the coefficients $(a, b, c, d)$ and thereby the expression for $dw(x_1)/dx$. The first derivatives for the two points at each boundary of the grid can be determined in this manner:

$$\begin{aligned} dw(x_1)/dx &= (1/(4!\Delta x))(-50w(x_1) + 96w(x_2) - 72w(x_3) \\ &\quad +32w(x_4) - 64w(x_5)) + O\left(\Delta x^4\right) \end{aligned} \tag{4.44}$$

$$\begin{aligned} dw(x_2)/dx &= (1/(4!\Delta x))(-6w(x_1) - 20w(x_2) + 36w(x_3) \\ &\quad -12w(x_4) + 2w(x_5)) + O\left(\Delta x^4\right) \end{aligned} \tag{4.45}$$

$$\begin{aligned} dw(x_{N-1})/dx &= (1/(4!\Delta x))(-2w(x_{N-4}) + 12w(x_{N-3}) - 36w(x_{N-2}) \\ &\quad +20w(x_{N-1}) + 6w(x_N)) + O\left(\Delta x^4\right) \end{aligned} \tag{4.46}$$

$$\begin{aligned} dw(x_N)/dx &= (1/(4!\Delta x))(6w(x_{N-4}) - 32w(x_{N-3}) + 72w(x_{N-2}) \\ &\quad -96w(x_{N-1}) + 50w(x_N)) + O\left(\Delta x^4\right) \end{aligned} \tag{4.47}$$

The resulting expression and the coefficient matrix is obtained:

$$d\overline{w}/dx = [1/(4!\Delta x)] \begin{bmatrix} -50 & 96 & -72 & 32 & -6 \\ -6 & -20 & 36 & -12 & 2 \\ 2 & -16 & 0 & 16 & -2 \\ -2 & 12 & -36 & 20 & 6 \\ 6 & -32 & 72 & -96 & 50 \end{bmatrix} \overline{w} + O\left(\Delta x^4\right) \tag{4.48}$$

The coefficient matrix is antisymmetric and its rows sum to zero each, satisfying the previously stated conditions. This expression is implemented in the Fortran90 subroutine DSS004 [33].

Higher order expressions can be obtained and used in discretizing the spatial derivatives, however these expressions will have derivatives with more roots, which indicates the number of minima and maxima and the degree of oscillation between these points. The increased number of roots causes an unrealistic oscillation in the solution of the PDEs with method of lines. Therefore a fourth-order approximation is good compromise between accuracy and minimization of oscillation.

### Formulas for Second derivatives

**Fourth-order approximation** A PDE model of the physical phenomena investigated here contains a combination of the first and second order spatial derivatives of the independent variables. In general PDEs obtained might include various orders of derivatives with linear and non-linear terms involved, which are all easily handled via this approach. MOL is a flexible method due to the straightforward application to any combination of derivatives with almost no modification to the initial code produced during programming.

MOL will permit step wise differentiation using the first-order derivative computation. Yet, it is desirable to have a direct derivation which will be applicable to all forms of problems. The central difference expression for the interior points is obtained by writing Taylor series for $w(x_i)$ at $x_{i-2}$, $x_{i-1}$, $x_{i+1}$, and $x_{i+2}$, and multiplying with coefficients. The equations are summed and the term $d^2w(x_i)/dx$ is retained and the higher derivatives are eliminated:

$$\begin{aligned} dw^2\left(x_i\right)/dx^2 &= \left(1/\left(4!\Delta x^2\right)\right)\left(-2w\left(x_{i-2}\right)+32w(x_{i-1})-60w\left(x_i\right)\right. \\ &\quad \left.+32w(x_{i+1})-2w(x_{i+2})\right)+O\left(\Delta x^4\right) \end{aligned} \tag{4.49}$$

The fourth-order expressions for the second derivative at the points $i = 1, 2, N-1, N$ are obtained based on [33], such that the first derivation includes the Neumann type and next the Dirichlet type boundary condition effects at $i = 1, N$. The

derivative at $i = 2, N-1$ are obtained taking linear combinations at $i = 1, 3, 4, 5, 6$ for $d^2w(x_2)/dx^2$ and at $i = N-5, N-4, N-3, N-2, N$ for $d^2w(x_{N-1})/dx^2$. The coefficients are summed to retain the second and to drop the first, third, fourth and fifth order derivative terms and achieve the required accuracy. The solution of the simultaneous linear equations for the coefficients is then obtained and used in obtaining the expression for the second derivative terms:

$$\begin{aligned} dw^2\left(x_2\right)/dx^2 &= \left(1/\left(4!\Delta x^2\right)\right)\left(20w\left(x_1\right) - 30w(x_2) - 8w\left(x_3\right)\right. \\ &\quad \left. +28w(x_4) - 12w(x_5) + 2w(x_6)\right) + O\left(\Delta x^4\right) \end{aligned} \tag{4.50}$$

$$\begin{aligned} dw^2\left(x_{N-1}\right)/dx^2 &= \left(1/\left(4!\Delta x^2\right)\right)\left(20w\left(x_N\right) - 30w(x_{N-1}) - 8w\left(x_{N-2}\right)\right. \\ &\quad +28w(x_{N-3}) - 12w(x_{N-4}) \\ &\quad \left. +2w(x_{N-5})\right) + O\left(\Delta x^4\right) \end{aligned} \tag{4.51}$$

The remaining expressions for the second derivative at $i = 1, N$ are obtained in two sets as stated above. The first set incorporates the Neumann $(dw(x)/dx)$ and the second set incorporates the Dirichlet $(w(x))$ type boundary conditions into the expressions for the second derivative at the boundaries. The linear combination of the coefficients and equations are written for $w(x_i)$ at $i = 2, 3, 4, 5$ and for $dw(x_i)/dx$ at $i = 1$. Similar linear combination is applied for the boundary at $N$, at points $i = N-1, N-2, N-3, N-4$ and the first derivative at $i = N$. The simultaneous equations of the coefficients are formed by retaining the second and dropping the first, third, fourth and fifth order derivative terms. The solution of these equations for the coefficients will allow forming the second derivative expressions at the boundaries where the Neumann type conditions are embedded in the formation:

$$\begin{aligned} dw^2\left(x_1\right)/dx^2 &= \left(1/\left(4!\Delta x^2\right)\right)\left(\left(-415/3\right)w\left(x_1\right) + 192w(x_2) - 72w\left(x_3\right)\right. \\ &\quad + \left(64/3\right)w(x_4) - 3w(x_5) - 100(dw(x_1)/dx)\Delta x) \\ &\quad \left. +O\left(\Delta x^4\right)\right) \end{aligned} \tag{4.52}$$

$$\begin{aligned} dw^2\left(x_N\right)/dx^2 &= \left(1/\left(4!\Delta x^2\right)\right)\left(\left(-415/3\right)w\left(x_N\right) + 192w(x_{N-1}) - 72w\left(x_{N-2}\right)\right. \\ &\quad + \left(64/3\right)w(x_{N-3}) - 3w(x_{N-4}) + 100(dw(x_N)/dx)\Delta x) \\ &\quad \left. +O\left(\Delta x^4\right)\right) \end{aligned} \tag{4.53}$$

Another set incorporating the Dirichlet BCs for $i = 1$ and $N$ is obtained from linear combination of the Taylor series for five adjacent points and dropping higher order derivative terms.

$$\begin{aligned} dw^2\left(x_1\right)/dx^2 &= \left(1/\left(4!\Delta x^2\right)\right)\left(90w\left(x_1\right) - 308w(x_2) + 428w\left(x_3\right)\right. \\ &\quad -312w(x_4) + 122w(x_5) - 20w(x_6)) \\ &\quad +O\left(\Delta x^4\right) \end{aligned} \tag{4.54}$$

$$\begin{aligned} dw^2\left(x_N\right)/dx^2 &= \left(1/\left(4!\Delta x^2\right)\right)\left(90w\left(x_N\right) - 308w(x_{N-1}) + 428w\left(x_{N-2}\right)\right. \\ &\quad -312w(x_{N-3}) + 122(x_{N-4}) - 20w(x_{N-5})) \\ &\quad +O\left(\Delta x^4\right) \end{aligned} \tag{4.55}$$

The fourth-order expressions for the central points and at the boundaries including the Neumann and Dirichlet conditions are obtained and implemented in Fortran90 subroutine DSS044. One of the critical arguments of this subroutine is the type of the boundary condition at both ends: being Neumann or Dirichlet such that the correct expressions at these ends would be used and the MOL user would not need to deal with defining fictitious points and coding a new formulation for each different PDE problem.

The advantages of using expressions derived directly for the second derivative terms are: 1) ability to handle more classes of PDEs compared to step wise differentiation, 2) all types of BCs can be included without approximation. The disadvantages to the direct formulation are: 1) the second order derivative terms can not handle the nonlinear term occasionally embedded after the first derivative, 2) the implementations to more than one-dimension becomes cumbersome.

Other types of methods and implementations can also be used to develop generic coding for MOL. Typical examples include the use of Lagrange interpolation polynomials, cubic splines and orthogonal collocation. Problem specific issues, such as the numerical oscillations developed in first-order hyperbolic problems ($w_t = -v.w_x$), due to the advective term are also handled by using upwind approximations of the

spatial derivative term [33]. This type of approximation will spread out the oscillation in the temporal as well as the spatial domain causing the numerical solution to lag behind the exact solution.

This illustrates the importance of the quality of the solution to the understanding the physical and numerical systems and thereby defining the proper representation that allow dependable simulation of the actual process. A similar care should also be taken in handling hyperbolic PDEs with inconsistent initial and boundary conditions as stated earlier.

## 4.4 Time integration

The set of PDEs describing the physical system is converted to an initial value ODE problem at this point by approximating the spatial derivative terms with a finite difference polynomial discretization. The next step is the numerical integration of this initial value ODE problem. A quality integrator offers accuracy and stability in the solution of the ODEs. Both of these integrators have good accuracy and stability within their own type; explicit vs. implicit integrators. The stiffness of the set of ODEs effects the stability of a quality ODE integrators. Two types of integrators: RKF45 and LSODE are considered for this purpose.

The stability conditions (separation in the eigenvalues) and the structure of the coefficient matrix (full, dense, sparse or banded) determines the type of integrator to be used. In general a stiff problem originates from the difference in the order of magnitude in the eigenvalues obtained for the characteristic equation generated from taking the determinant of a coefficient matrix (the Jacobian matrix in the case of a nonlinear problem) and setting it to zero. Rate of stiffness, is often used as a measure which, is the ratio of the largest to the smallest real part of the eigenvalues. Typically stiff problems are characterized by a stiffness ratio larger than 1000 (difference of 3 in order of magnitude). The stiff equations in general are generated while modeling physical phenomena occurring on several different time scales. This is specially evident while dealing with two coupled phenomena such as

temperature and pressure which are on different time scales.

### 4.4.1 Stability issues

The stability of the solution can be expressed in two groups; one being the *stability of the ODE problem* and the other the *stability of the numerical method*. The stability of a set of linear-constant coefficient ODEs are briefly discussed here and the nonlinear ODE stability is based on similar thought pattern [33].

#### Stability of the ODE problem

**Stability of linear first-order ODEs with constant coefficients** A typical problem statement for $w(t)$ is:

$$d\overline{w}/dt = \overline{A}\overline{w} \tag{4.56}$$

assuming that they represent a $2X2$ system:

$$d\overline{w}/dt = \begin{bmatrix} dw_1/dt \\ dw_2/dt \end{bmatrix} \quad \overline{w} = \begin{bmatrix} w_1 \\ w_2 \end{bmatrix} \quad \overline{A} = \begin{bmatrix} a_{11} & a_{12} \\ a_{21} & a_{22} \end{bmatrix}$$

The assumed exponential solution vector for the system above is stated in equation (4.57) which is then substituted into the ODE expression in equation (4.56). After eliminating the exponential terms, a set of expressions is obtained for the coefficients, $\overline{C}_{2X2}$, which can be written in the form of equation (4.58), and its determinant set to zero to have a nontrivial solution, (equation 4.59):

$$\overline{w}(t) = \overline{C}e^{\lambda t} \tag{4.57}$$

$$\left(\overline{A} - \lambda\overline{I}\right)\overline{C} = \overline{0} \tag{4.58}$$

$$\det\left(\overline{A} - \lambda\overline{I}\right) = \overline{0} \tag{4.59}$$

Equation (4.59) is the characteristic equation, which is an $n$-th order polynomial defining $n$ eigenvalues, $\lambda_1$, $\lambda_2$, ..., $\lambda_n$. For the $n$ linear first-order DEs to be stable (for the solution 4.57 not to grow exponentially), all the eigenvalues must have negative real parts.

The selection of the ODE method depends on the properties of coefficient matrix $\overline{A}$. The separation of its eigenvalues determines the stiffness of the problem requiring use of a stiff integrator. The structure of $\overline{A}$ matrix, being sparse, full, or banded also effects the implementation of the integrator.

**Stability of nonlinear ODEs** A typical nonlinear set of ODEs and the initial conditions:

$$d\overline{w}/dt = \overline{f}\,(\overline{w}, t) \tag{4.60}$$

$$\overline{w}(t_0) = \overline{w}_0 \tag{4.61}$$

Expanding the RHS of equation (4.60) in Taylor series about point $(\overline{w}_s, t_s)$and ignoring after the linear term:

$$d\overline{w}/dt = \overline{f}\,(\overline{w}_s, t_s) + \overline{J}(\overline{w}_s, t_s)\,(\overline{w} - \overline{w}_s) \tag{4.62}$$

$$\overline{J} = \begin{bmatrix} f'_{11} & f'_{12} & . & f'_{1n} \\ f'_{21} & f'_{22} & . & . \\ . & . & . & . \\ f'_{n1} & . & . & f'_{nn} \end{bmatrix} \tag{4.63}$$

The $nXn$ Jacobi matrix on the RHS, represents the first derivatives of $\overline{f}$ with respect to members of $\overline{w}$ which is constant for a linear set of ODE. $J$ becomes a function of $\overline{w}$ for nonlinear ODEs and is evaluated at $(\overline{w}_s, t_s)$ which is a constant at each time (requiring evaluation as solution evolves in $t$ for each new value of $w$). Therefore the Jacobi matrix may act similar to the coefficient matrix in the linear form and can play a similar role in defining the stability and type of integrator needed.

**Stability of the numerical method**

The stability of numerical process can be expressed based on the type of the integrator: explicit vs. implicit. The explicit methods determine the solution at a given time based on the known information at the previous time step. The implicit integration approach however requires the values at the unknown times which then have to be solved simultaneously. The stability of each method is briefly discussed and

the use of two industry standard integrators: RKF45 and LSODE, their structure and application for the solution of the ODEs generated in this case are presented.

**Stability of explicit method** The simplest explicit integration is by Euler method. This method uses the solution at time $n$, which is known as $\overline{w}_n$, to obtain the solution at the next time step. It is first order and computes the next solution point by the projection from $t_n$ to $t_n + \Delta t$ along a tangent to the solution at $t_n$:

$$\overline{w}_{n+1} = \overline{w}_n + (d\overline{w}_n/dt)\Delta t = \overline{w}_n + \overline{f}(\overline{w}_n, t_n)\Delta t \tag{4.64}$$

A solution for a $2X2$ linear system with constant coefficients is given by [33], in terms of $\beta_1$ and $\beta_2$. Satisfying the unboundedness condition, the stability conditions for eigenvalues $\lambda_1$ and $\lambda_2$ results in:

$$|\beta_1| = |1 + \lambda_1 \Delta t| \leq 1 \tag{4.65}$$

$$|\lambda_i \Delta t| \leq 2 \tag{4.66}$$

This indicates that the explicit Euler integration is stable for a system of $N$ first-order, linear, constant-coefficient ODEs if $\lambda_i \Delta t$, $i = 1, 2, ..., N$ fall within a unit circle centered at the point $(-1, 0j)$ $\left(j = \sqrt{-1}\right)$ in the complex plane, for all $i$ [33]. It is clear that to satisfy the stability condition, specially with ODEs having separated eigenvalues, it requires to have very small time steps, resulting in large number of integrations. The largest eigenvalue defines the maximum step size which is the main limitation of the Euler's method when the problem is sufficiently stiff.

**Stability of implicit method** Similarly the implicit Euler method where the derivative term is evaluated at point $n + 1$:

$$\overline{w}_{n+1} = \overline{w}_n + (d\overline{w}_n/dt)\Delta t = \overline{w}_n + \overline{f}(\overline{\overline{w}}_{n+1}, t_{n+1})\Delta t \tag{4.67}$$

and the solution in terms of $\beta_1$ and $\beta_2$ is [33]:

$$\beta_1 = \tfrac{1}{1-\lambda_1 \Delta t} \quad \beta_2 = \tfrac{1}{1-\lambda_2 \Delta t} \tag{4.68}$$

indicating that the solution remains stable for all values of $\Delta t$, and implicit Euler method is unconditionally stable. For nonlinear problems root-finding methods like Newton's method are applied to determine the required solution.

### 4.4.2 Accuracy issues

The Euler's methods described above are relatively inaccurate (only first-order), yet sufficiently applicable to illustrate the problems involved in stability during integration. The accuracy of the solution can be improved either by decreasing the time interval $\Delta t$, or increasing the order of the method used. The current 32 or 64 bit computational capability allows limited decrease in time interval $\Delta t$, to achieve the required accuracy. Therefore higher order terms are required to achieve the desired accuracy in solution without creating numerical instability in the solution, especially in the case of explicit integration methods. The higher order methods will allow taking larger time steps without compromising the accuracy of the solution.

### 4.4.3 RKF45

The name of the numerical integration algorithm RKF45 [15], designates the Runge-Kutta-Fehlberg (RKF) with a fourth-order method that is embedded in a fifth-order method. The solution is calculated with the fourth-order RK algorithm, and also with fifth-order RK algorithm. The two solutions are compared to estimate the error in the numerical solution. If the error term exceeds the user defined tolerance, the solution is repeated with a smaller step in time to improve the accuracy of the integration in $t$. RKF45 is primarily designed to solve non-stiff and mildly stiff differential equations when derivative evaluations are inexpensive. Use of fourth- and fifth-order methods in RKF45 improves the accuracy of the solution without the need of smaller time steps. However the stability criterion for the fourth-order Runge-Kutta method is:

$$|\lambda \Delta t| < 2.875 \tag{4.69}$$

indicating that the stability interval is only increased slightly in the price of calculation of four derivative evaluations per step. The eigenvalue $\lambda$ can be complex, on both real and imaginary axes. Unlike the explicit Euler method where the stability region was a unit circle centered at $(-1, 0j)$, the region for fourth-order method is slightly larger and irregular [33].

RKF45 is suitable for problems where the accuracy of the solution is not very critical [15]. The tolerance level set by the user might not be achieved in some cases and the method will fail. The applications of this method is illustrated in the case of simulation of pressure propagation in porous media where the physical problem did not have stiff characteristics. However the coupled problems involve various physical phenomena in different time scales resulting in separated eigenvalues and naturally stiff problems. The solution of the stiff problems require a stiff integrator based on the implicit method. Integrators based on the backward differentiation formula (BDF) use the implicit derivative term in evaluation of the solution at the next step thereby providing the necessary accuracy and stability as in the case of LSODE.

### 4.4.4 LSODE

The implicit Euler formula, equation (4.67), is obtained from the generalized form where; $q = 1$ (order of the method), and $\alpha_0 = \beta_0 = 1$ (constants for particular order):

$$\overline{w}_{n+1} = \sum_{l=0}^{q-1} \alpha_l \overline{w}_{n-l} + \Delta t \beta_0 (d\overline{w}_{n+1}/dt) \tag{4.70}$$

The BDF method in equation (4.70) is explicit due to the use of only past values $\overline{w}_{n-1}$ and is implicit in one of the derivatives $d\overline{w}_{n+1}/dt$. The BDF is a multistep method using more than one past value in solution where as RK used only the current for the solution at the next step. The coefficients $\alpha_0$ and $\beta_0$ depend on the order of the method ($q$) [18]. BDF starts as a first-order method initially at $t_0$, since $w_0$ is the only available set of known values, and as additional points are calculated it develops to a higher-order method. This indicates that the step size and the order of the method are both handled making BDF a variable-step, variable-order implicit method suitable for solution of the stiff problems.

The use of past values for the current solution requires these values to be stored. The variation of the time step size for accuracy of the integration also requires these previous values to be available at the current integration time step, which results in

the requirement for interpolation of the previous values at the current time step size. The higher-order methods ($q > 2$) are not absolutely stable, but the coefficients are selected as such to achieve a compromise between accuracy and stability. In general physical problems (ODEs) have real eigenvalues where the method is stable.

As a result of BDF, a set of linear algebraic equations are obtained where a form of root finding is required for solution at the unknown time steps. Newton's method is used to iterate and converge starting from a solution and using conventional linear algebra methods such as Gauss row reduction. The main computational effort using BDF is due to the necessity for an updated Jacobian matrix at each iteration. However it is also noted that using a Jacobian matrix that is not current does not introduce any additional error in numerical solution as long as the Newton iteration converges [33]. Therefore the BDF integrators are designed such that the Jacobian gets updated only when it is required for convergence. The BDF algorithm can also take advantage of the structure of the Jacobian matrix during numerical manipulation. Substantial saving in computational time is possible when the matrix is not full or is banded with a bandwidth $M$. The ratio of the number of operations for an $NXN$ Jacobian matrix at full case to a banded case using a typical gauss row reduction is expressed as: $N^3/N^2M$. This reduces the operations by 1000 times for a Jacobi of size $N = 1000$ with a bandwidth of $M = 30$ [33]. Since the analytical computation of the partial derivative terms are often complicated, BDF methods incorporate a numerical Jacobian by finite differences for large ODE problems.

The Livermore Solver for Ordinary Differential Equations, "LSODE" was developed for integrating system of ODEs with full or banded Jacobian matrix [21].

LSODE is capable of solving problems designated as non-stiff (by Adams formula) or stiff (by BDF method). The integrator states the last order of the method used (achieved) and the number of function ($dw/dt$) and Jacobian evaluations. The Jacobian evaluations can be either provided in a separate subroutine or a dummy subroutine given and the matrix evaluated numerically.

Other applications include the solvers for the problems with; sparse Jacobian matrix, more than one time derivative appearing in an ODE, and BDF implementations where the storage of the matrices is not required.

## 4.5 Simulation environment

A simulation environment is constructed by assembling a set of various components coded for the solution of a PDE system. The various components for the input-output, definition of initial conditions, the derivative equations, spatial discretization and time integration methods are prepared for modular coding. The modular software algorithm is assembled in a fashion to permit ease of update, interchange and modify any particular component. The modules are self-contained routines where various segments of NUMOL are implemented and linked with the rest. This approach allows interchangeability of the components. For instance, discretization routines can be easily upgraded or different ones linked to permit solution of a different set of PDEs. The integration routines are also similarly interchangeable once the required subroutine call is placed within the program flow. The modular assembly and algorithm also permits the integration of the standard commercial quality components whenever applicable.

### 4.5.1 PDE system simulator

The components/subroutines of the simulator for the numerical solution of the ODEs, PDEs are programmed in FORTRAN90 code. Initially numerical experimentation and solutions were developed using spatial discretization routines coded in low order finite difference approximations. Subsequent to this verification, the solutions are all developed with the use of higher-order spatial discretization of the DSS routines.

In general a typical simulator/solver consists of several independent components:

- MAIN PROGRAM, is the unit that initially inputs the required data from the files, communicates with various components, and coordinates multiple activities and the output requirements.

- INITAL, defines the initial conditions ($\overline{w}(\overline{x}, 0) = \overline{w}_0(\overline{x})$), equation (4.4), for the ODE problem, as well as the problem constants to be set once for the entire integration period.

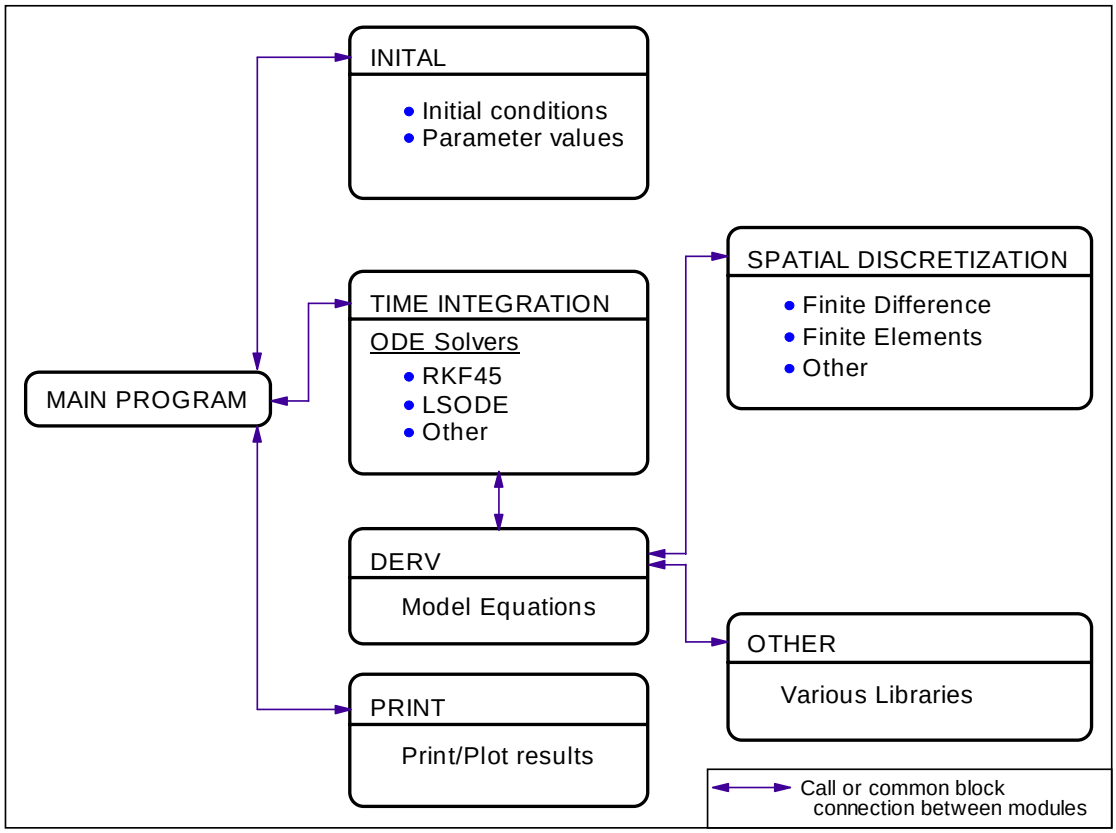


Figure 4.3: Modular component assembly diagram of the simulation environment

- TIME INTEGRATION, is a set of routines that carry out the integration of the ODEs using the previously described explicit or implicit methods (RKF45, LSODE, etc.). It also generates the required form of ODEs by accessing problem definition and discretization components for the PDE system.

- DERV, defines the derivative equations, ($\overline{w}_t = d\overline{w}/dt$), equation (4.1), to be integrated in time (model equations). This routine might access other generic components for discretization of the spatial derivatives in equation (4.1).

- SPATIAL DISCRETIZATION, are various routines that permit finite difference discretization of the spatial derivatives forming the RHS of the original PDE system, equation (4.1).

- PRINT, is where the various output schemes for plotting or multiple I/O purposes are combined.

The operations are controlled by a main program which reads the data file that defines the parameters specific to the problem (initial, final, print interval values of time, error tolerance, etc.), calls the INITAL to define the initial conditions. The repeated calls to ODE solver are made to step through and obtain the solution at $t = 0, t_1, t_2$. An error check (flag) is made at each time step $t_i$. The PRINT subroutine is called to print the solution at that time step for a successful integration, otherwise an error message is generated providing the status of the error. Program structure is illustrated in Figure 4.3.

The general purpose discretization (DSS/2) and integration routines allow relatively easy approximation to the solution of wide variety of one-, two- and three-dimensional, adaptive grid problems. New algorithms and libraries can easily be added and linked due to modularity of the software.

### 4.5.2 Other MOL applications

Computational packages using MOL have been developed using similar modular components. Some examples include DSS/2 [34] consisting of various discretization and integration routines , SPRINT [3] modular open-ended software tool for one-dimensional PDEs with discretization methods of finite differences and elements, polynomials and adaptive meshing with integrators for stiff systems. Other sources include mathematical libraries for numerical methods; NAG (Numerical Algorithms Group), and IMSL (International Mathematics and Statistics Libraries) [1] which contain PDE software with various MOL routines.

## 4.6 Typical applications

Typical applications of MOL to various segments of problem are illustrated in this segment. Various set of boundary and initial conditions for the selected set of cases and assumptions similar to those listed earlier in Chapter 3 are shown. Chapter 5 discusses use of simulation environment in conjunction with the parameter identification routine in bringing numerical simulation and experimental responses together to obtain the desired diffusivity coefficients.

### 4.6.1 Simulation under hydraulic gradient application

The pressure distribution for a typical sample is simulated under hydraulic gradient at loading stage (Figure 4.4). The simulation is performed for a saturated sample with a zero initial pressure distribution under closed material boundary conditions. The diffusivity for this simulation is $0.753\,\mathrm{cm}^2\,/\,\mathrm{sec}$. The initial and boundary conditions for the system can be listed as:

| **Gradient Type** | **Boundary** | **Initial Conditions** | **Boundary Conditions** |
|---|---|---|---|
| Hydraulic | Closed | $p\,(x,0) = 0psi$ | $p\,(0,t) = 5psi$<br>$\frac{\partial p}{\partial t}\vert_{x=L} = 0$ |

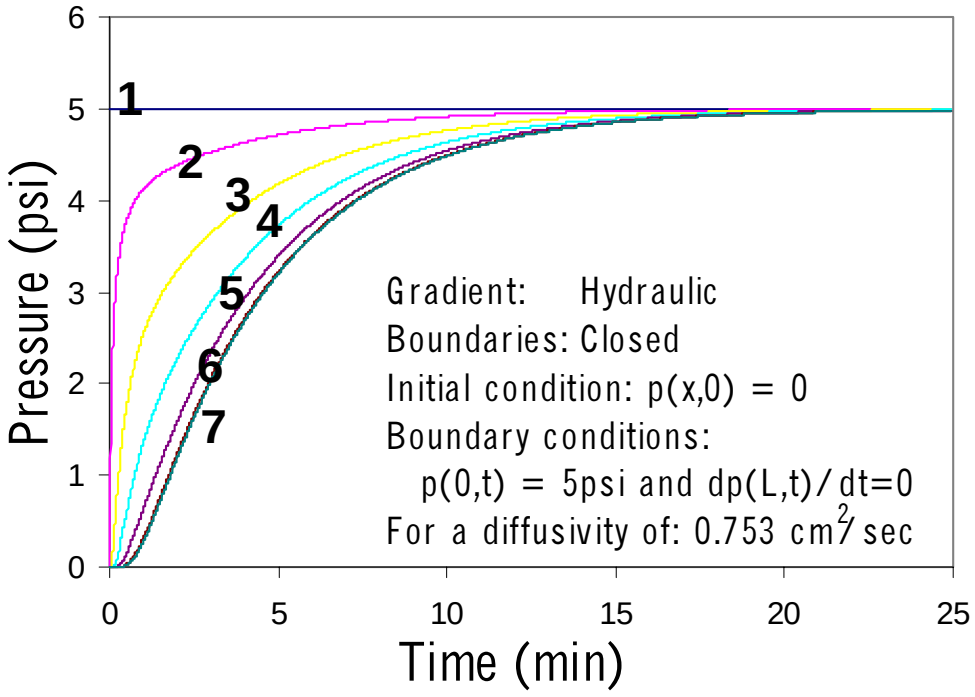


Figure 4.4: Simulated pressure distribution under hydraulic gradient

### 4.6.2 Simulation under thermal gradient application

Similar simulations are performed for a one-dimensional system under applied thermal gradients. A system with an internal heat source located at the left of the specimen (station no.2) is simulated, which is initially at room temperature, $T(x,0) = 20\,^{\circ}\mathrm{C}$. The temperature distribution at 9 stations along the first half of the uninsulated specimen is plotted for comparison with experimental results. The simulation is performed for a specimen with a thermal diffusivity of $0.5678\,\mathrm{cm}^2\,/\,\mathrm{min}$ (Figure 4.5).

| Gradient Type | Boundary | Initial Conditions | Boundary Conditions |
|---|---|---|---|
| Thermal | Un-insulated | $T(x,0) = 20\,^{\circ}\mathrm{C}$ | $\frac{\partial T}{\partial t}\|_{x=0} = 0$ <br> $\frac{\partial T}{\partial t}\|_{x=L} = 0$ |

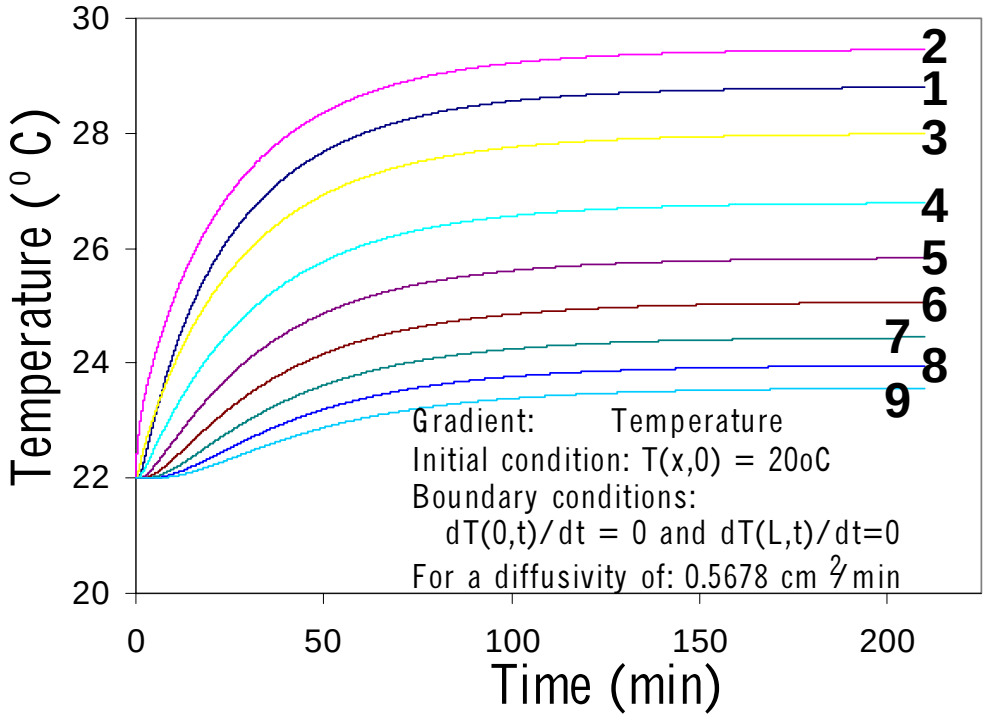


Figure 4.5: Simulated temperature distribution for half of sample with heater at the left end of sample

### 4.6.3 Simulation for multi-dimensional response

The simulation environment and various components are designed to be flexible in handling different boundary conditions and spatial derivatives in one or more

dimensions. Two simulations for temperature distribution in the specimen elevated temperature values at the left end and the quarter of the specimen are shown. Figure 4.6 is plotted for a only a quarter of the cylindrical sample taking advantage of the symmetry. Temperature profiles at 5 time segments are shown caused by the applied temperature raise at the left boundary of the specimen. The initial and boundary conditions used in simulation of the profiles shown in Figure 4.6 are:

| **Gradient Type** | **Boundary** | **Initial Conditions** | **Boundary Conditions** |
|---|---|---|---|
| Thermal | $T(x, R, t) = 22\,^{\circ}\mathrm{C}$ | $T(x, r, 0) = 22\,^{\circ}\mathrm{C}$ | $T(0, r, 0) = 30\,^{\circ}\mathrm{C}$<br>$T(L, r, 0) = 22\,^{\circ}\mathrm{C}$<br>$T(x, R, 0) = 22\,^{\circ}\mathrm{C}$<br>$\frac{\partial T}{\partial r}\|_{r=0} = 0$ |

Similarly, a specimen with initially raised temperature value at the left quarter is shown in Figure 4.7. The heat dissipation along the specimen at 3 time segments in terms of two-dimensional temperature profile is shown. The initial and boundary conditions are defined as:

| **Gradient Type** | **Boundary** | **Initial Conditions** | **Boundary Conditions** |
|---|---|---|---|
| Thermal | $T(x, R, t) = 22\,^{\circ}\mathrm{C}$ | $T(x, r, 0) = 22\,^{\circ}\mathrm{C}$<br>$T(L/4, r, 0) = 30\,^{\circ}\mathrm{C}$ | $T(0, r, 0) = 22\,^{\circ}\mathrm{C}$<br>$T(L, r, 0) = 22\,^{\circ}\mathrm{C}$<br>$T(x, R, 0) = 22\,^{\circ}\mathrm{C}$<br>$\frac{\partial T}{\partial r}\|_{r=0} = 0$ |

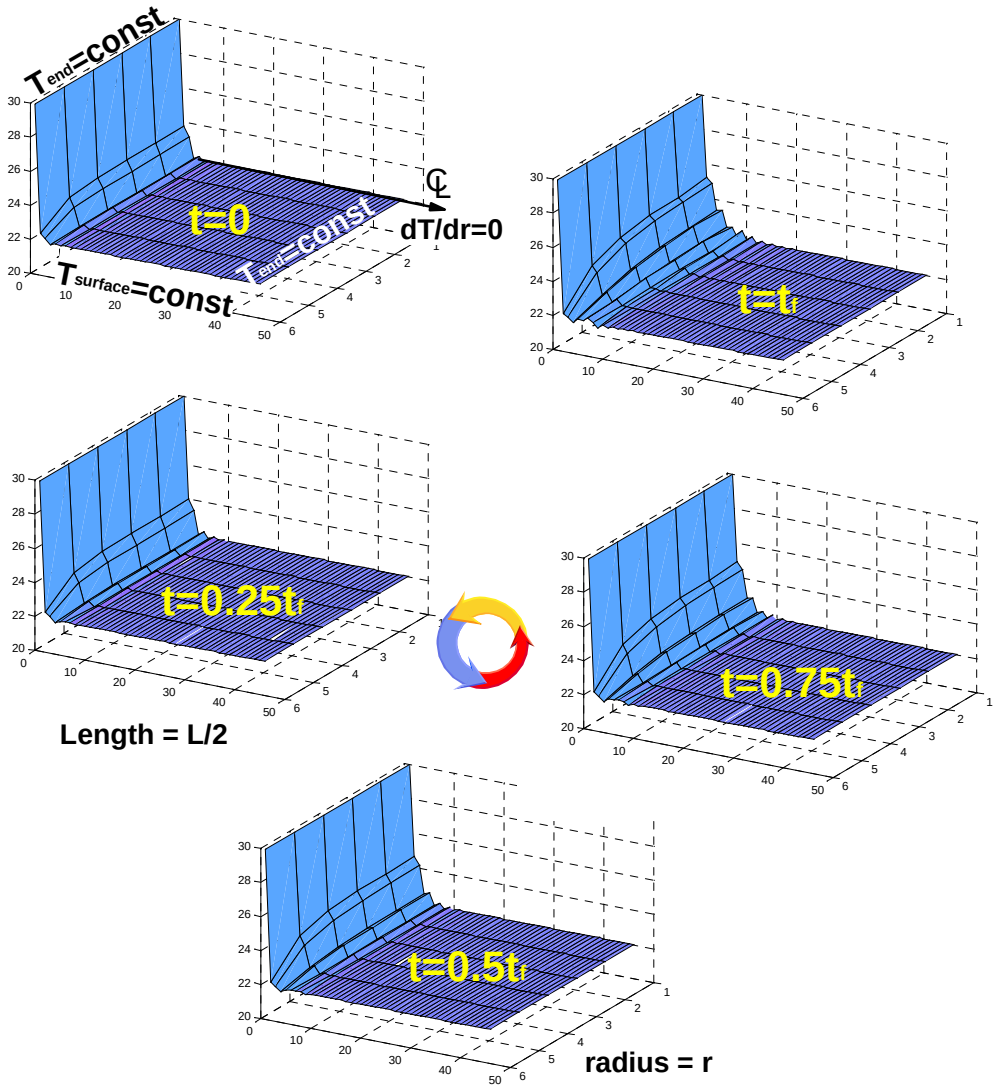


Figure 4.6: Simulated two-dimensional temperature distribution for first quarter of the specimen

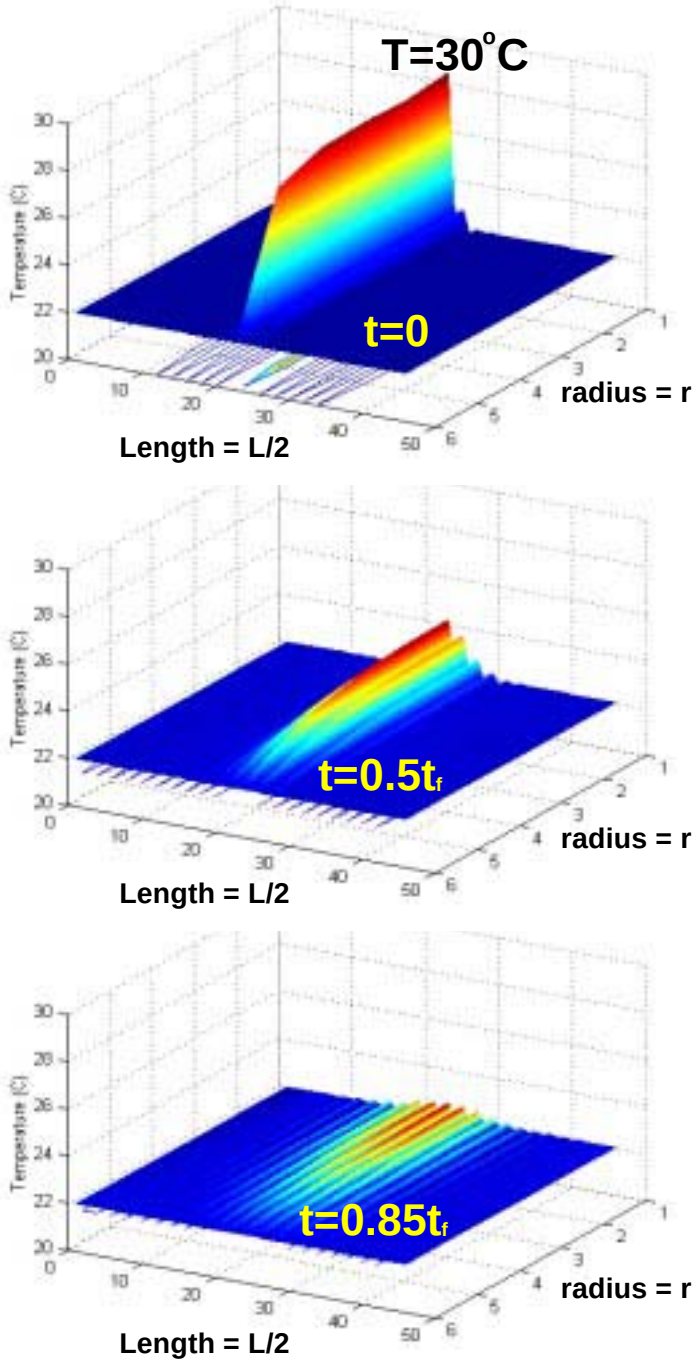


Figure 4.7: Simulated two-dimensional temperature distribution for first quarter of the specimen

# Chapter 5

# Parameter Identification

The derivation of a distributed parameter model is based on development of a structural model and the parameter identification. The structural model is the backbone of the entire system representing the process and the interrelationships. The required relationships in this case, were introduced in Chapter 3. The model for the transient coupled flow process in porous media subject to thermal and hydraulic gradients was derived from physical laws and the governing partial differential equations (PDEs) were obtained. The derived governing equations have unknown parameters that might be constants or variables of time, space or the state. Often some parameters used in a simplified models might lose their physical significance as they may be combined in a manner that represent several physical processes at once. This results in two types of parameters in the model, one being the physical parameters known from the analysis of the system and the other the parameters that have no direct physical interpretation and yet have to be identified.

The parameter identification is used to determine the unknown parameters such that the output from the numerical simulations performed on the model would match the experimentally obtained data under similar boundary and initial conditions as close as possible [38]. The application of the parameter identification requires the definition of an error criterion as an objective function representing the distance between the model output and the experimental data. Another issue is the selection of a numerical algorithm to minimize the objective function.

The essence of the parameter estimation process is the simulation program developed in Chapter 4, which allows discretization of the equations in a suitable form for numerical integration, solution and optimization. The selection of the error criterion, and the optimization algorithm for parameter identification are described in this chapter. The coupled flow parameters are estimated by making use of a Quasi-Newton method with finite difference gradient of the objective function implemented in the mathematical IMSL Fortran subroutines library [1].

## 5.1 Optima problem

The definition of the problem and obtaining the optimal solution by satisfying the minimization condition defined by a function $f(x)$, is addressed here. Short discussions on single variable and multiple variable optimization methods are presented. The direct search and gradient based methods are summarized and the Newton's, modified Newton's and Quasi-Newton's methods are described in detail as part of the quadratic gradient method. The algorithm used in Quasi-Newton Method (QNM) [14] is also briefly discussed. Parameter identification is performed by using the optimization approach integrated with the simulated and the experimental responses of the system, described in the previous chapters.

The problem of optimization of a given objective function $f(x)$, is often the problem of finding the value of $x = x^*$ that minimizes the value of the function $f(x^*)$. A unimodal function is monotonic on either side of the single optimal point $x^*$. The statement for the monotonic function can be shown as:

$$\text{for } x_1 \leq x_2, \qquad \underbrace{f(x_1) \leq f(x_2),}_{\text{monotonically increasing}} \qquad \text{or} \qquad \underbrace{f(x_1) \geq f(x_2),}_{\text{monotonically decreasing}} \tag{5.1}$$

Similarly a definition of a unimodal function for a minimum at $x^*$ can be stated as:

$$\begin{aligned} \text{for} \quad & x^* \leq x_1 \leq x_2, \quad f(x^*) \leq f(x_1) \leq f(x_2) \\ & x^* \geq x_1 \geq x_2, \quad f(x^*) \leq f(x_1) \leq f(x_2) \end{aligned} \tag{5.2}$$

which indicates that the point is either a local or a global minimum.

The definitions for identification of the stationary points, the regions, and the estimation for local and global optimum points using different methods are described in the subsequent segments.

### 5.1.1 Single variable optima

The Taylor series expansion of a single variable function $f(x)$, over the interval $x \in (a, b)$, in which it is differentiable to the $n^{th}$ order, is:

$$f(x^* + \varepsilon) - f(x^*) = \varepsilon \frac{df}{dx}|_{x=x^*} + .... + \frac{\varepsilon^n}{n!} \frac{d^n f}{dx^n}|_{x=x^*} + O_{n+1}(\varepsilon) \tag{5.3}$$

At an assumed local minima ($x^*$), there exists a neighborhood ($x = x^* + \varepsilon$), such that $f(x) \geq f(x^*)$:

$$\varepsilon \frac{df}{dx}|_{x=x^*} + .... + \frac{\varepsilon^n}{n!} \frac{d^n f}{dx^n}|_{x=x^*} + O_{n+1}(\varepsilon) \geq 0 \tag{5.4}$$

where $\varepsilon \frac{df}{dx}|_{x=x^*}$ is a good approximation for small values of $\varepsilon$.

It follows that for the function $f(x)$ to be a local minima (an optima) at $x^*$ on an open interval $(a, b)$, the stationary point $\frac{df}{dx}|_{x=x^*} = 0$ is a necessary condition with $\frac{d^2 f}{dx^2}|_{x=x^*} \geq 0$. In general with the stationary point condition satisfied, the first non-zero higher-order derivative of order $n$ determines whether it is an inflection point ($n =$ odd) or a local optima ($n =$ even) [30]. One method of determining the global optimum for an $f(x)$ bounded in an interval $[a, b]$ (in this case of minima), is to calculate the function values for local optima points as well as at the boundaries.

There are many rudimentary methods that require the function to be only unimodal within the interval of interest. In fact methods like region elimination don't even require the function to be differentiable and work by eliminating the subintervals. Region halving and golden section search are among this group. However, polynomial approximation (point-estimation) methods take advantage of the magnitude of the difference between the consecutive function values, which require the function to be sufficiently smooth. Quadratic estimation, successive quadratic estimation are within this group, requiring the function to be unimodal and continuous. Another group makes use of the derivatives of the function which requires continuity

and differentiability. Typical derivative methods are: Newton-Raphson, bisection, secant, and cubic search methods. Improper selection of the initial search point can cause the solution to diverge with Newton-like methods.

### 5.1.2 Multi-variable optima

The problem statement requiring the optimization of functions of several variables is:

$$\begin{array}{rl} \text{Minimize} & f(x), \quad \text{where } x \in R^N \\ f: & \text{scalar objective function} \\ x: & \text{vector of design variables} \end{array} \tag{5.5}$$

It is assumed that the first derivative vector, $\nabla f = \left[\frac{\partial f}{\partial x_1}, \frac{\partial f}{\partial x_2}, ...., \frac{\partial f}{\partial x_N}\right]^T$, exists and is continuous everywhere. Next, the optimality criteria is developed starting from Taylor expansion:

$$f(x) = f(\overline{x}) + \nabla f(\overline{x})^T \Delta x + \frac{1}{2}\Delta x^T \nabla^2 f(\overline{x}) \Delta x + O_3(\Delta x) \tag{5.6}$$

where $\Delta f(x) = f(x) - f(\overline{x}) = \nabla f(\overline{x})^T \Delta x + \frac{1}{2}\Delta x^T \nabla^2 f(\overline{x}) \Delta x$ and for point $\overline{x}$ to be a minimum (local or global):

$$\begin{array}{lll} \overline{x} \text{ is global minimum} & \Delta f(x) = f(x) - f(\overline{x}) \geq 0 & \forall x \in R^N \\ \overline{x} \text{ is local minimum} & \Delta f(x) = f(x) - f(\overline{x}) \geq 0 & ||x - \overline{x}|| \preceq \delta,\ \delta > 0 \end{array} \tag{5.7}$$

where sign of $\Delta f(x)$ determines if its a maxima, minima or a saddle point and with the stationary point ($\nabla f(\overline{x}) = 0$) requirement, a quadratic form is obtained for $\Delta f(x)$:

$$\Delta f(x) = \frac{1}{2}\Delta x^T \nabla^2 f(\overline{x}) \Delta x \tag{5.8}$$

The definition for determination of minima, maxima or saddle point is illustrated in a diagram in Figure 5.1, starting from the stationary point at $\overline{x}$ and the quadratic expression in equation (5.8). The search direction vector $S(\overline{x})$ and the step size $\alpha$, used in determination of the next approximation towards the minima are also shown. The necessary conditions for the existence of a minima are: existence of a

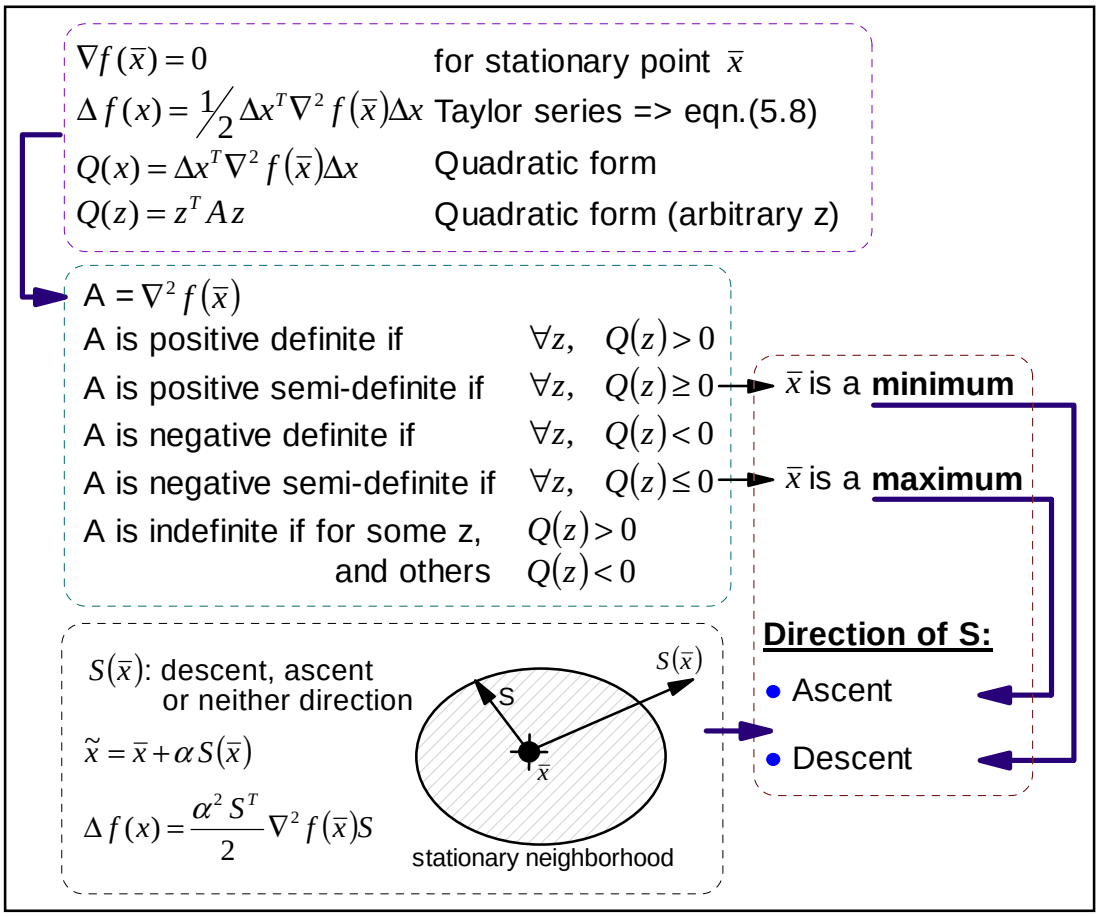


Figure 5.1: Diagram for minimum, maximum and direction vector.

stationary point and a positive semi-definite Hessian matrix, $\nabla^2 f(\overline{x})$. But having a positive definite Hessian is a sufficient condition for an isolated local minima of the function to exist. A local minima is a global one if $\Delta x^T \nabla^2 f(\overline{x}) \Delta x \geq 0$ is satisfied for all $x$ [14], [20]. This is identical to saying that the function is convex. First, the Hessian matrix is constructed. Then different $z = \Delta x$ vectors are tried, which ultimately result in the global minima vector.

### 5.1.3 Direct search methods

Direct search methods are iterative ways of producing the minima vector using the function values alone. These are grouped in the heuristic and theoretically based techniques. Some of the heuristics methods known are simplex search ($S^2$ method) and Hooke-Jeeves pattern search methods [14]. Powell's conjugate direction method is a good example of the direct search method that are based on theory. This method includes history of iterations and combines moves in one variable at a time with acceleration moves. These methods are suitable when only a set of function values are available and the search is to be performed within those and no further information on the form of the function itself is available or used in the search.

### 5.1.4 Gradient based methods

Gradient based methods require the function $f(x)$, the first derivatives $\nabla f(\overline{x})$ and the Hessian Matrix $\nabla^2 f(\overline{x})$, to exist and be continuous [14]. The method works by identifying the steepest descent direction and stepping in the descent direction at each iteration. Cauchy method uses the most local descent ($-\nabla f(\overline{x})$) for the direction vector and adjusts the scale ($\alpha$) at each step. Newton's method uses a Taylor's expansion including a quadratic term for approximating the function for the $k^{th}$ iteration point. The method uses step size of $\Delta x = -\nabla^2 f\left(x^{(k)}\right)^{-1} \nabla f\left(x^{(k)}\right)$, which is obtained by setting the gradient of the approximation to the function at the $k^{th}$ step to zero. Newton's method converges with a quadratic rate however ascent or descent is a function of the sign of the Hessian matrix with convergence depending on the starting point. If the starting point is far from the optima the step size might

become large causing the procedure to diverge. Modified Newton's method includes the scaling factor ($\alpha$) to adjust for the step at each iteration. The Marquardt's method combines the Cauchy and the Newton's methods and requires $2^{nd}$ order information. A coefficient ($\lambda$) is used in this method to control both direction and length of step. The initial value for this constant starts from a very large number indicating a Cauchy like approach and as $\lambda$ decreases it works as Newton's method. The value of the method is in; Cauchy's method being effective when away from the minima and Newton's method is when closer to minima which is put to use in application of the conjugate methods where the change in gradient of the function from one iteration to the next is used in updating the search direction.

**Quasi-Newton methods** The disadvantage of Newton-like methods is the need to supply derivative formulas so that the second order derivative matrix can be calculated from it. Finite difference representations of the first derivatives can be supplied so that the Hessian matrix can be obtained using the differences in the gradient vectors. The Quasi-Newton method approximates the inverse of the Hessian matrix with a symmetric definite one (metric, $A_{(N\times N)}$) that is corrected and updated at each iteration [16], [14]. The typical line search process is performed for a new value at $(k+1)^{th}$ step, $\left(x^{(k+1)} = x^{(k)} + \alpha^{(k)} S\left(x^{(k)}\right)\right)$, where $S\left(x^{(k)}\right)$ is the search direction and can be expressed in terms of the metric which will eventually approach the inverse of the Hessian matrix, $A = G^{-1} = \nabla^2 f\left(\overline{x}\right)^{-1}$. The method uses the current metric at step $k$ to obtain a correction $\left(A_c^{(k)}\right)$ for it and updates the metric with the summation of the current and the correction, which is then used to obtain the direction of the descent to be used for step $k+1$.

a) set $S\left(x^{(k)}\right) = -A^{(k)} \nabla f\left(\overline{x}^{(k)}\right)$
b) line search along $S\left(x^{(k)}\right)$ gives $x^{(k+1)} = x^{(k)} + \alpha^{(k)} S^{(k)}$
c) update $A^{(k)}$ to $A^{(k+1)}$ by $A^{(k+1)} = A^{(k)} + A_c^{(k)}$

The initial matrix $A^{(1)}$ can be any positive definite matrix, even the identity matrix is usable for this purpose. The difficulty of this method is calculating $A^{(k)}$ and in updating the $A^{(k+1)}$ term, the aim being to push the initial estimate matrix towards

the inverse of the Hessian. One way is to use the difference in the values of the optima and gradients:

$$\delta^{(k)} = x^{(k+1)} - x^{(k)}$$
$$\gamma^{(k)} = \nabla f\left(\overline{x}^{(k+1)}\right) - \nabla f\left(\overline{x}^{(k)}\right)$$

and to use the Taylor series $\gamma^{(k)} = G^{(k)}\delta^{(k)} + ...$ where the higher terms are zero for a quadratic function. However since $A^{(k)}\gamma^{(k)} \simeq \delta^{(k)}$, where $(A = G^{-1})$, is not accurate, the relationship is usually better represented by:

$$A^{(k+1)}\gamma^{(k)} \simeq \delta^{(k)} \tag{5.9}$$

which is referred to as the quasi-Newton condition. Different methods are used to obtain the correction term $\left(A_c^{(k)}\right)$ to get to $A^{(k+1)}$. Rank one or rank two methods are available depending on the form used for the correction component.

$$\text{Rank one method:} \quad A^{(k+1)} = A^{(k)} + auu^T$$
$$\text{Rank two method:} \quad A^{(k+1)} = A^{(k)} + auu^T + bvv^T$$

where $u = \delta^{(k)} - G^{(k)}\gamma^{(k)}$ and $au^T\gamma^{(k)} = 1$ are to hold for rank one formula. Similar relationships for rank two formulas are available to obtain the components necessary for evaluation of the correction factor. DFP method by Fletcher and Powell [14], is a typical example for rank two formula which is more efficient than the steepest descent method and also more efficient than the conjugate gradient methods.

The method used in the implementation of the quasi-Newton method for this study is a rank two method given by Broyden [14] and others, referred to as the BFGS formula. It is similar to the DFP formula, but it represents the inverse of the matrix $A^{(k)}$ with another matrix and interchanges $\delta$ and $\gamma$. This type of approach is referred to as dual or complementary and also preserves the quasi-Newton condition in equation (5.9).

The DUMINF IMSL library is used for the problem solution.The FORTRAN90 subroutine DUMINF is a double precision application of the Quasi-Newton method with finite difference estimates of the gradient of the function.

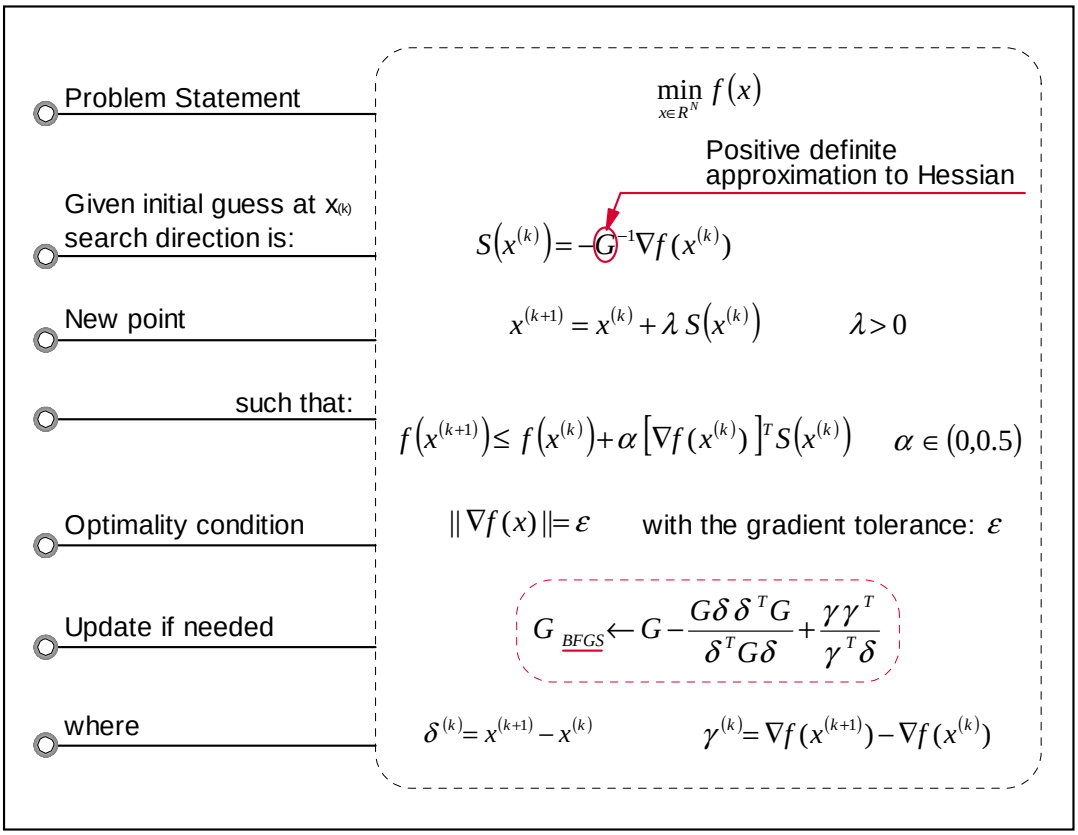


Figure 5.2: Diagram of Quasi-Newton (BFGS) method for optimization.

## 5.2 Parameter identification problem

The governing equations for the coupled flow process in porous media are obtained in terms of PDEs as given in Chapter 3. The unknown parameters appear in the differential equations and boundary conditions. Experimental response is also obtained in terms of measurements at various locations along the cylindrical saturated porous media, collected at different sampling intervals.

The derivation of the coupled flow process described in the previous chapters assumed parameters with constant values, which are independent of time, space and temperature. Naturally, these assumptions are not always valid, and some applications may require parameters expressed either as functions of space (for heterogeneous media) or state variables (to represent non-linearities). This requires discretization of the unknown parameters to express their functional forms.

The parameter identification is performed by collocation of the experimental and numerical results in terms of pressure and temperature response of the system to the applied boundary conditions. The experimental measurements are performed at seven locations along the porous sample as described in Chapter 2. The first and last measurements are performed at the boundaries. Figure 5.3a, illustrates the locations at which experimental measurements of pressure are taken. However, temperature measurements are recorded at smaller intervals.The numerical response simulation of the system (pressure and temperature) to the applied set of boundary conditions are computed at various spacings denoted by $dx$, as shown in Figure 5.3b. The measured values at the experimental measurement stations are then collocated with the numerical results and checked to obtain the best possible match. This process is described first by defining the objective function and then by the search method previously discussed.

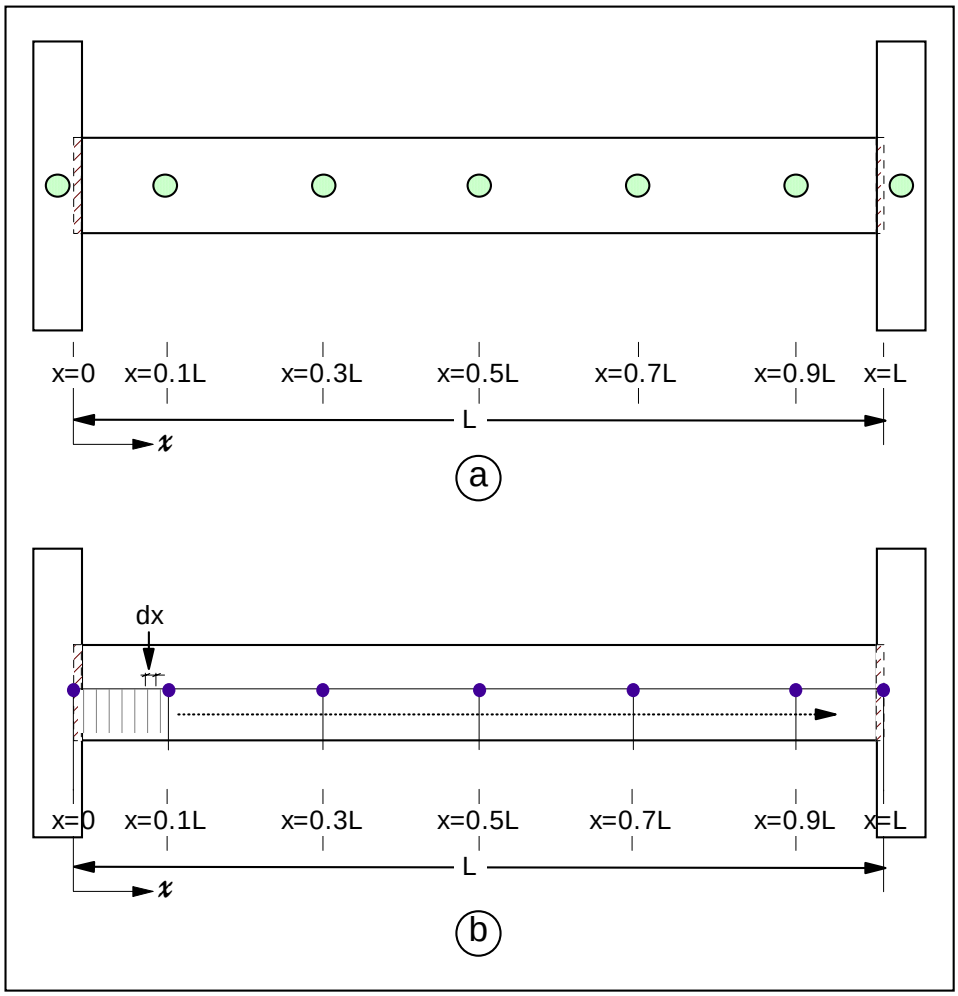


Figure 5.3: a) Experimental measurement points, b) Numerical simulation result output points, collocation.

### 5.2.1 Equation error criterion

The problem of optimization for parameter identification requires the objective function, an expression for error term, to be defined. As shown in figure 5.2, the optimization problem in terms of the required variable $x$ has the form of:

$$\min_{z \epsilon R^N} f(z) \tag{5.10}$$

**Sum of squares expression of error term**

The objective function, or the error expression, to be minimized is expressed in terms of collocation of the numerical results (subscript $n$) with the experimental ones (subscript $e$) at the measurement stations. The response of the system at these five interior points are then combined in terms of the sum of squares to obtain a cumulative error term. The sum of the squares expression between the two sets of data, experimental ($w_{ei}$) and numerical($w_{ni}$), is expressed as:

$$f(z) = \sum_{i=1}^{m} [w_{ei} - w_{ni}]^2 \tag{5.11}$$

The parameter $m$ is the total time steps taken for both the experimental and numerical data.

### 5.2.2 Error minimization

The physical sample can be represented by a discretized model, with various segments that allow modeling heterogeneous media.

**A single parameter model**

However a single parameter model is also capable of representing the sample here, which requires a single form of the parameter representing the entire porous media. This approach is suitable for homogeneous media where variations in the properties with space is insignificant. A single parameter model is shown in Figure 5.b, where equation (5.11) is good representation of the objective function. The single

parameter model can be expressed with a single objective function which combines the sum of squares of the terms at all five interior measurement stations, as given in equation (5.12):

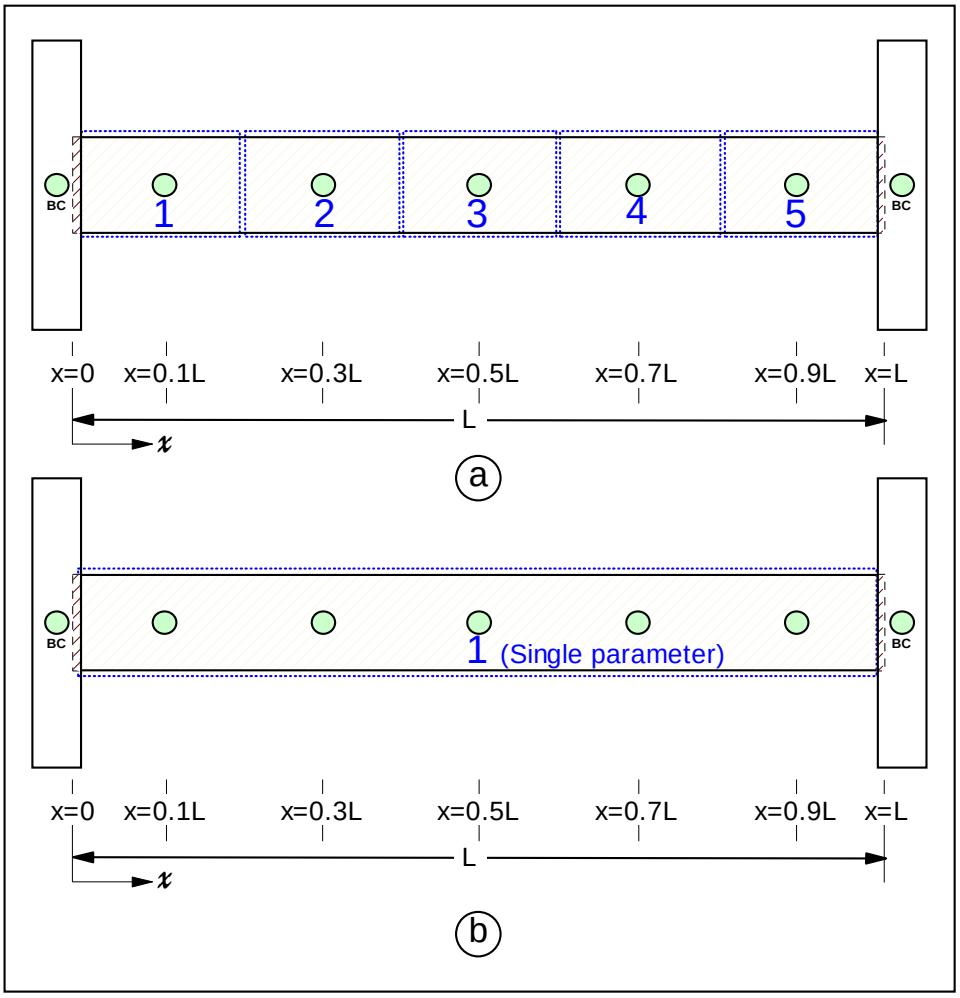


Figure 5.4: a) A discrete (five) parameter model, b) Single parameter model.

$$f(z) = \sum_{j=1}^{5} \sum_{i=1}^{m} [w_{eij} - w_{nij}]^2 \tag{5.12}$$

The single error term here combines all the deviations of the measured quantity (pressure or temperature) at all stations for the required time period of the test data.

This simply collocates the experimental and numerical values in space (five stations) and time (at every measurement-integration step). Equation (5.12) becomes the objective/error function to be minimized. However, to have a uniform measure of error term with respect to various tests and studies, the error term is normalized with the total number of data points involved in the summation ($E(z) = f(z)/(5m)$). The minimization of the single parameter model then is simply in the form of equation (5.13) with a second derivative term less than zero.

$$\frac{dE(z)}{dz} = 0 \tag{5.13}$$

The single parameter model simply represents the entire (homogeneous) soil specimen with a single parameter. Equation (5.13) is a simple case where the unknown parameter is in the form of a constant (single unknown). In the case of a functional form for the required parameter $r$, say in the form of a polynomial $r(x)$, with unknown coefficients $a_0$, $a_1$, and $a_2$ (shown as second order here),

$$r(x) = a_0 + a_1 x + a_2 x^2 \tag{5.14}$$

the error term is minimized in terms of each unknown parameter (coefficient),:

$$\frac{dE}{da_i} = 0 \tag{5.15}$$

which results in three equations for three unknown coefficients in the second order polynomial equation (5.14).

**A distributed parameter system**

However a distributed parameter system, represents a heterogeneous system by allowing various segments to be expressed by different parameters or a form of parameters (Figure 5.4a). A model with constant form of parameter for each five segments will require separate error terms for each segment. This can be approximated by assuming that each station approximates the average response at the mid point of that section, as illustrated in Figure 5.4a. The resulting error term (objective

function) for a constant unknown at each segment will take the form:

$$f(z_j) = \sum_{i=1}^{m} [w_{eij} - w_{nij}]^2 \tag{5.16}$$

$$E_j = f(z_j)/m \tag{5.17}$$

$$\frac{dE_j}{dz_j} = 0 \tag{5.18}$$

where $j = 1, 2, ..., 5$, resulting in five equations, each minimizing the response in one segment for the optimum parameter of the segment. If a form of parameter is applied to each segment, then each segment's error term should be minimized with respect to the unknowns in the corresponding assumed form of the parameter.

The single and discrete parameter forms of optimization with a constant parameter were both carried out for the system at hand in this work. The application of the discrete parameter model permits the check for possible inhomogeneity of the sample.

## 5.3 Optimization environment

The computer implementation of the identification via optimization is shown in Figure 5.5. The process requires three components: 1) a real system generating data from physical set-up, 2) a simulation program computing model outputs based on applied forcing function and current value of parameter $z$, 3) an optimization segment to minimize the objective function and update the parameter $z$.The optimization program should be iterative and be able to call the simulation routine repeatedly in order to calculate updated numerical responses to be used in obtaining the future values of the error components. An interface between the simulation component and the optimization routine is required to manage the information exchange. The coding for the simulation program is also expanded to include the computation of the criterion value using the measured data stored in external files. The estimation of the unknown parameters are carried out by interfacing the simulation program explained in Chapter 4 and the optimization routine of IMSL libraries [1] implementing the quasi-Newton method with numerical derivatives. The libraries are

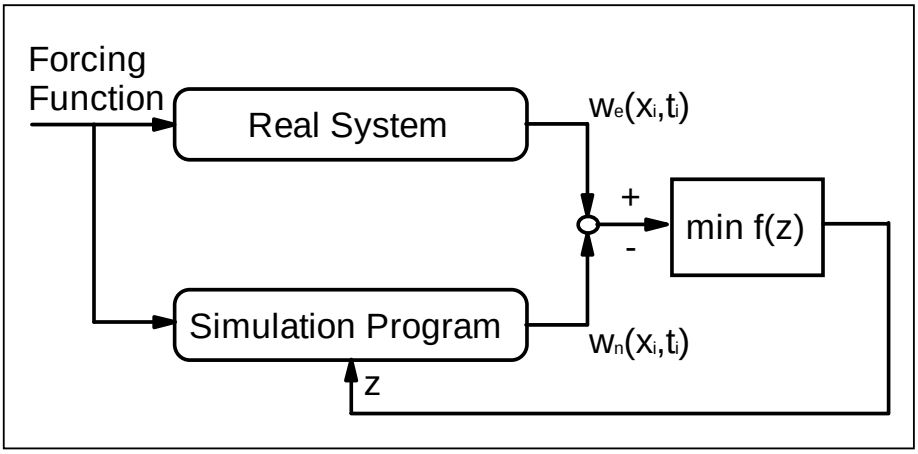


Figure 5.5: Model matching with the real system thru output minimization.

all written in FORTRAN90, and the integration between the components and the external sources is outlined in Figure 5.6. The lower half of the flow chart in Figure 5.6 is the simulation set already discussed in Chapter 4. Some modifications to the individual modules within the simulation segment are made to allow transfer of the optimization parameters. The two files for input and output shown within the simulation components are: 1) the data files that provide the initial, final time and output interval and error tolerances required for solution of ODEs by integration, 2) the numerical output files of pressure or temperature record determined at the experimental measurement locations at the time steps identical to the experimental time steps. The upper half of the flow chart illustrates the additional optimization components. Those components are:

- MAIN PROGRAM, this unit inputs the required data from the files (inrkf and inlsode), defines the size of the problem (dimension of the parameter set), initializes the optimization variables, communicates with various components, and coordinates multiple activities and the output requirements.

- DATAFILEs, inrkf and inlsode provide the initial starting point values for optimization of the parameters.

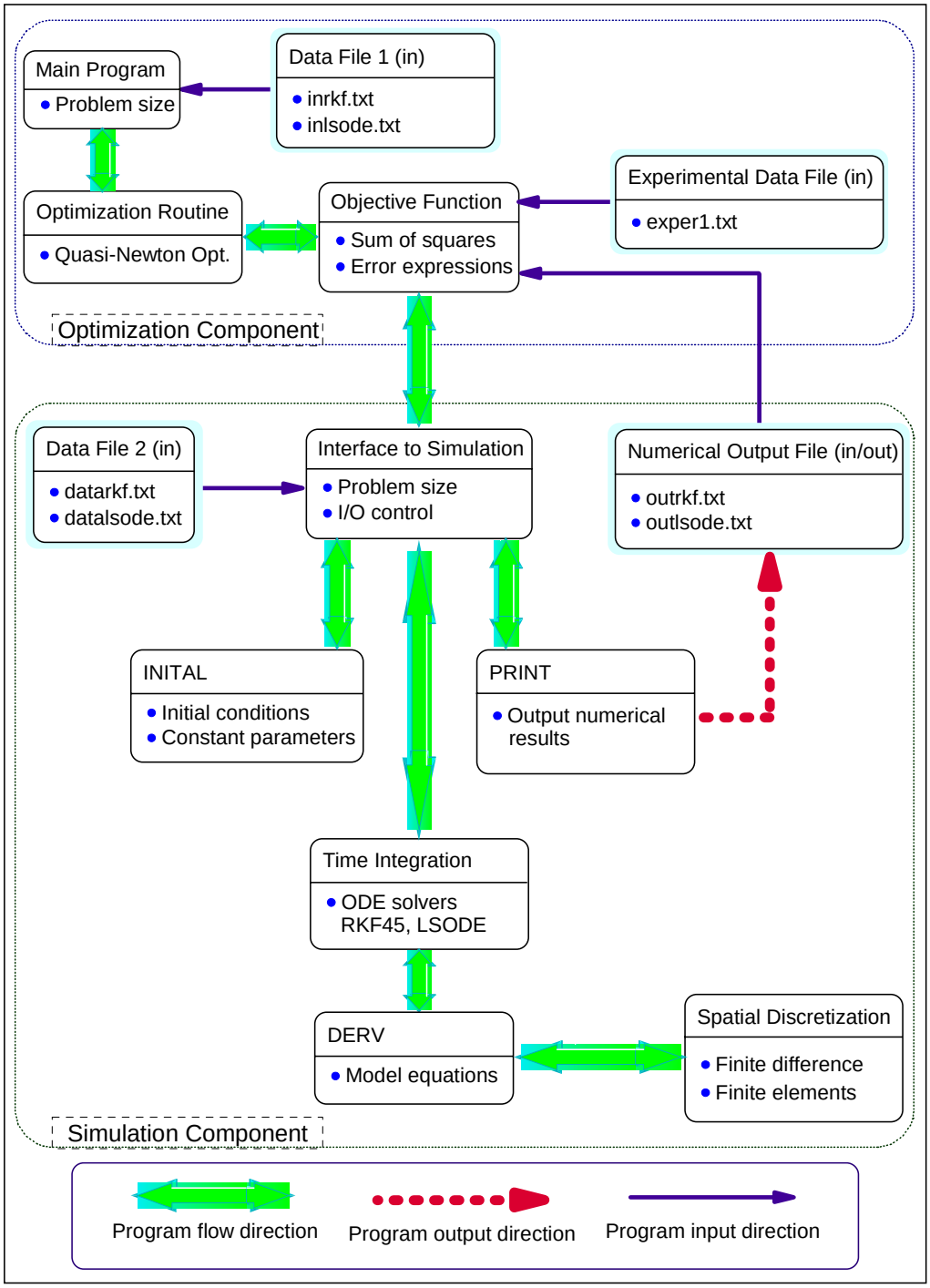


Figure 5.6: Simulation and optimization flow chart.

- OPTIMIZATION ROUTINE, is the IMSL library DUMINF where a double precision version of the quasi-Newton method with numerical derivatives is implemented.
- OBJECTIVE FUNCTION, defines the sum of the squares and the error term by accessing the simulation program to generate the numerical response and experimental response available in a data file (exper1).

The operations are controlled by the main program as stated above. The optimization routine continues iteration by making subsequent calls to the simulation routine and minimizing the sum of the squares error term to obtain the required improved form of the parameters.

A useful feature of the components (modules) shown in Figure 5.6 is that they all are written in FORTRAN90 and are therefore portable. These components can easily be used on a PC allowing a fast, low cost simulation environment. However, the system described in here was originally constructed on the computer server machines and Unix Operating System at the Lehigh University.

## 5.4 Experimental and numerical systems

The appropriate form and type of input signals and measurements should be identified and selected carefully. The successful estimation of the parameters depends on the accumulation of sufficient and quality data.

Single (Figure 5.4b) and distributed (Figure 5.4a) parameter type estimations are performed on the responses obtained from measurement stations. Both simulation routines: explicit (RKF45) and implicit (LSODE) are used for this purpose. The soil sample is divided to various segments as illustrated in figure 5.4b for the implementation of distributed parameter type estimation. Each segment is considered homogeneous within itself, while the entire soil consists of several segments represented by different parameters. This permits a heterogeneous representation of the soil sample. However, during the initial studies, it was observed that the variation of parameters from different parts of the same sample are small and the parameters

obtained from the distributed and the single type system are comparable. Therefore, the subsequent numerical and parameter estimation studies were performed based on the homogeneous medium assumption using the single parameter system.

A coarser spatial discretization is used for implementation of the explicit (RKF45). This is mainly due to stability problems of the method itself, caused by the need to match the numerical integration outputs to the experimental data in the temporal domain, which as a result requires the use of smaller time steps in integration. The use of explicit integration method in RKF45 for one-dimensional solution permits up to 21 nodes in spatial discretization along the sample. The sample is then simulated with 1 cm segments, which is acceptable since the smallest pressure sensor spacing (2.1 cm) and the thermocouple spacing (1.05 cm) are both larger than this value. The LSODE and the implicit mode of numerical solution is developed further and replaced the RKF45 for all integration purposes. Spatial discretizations up to 401 nodes, (half a millimeter), can be used with the LSODE. However, the system is well defined spatially when discretized into 101 nodes. It was observed that further increase in discretization beyond this number did not provide further improvements on the quality of the solution. The further increase beyond this point would only lengthen the solution and the time required for parameter estimation and optimization. Although not investigated in here, further discretization is possible, to study or model a localized feature or occurrence within the system.

The behavior of the experimental and numerical systems subject to the same conditions are obtained and used in the search for the desired parameters. The pressure and temperature responses of the experimental set-up stamped with location and time are reproduced at the same spatial and temporal steps numerically with the use of appropriately simplified form of the governing equations as described in Chapter 3. The application of the optimization method in terms of minimization of the objective function and error terms were described earlier in this chapter. The pressure and temperature error terms, objective functions and the minimization criterion for each are given in equations (5.12) and (5.13).

$$E_p\left(z_p\right) = \frac{\sum_{j=1}^{n}\sum_{i=1}^{m}\left[p_{eij} - p_{nij}\right]^2}{m \cdot n} \tag{5.19}$$

$$E_T(z_T) = \frac{\sum_{j=1}^{n}\sum_{i=1}^{m}\left[T_{eij} - T_{nij}\right]^2}{m \cdot n} \tag{5.20}$$

$$\frac{dE_p(z_p)}{dz_p} = 0 \quad \text{and} \quad \frac{dE_T(z_T)}{dz_T} = 0 \tag{5.21}$$

The upper bounds in summation terms; $m$ and $n$ above are the time and spatial discretization numbers. The error terms are obtained for pressure ($E_p$) and temperature ($E_T$) as a function of the required parameters in each case ($z_p, z_T$).

The governing equations stated in Chapter 3 involve many unknown parameters. As a result of the simplifying assumptions based on the nature of the physical model, and the type of conducted test, or by combination of several parameters into a single parameter, the ambiguous "curve fit" type approach was not considered, and where ever possible physical values and representations for the parameters involved were utilized. Two of the important soil parameters (thermal diffusivity $\alpha$, and rate of compressibility of the media $c_v$) for the thermal and hydraulic processes for a two-phase porous media are determined as a validation of the unified system constructed for nondestructive study of coupled. The determination of these two soil parameters using the system are discussed below.

### 5.4.1 Hydraulic gradient

In Chapter 2, the application of step-function type hydraulic gradients and the corresponding response of the soil medium were discussed. The loading and unloading stages for gradient applications and the corresponding transient pressure response for the representative samples were included in the same chapter.

The numerical solution of the simplified form of the governing equations in Chapter 3 are obtained using the simulation environment in Chapter 4. The numerical solutions are obtained for various levels of discretizations as shown in Chapter 4. The numerical responses corresponding to the experimental hydraulic gradient measurement stations are then used for comparisons with the experimental results at these locations. The responses at the measurement locations are collocated in the form of least square type error terms as described above and minimized to obtain parameters of interest.

The hydraulic gradient case of the system is simply expressed as:

$$\begin{aligned} \frac{\partial p}{\partial t} &= \left[\frac{K\,(1+e_0)}{\rho_f \cdot g \cdot a_v}\right]\nabla^2 p \\ &= C_1 \nabla^2 p \end{aligned} \tag{5.22}$$

By making use of the equation of motion for the regime immediately after the onset of the flow, and including the inertial effects on the continuity equation, the transient pressure variation is represented as:

$$\frac{\partial V_x}{\partial t} = -\frac{1}{\rho_f}\frac{\partial p}{\partial x}$$

$$\frac{\partial p}{\partial t} = -\frac{1}{\left(n\beta_p + \frac{a_v}{1+e_0}\right)}\frac{\partial V_x}{\partial x} \tag{5.23}$$

**Open material boundary**

The experimentally obtained transient pressure response of the system under open boundary conditions were illustrated and discussed in Figures 2.14 and 2.18 in Chapter 2. A convective and conductive type of model is used to represent the pressure response under open boundary conditions. The governing PDEs are discretized and the generated ODEs are integrated to produce a representative pressure response based on the initial estimate (guess) of the system parameter.

The typical open system numerical pressure responses after completion of the parameter identification stage for various discretizations simulated with implicit integration of the ODEs are illustrated in Figure 5.7. The numerical results are plotted for total node numbers of: 11, 21, 101 and 401. The experimental transient pressure of the actual system can be observed in Figure 5.7e. Almost identical parameters and pressure distributions are obtained from various spatial discretization schemes. The simulation-optimization characteristics and the obtained parameters are discussed and tabulated under the model validation segment of this chapter.

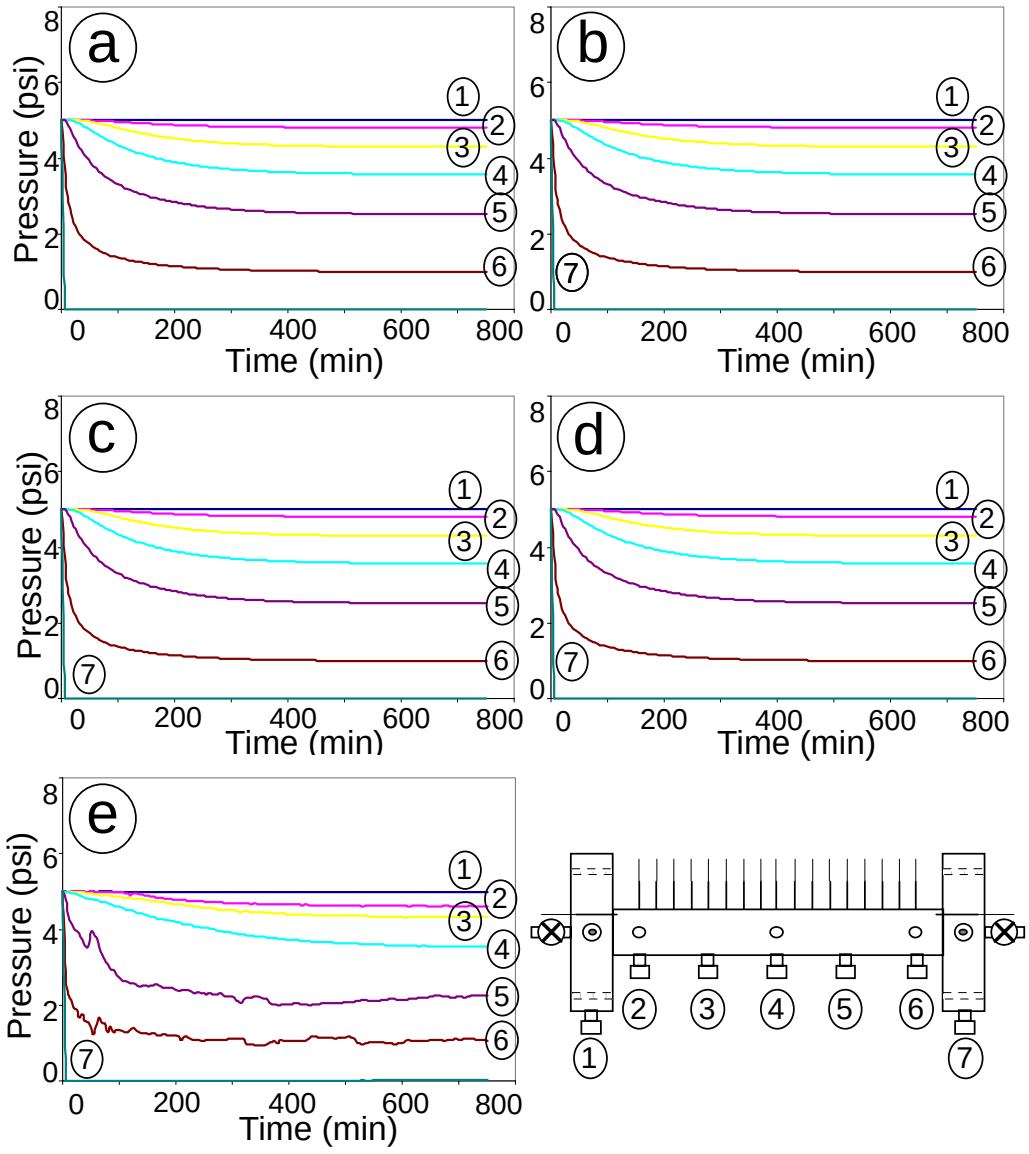


Figure 5.7: Unloading stage simulation under open conditions for total node numbers of, a) 11, b) 21, c) 101, d) 401, e) experimental plots.

### Closed material boundary

The typical transient experimental response of the system to loading and unloading under closed boundary conditions were previously shown in Figures 2.21 and 2.33 in Chapter 2. The numerical responses of the system obtained for various discretizations is represented in terms of the parabolic PDE, equation (5.22). The simulated system response with an initial guess for the parameter is collocated with the experimental response to optimize the numerical solution and obtain the desired parameter (rate of compression).

The responses of the numerical system for different discretizations at the end of the estimation routine under loading stage are shown in Figure 5.8. Figure 5.8a to d are the numerical solutions obtained with optimized parameter for 11, 21, 101 and 401 node system. Figure 5.8e, is the experimental response of the system.

Similarly, Figure 5.9 illustrates the numeric responses obtained with the optimized parameter (Figure 5.9a-d) and the corresponding experimental variation of the pressure (Figure 5.9e) along the same sample.

## 5.4.2 Thermal gradient

The application of thermal gradients at various locations within the cylindrical sample and the recorded measurements of system response in terms of transient temperature values were discussed in Chapter 2.

Repeated heating and cool-down cycles are applied to the saturated sample via heaters installed at the ends and inside the sample. The real time experimental temperature variation along the specimen is shown in Figures 2.25 and 2.27 for the heating and in Figures 2.29 and 2.31 for the cool-down segments. The plots shown in Chapter 2 are representative experimental responses of the system to the applied inputs.

A full coverage of the sample length with thermocouples was not possible due to limited number of available data acquisition channels. Therefore only a total number of 8 channels were allocated for temperature measurements. These channels were distributed evenly along the length of the sample. However, it was not possible

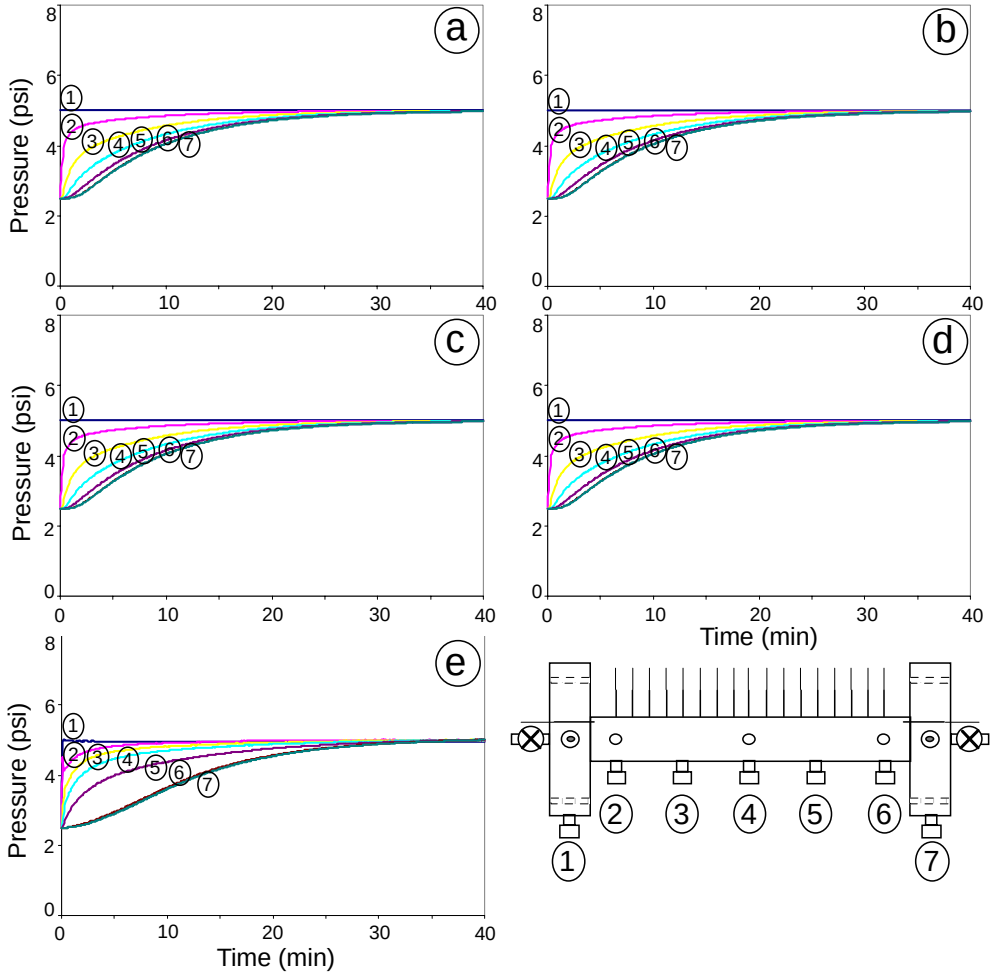


Figure 5.8: Loading stage simulation under closed conditions for total node numbers of, a) 11, b) 21, c) 101, d) 401, e) experimental plots.

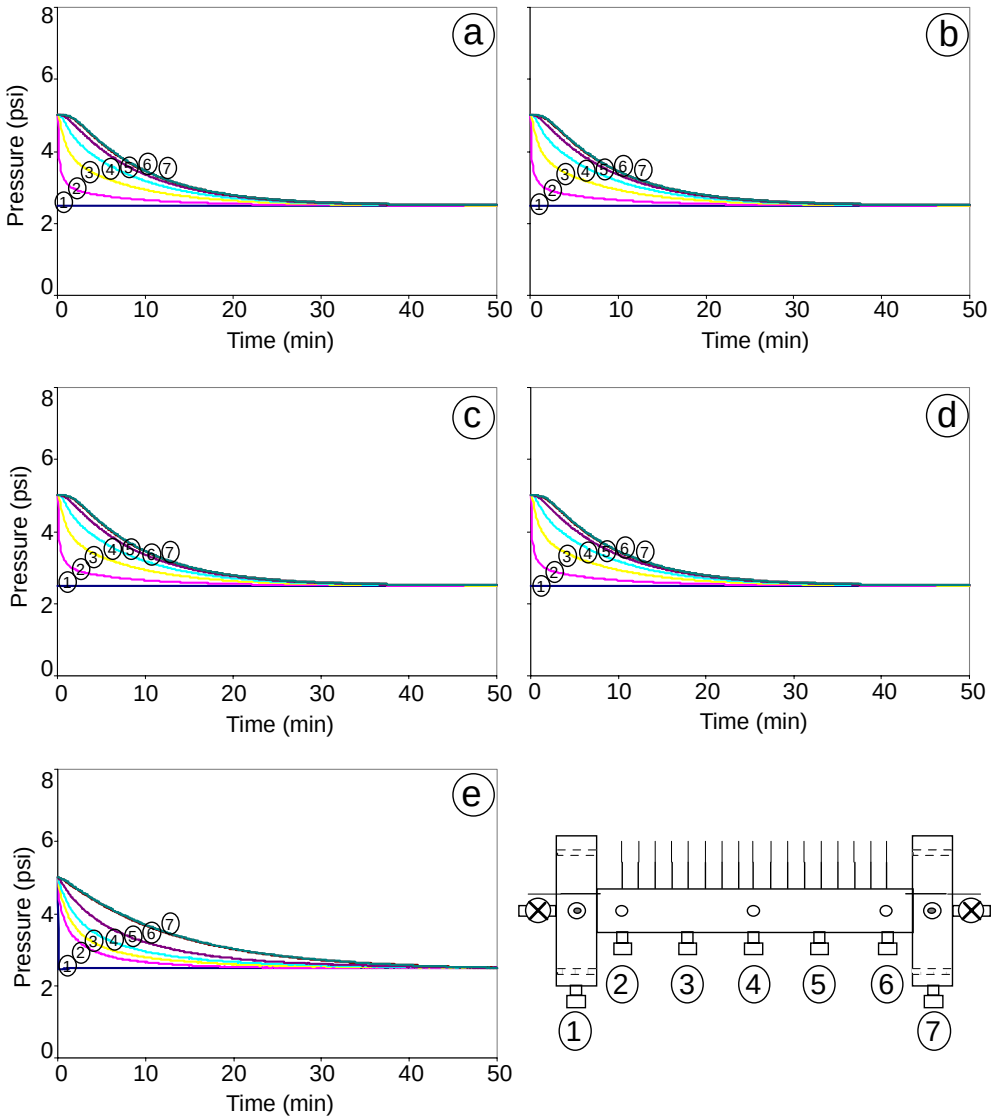


Figure 5.9: Unloading stage simulation under closed conditions for total node numbers of, a) 11, b) 21, c) 101, d) 401, e) experimental plots.

to capture a well representative temperature distribution along the full length of the sample with evenly distributed thermocouples due to presence of surface heat loss at room the temperature. As a result, a reduced spacing of the thermocouples were used instead and only the first half of the specimen was fully monitored and the temperature values were recorded. However, the entire sample length was monitored for the hydraulic case and the pressure response measured along all the stations.

Making use of symmetry, the heat source was placed at the center and the experimental response was obtained for half of the sample. The numerical solution was obtained for a sample of half length also, with heater located at the end of the sample.

The numerical simulations of the case with heater located at the boundary is performed for the full length of the sample. The numerical response along the first half of the sample is then collocated with the experimental measurements to provide the objective function in terms of the required system parameters. This partial system response proved to be sufficient in allowing successful parameter estimation for the tested sample.

**Equation of energy**

The equation for energy conservation of the system was derived in Chapter 3. Equation (3.10.5) was simplified under a set of assumptions in Chapter 4 for simulation purposes. Assuming constant thermal conductivity the equation for energy conservation is:

$$\frac{dT}{dt} = \alpha \nabla^2 T + G\left(x, y, z, t\right) \tag{5.24}$$

where

$T$ : Temperature at a point

$\nabla^2$ : Laplacian operator

$G$ : Heat generation - dissipation terms

$\alpha$ : Thermal diffusivity $\left(\frac{\lambda}{\rho c_v}\right)$

Equation (5.24) above [10] can be reduced to equation (5.25) under the closed

boundary conditions where convective transfer is eliminated due to lack of material flow, and where the contribution from the internal heat generation and surface heat loss terms are expressed individually.

$$\frac{\partial T}{\partial t} = \alpha \left[ \nabla^2 T - \frac{h}{\lambda}(T - T_s) \right] + q^{"} \tag{5.25}$$

where $h$, is the convective heat loss coefficient due to free convection around the surface and $T_s$, is the surface temperature.

The numerical solution of the equation of energy (5.20) given above, is collocated with the experimental response of the system to determine the unknown coefficients. The thermal diffusivity, free convection coefficient, conduction and the internal heat generation terms are all non-measurable quantities during a given test. The system response is obtained only in terms of the transient temperature variation along the sample. A simulation for the correct numerical temperature response is required to be able to estimate the unknown parameters.

One of the main goals of the approach is to keep the number of unknown parameters to be determined at a minimum. The use of minimal number of parameters and their constant forms are important requirements that will prevent the use of empirical forms or the development of the method as a curve fitting process.

One common method often used by many numerical applications is to handle all of the unknown parameters (i.e. $\alpha$, $\lambda$, $h$, and $q^{"}$) numerically and search for their final form and value as part of the parameter estimation routine. This approach however will take the form of a generic "curve fitting" process that will match the output of the numeric system by rearranging a set of unknown parameters based on the assumed empirical forms.

No matter how applicable, the above procedure is, it is preferred to obtain the parameters or their ratios from the known characteristics of the heater, or the final temperature profile along the length of the sample, prior to the optimization routine. This will reduce the unknown parameter to only thermal diffusivity, $\alpha$, which can be estimated in a deterministic manner.

**Heat source** The applied heat is controlled via the power supply and the voltage input. As previously discussed in Chapter 2, the internal heaters are operated at approximately 20 V to obtain a stable temperature response with minimum oscillation. The power input is calculated based on the provided rating of the heater at 120 V to be $W_{20\,\mathrm{V}} = 0.6499\,\mathrm{W}$. The term $q^{"}$ in the equation is the rate of temperature increase obtained from the volumetric heat input of the heater divided by the density and the heat capacity of the media. The average mass density of the samples used were $1.876\,\mathrm{g}\,/\,\mathrm{cm}^3$ and the range of heat capacity of $90 - 130\,\mathrm{J}\,/\,\mathrm{kg\,K}$, which resulted in a heat generation rate term of $q^{"} = 15 - 20\,\mathrm{K}\,/\,\mathrm{s}$ [**?**], [23], [22].

The heat generation component can be eliminated from the numerical calculations completely by studying the cool-down period. The initial temperature distribution of the sample during the cool-down period is obtained from the steady state profile at the end of the heating period. The cool-down, as a result of free convection from the surface provides the transient state temperature distribution at this stage, which is again used by the parameter estimation method to minimize the error between the numerical and the experimental temperature responses.

**Surface heat loss and convection coefficient** The sample is tested under room temperature conditions with no insulation. The heat loss coefficient due to free convection on the sample surface can either be directly obtained as a parameter set to be identified by the optimization routine, or obtained from the experimental steady state temperature distribution. The latter is used here. This procedure permits only the representation of the ratio of the convective heat loss coefficient to the heat conduction coefficient. This ratio (similar to Nusselt number) can then be used as a known system parameter within the numerical simulation of the governing equation and conduct the required optimization for the thermal diffusivity coefficient as previously discussed.

At steady state, the energy balance at the surface which satisfies the balance between the heat conduction along the sample and the heat loss from its surface is shown in Figure 5.10 and by equation (5.26).

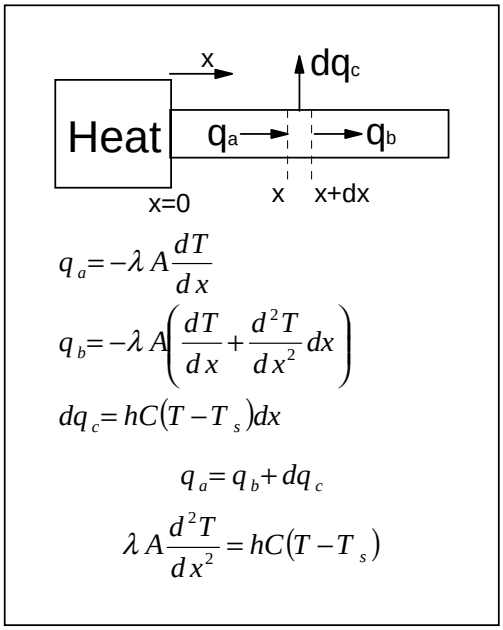


Figure 5.10: Steady state cylinder surface heat loss with a heat source at one end.

$$\lambda A \frac{d^2T}{dx^2} = hC\,(T - T_s) \tag{5.26}$$

where $A = \pi r^2$, is the cross sectional area, $\lambda$ is the thermal conductivity of the medium and $C = 2\pi r$ is the circumference of the cross section of the sample. Interchanging the temperature variables with $\Theta = T - T_s$, equation (5.26) can be re-written as:

$$\lambda \pi r^2 \frac{d^2\Theta}{dx^2} = h 2\pi r \Theta$$

Simplifying the above equation to its final form:

$$\frac{d^2\Theta}{dx^2} = m^2\Theta \tag{5.27}$$

The exact solution of equation (5.27) is : $\Theta\,(x) = C_1 e^{mx} + C_2 e^{-mx}$. The internal diameter (ID) of the test set-up is 2.54 cm. The steady state temperature profile at three or more locations along the sample for every test is used to obtain the unknown coefficients: $C_1$, $C_2$ and $m$ numerically, where $m^2 = \frac{2h}{\lambda r}$. The desired ratio

of convection to conduction coefficient is then represented by $\frac{h}{\lambda} = \frac{m^2 r}{2}$ and is used as a constant parameter in the numerical solution and simulation of the energy equation:

$$\frac{\partial T}{\partial t} = \alpha \left[ \nabla^2 T - \frac{m^2 r}{2}(T - T_s) \right] + q^{"} \tag{5.28}$$

Equation (5.28) is the generic form to be used in numerical solution under the applied source and boundary conditions.

**Loading stage - heating**

The thermal gradient and the desired temperature level is achieved by the heater and controller sets described in Chapter 2. The heaters are installed at the ends and center of the sample. The transient temperature response is recorded as shown in Figures 2.25, and 2.27 (Figure 5.11d). Figure 5.11 illustrates the numerical temperature responses for the case with the heater at the left end of the sample. Limited number of thermocouples (eight) were used during the test, and the parameter identification was based only on the partial set of data obtained from the first half of the sample. The effect of discretization and the error for the estimated parameters, along with the performance and characteristics of the estimation method are discussed at the end of this chapter.

**Unloading stage - cool down**

The transient temperature distribution obtained experimentally for the cool-down period of a test is handled similarly to calibrate the numerical simulation model. The initial temperature distribution of the sample during the cool-down period is obtained from the steady state profile at the end of heating segment. A typical curve fit with a polynomial approximation is used on the steady state distribution obtained at the end of the heating period; $T(x,0) = a_0 + a_1 x + a_2 x^2 + a_3 x^3 + a_4 x^4$. A typical initial temperature distribution for cool down is shown in Figure 5.12. This distribution is obtained by a fourth order polynomial approximation to the steady state distribution achieved at the end of the heating period. The initial temperature distribution is necessary to obtain the numerical solution of the ODE system. The

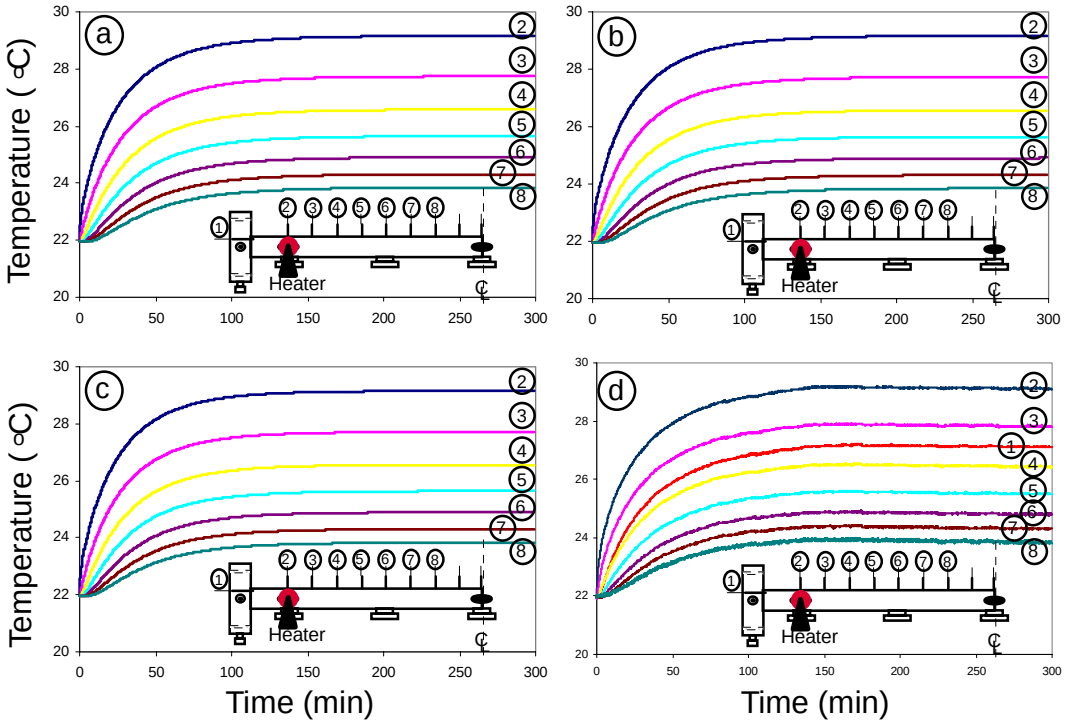


Figure 5.11: Loading stage for total number of nodes of, a) 101, b) 201, c) 401, d) experimental plot.

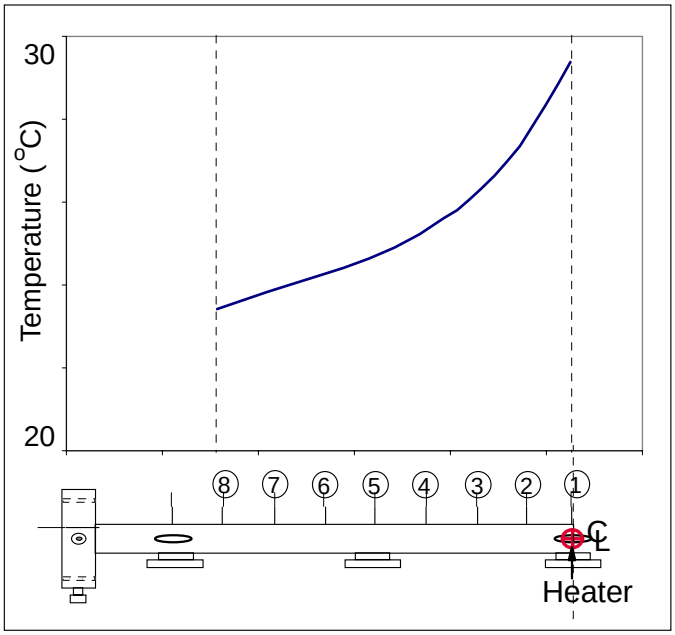


Figure 5.12: Initial temperature distribution for cool-down stage.

simulated temperature responses with the optimized parameter for the cool down period are shown for various discretizations in Figure 5.13. The results for 11 and 101 node simulations and the corresponding experimental measurement are carried up to the steady state condition ($t_f = 200\,\text{mn}$).

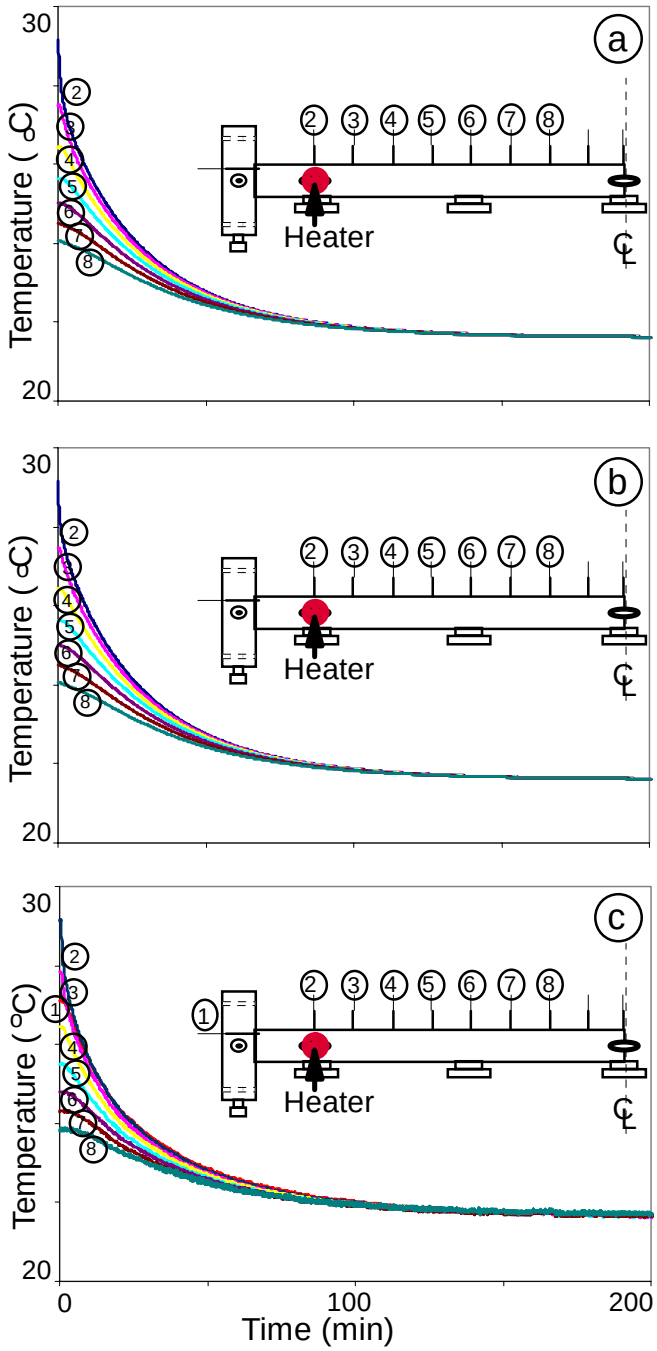


Figure 5.13: Unloading stage for total number of nodes of, a) 11, b) 101, c) experimental plot.

## 5.5 Model validation and parameters

In here, the estimated parameters are listed for various types of tests and selected soil types, and their physical significances are discussed briefly. The performance of the parameter identification method in terms of errors, convergence and effects of discretization on the numerical solutions with respect to the experimental response are presented in this section also.

### 5.5.1 Hydraulic response related parameters

The measured transient hydraulic response of the system is used to obtain the average molecular diffusion and the velocity of the propagation of the applied hydraulic pressure across the sample. The values of these parameters obtained for different samples are tabulated here.

Typical values for the diffusion coefficient for pressure migration $\left(\frac{\partial p}{\partial t} = D\frac{\partial^2 p}{\partial x^2}\right)$ under closed boundary conditions, and the velocity of the flow obtained from the equation which includes the convective contribution $\left(\frac{\partial p}{\partial t} = D\frac{\partial^2 p}{\partial x^2} - v\frac{\partial p}{\partial x}\right)$ under open boundary conditions were estimated. The average flow velocity values were then used based to obtain an average value of the hydraulic conductivity for the entire duration of test (onset - steady state), based on generalized Darcy's law.

Table 5.1: Flow related parameters due to hydraulic gradient application

| Test No. | Load Stage | Unload Stage | Diffiusivity $D$ (cm$^2$ / s) | Velocity $v$ (cm / s) | Hyd. Cond. $K$ (cm / s) | Error $\frac{f(z)}{5m}$ |
|---|---|---|---|---|---|---|
| A1 | ★ | | 0.7531984 | – | | 0.0521 |
| A2 | ★ | | 0.7535381 | – | | 0.0502 |
| B1 | | ★ | 0.7627432 | – | | 0.0382 |
| B2 | | ★ | 0.7442542 | – | | 0.0382 |
| C1 | ★ | | 0.6532783 | $1.34e-03$ | $5.27e-04$ | 0.0496 |
| C2 | ★ | | 0.7335768 | $4.28e-03$ | $4.26e-04$ | 0.0500 |

The parameters listed in Table 5.1 are obtained from optimization of the numerical and experimental data for an assumed constant form. Therefore, the table above

represents the average value of the parameters for the entire period of transient to steady state condition. These parameters can be estimated at different stages of the test, representing their variation over the transient period.

### 5.5.2 Thermal response related parameters

The transient temperature distribution obtained for heating and cool-down stages of the tests are used to determine the thermal diffusivity of the two-phase soil sample. However, the ratio of the convective heat loss at the surface to the conductive heat along the length is also obtained from the steady state distribution of the temperature at the end of the heating segment. The average Nusselt number for the experiment can be expressed as $Nu = \frac{hL}{\lambda}$, which is the measure of convective heat transfer at the surface or by the same reasoning the dimensionless temperature gradient at the surface. The average Nusselt number over the length of the sample ($L = 21\,\text{cm}$) under room temperature conditions is calculated as: $Nu = 1.04$. This value is fairly constant for different samples due to similar heater input (power) and similar temperature rise and room conditions.

The representative tests and the resulting thermal diffusivity values obtained from parameter estimation routine for these tests and their heating and cool-down segments are listed in Table 5.2.

Table 5.2: Heat flow related parameters due to thermal gradient application

| Test No. | Heater Location | Heating Stage | Cool-down Stage | Thermal Diffusivity $\alpha$ ($\text{cm}^2\,/\,\text{h}$) | Error $\frac{f(z)}{n \cdot m}$ |
|---|---|---|---|---|---|
| A1 | Left end | ★ | | 33.17 | 0.009 |
| A2 | Left end | ★ | | 33.38 | 0.01 |
| A3 | Left end | | ★ | 33.01 | 0.007 |
| B1 | Center | ★ | | 27.90 | 0.13 |
| B2 | Center | | ★ | 37.12 | 0.01 |
| C1 | Center | ★ | | 25.81 | 0.03 |
| C2 | Center | | ★ | 26.39 | 0.04 |

It is observed that the average diffusivity obtained for a soils did not show much

dependence on the location of the heather or the stage of the test. The repeatability of the measurements were checked by duplicating each test more than once and also by comparing outputs from various stages and heater locations. Duplicate test and application of various testing scenarios demonstrated clear repeatability trends.

The thermal diffusivity of the soil medium obtained here is a parameter indicating the rate of heat flow in the medium. The parameter identification was performed for each experiment and it was combined with numerical solutions of various sample discretizations $(11, 21, 101, 201,$ and $401)$. Each parameter estimation process generated an optimized form of the required parameter, output the total number of iterations performed, the number of times the function (objective function) is evaluated, the number of times the gradient is evaluated (to update the Jacobian matrix) and the final magnitude of the error (objective function) obtained for the parameter. The magnitudes of the objective (error) function corresponding to a particular iteration are also listed below. Other variations of the optimization statistics for several tests with respect to discretization size are listed in Table 5.3.

Table 5.3: Optimization statistics

| Test No. | Total Nodes | No. of Iterations | No. of Fcn. Evaluations | Gradient Evaluations | Objective Function |
|---|---|---|---|---|---|
| A1 | 101 | 7 | 27 | 8 | $.8866e-02$ |
| A1 | 201 | 17 | 46 | 21 | $.8965e-02$ |
| A1 | 401 | 24 | 94 | 46 | $0.1018e-01$ |
| B1 | 101 | 29 | 75 | 42 | 0.1392306 |
| B1 | 401 | 8 | 33 | 12 | 0.1392292 |
| B2 | 21 | 8 | 31 | 14 | 0.2053521 |
| B2 | 401 | 12 | 33 | 16 | 0.2053557 |

**Error and convergence**

The objective function was evaluated based on a single parameter model as discussed earlier in this chapter. Preliminary studies based on a distributed parameter model for a soil sample consisting of 5 segments resulted in very closely optimized

parameters for each segment, thereby in the assumption of homogeneous soil sample and representation with a single parameter model as shown above. The error term however is not normalized for the maximum magnitude of the temperature or pressure value, therefore the comparisons of error terms between different tests with different set points are not valid. Yet it is a good measure for the individual test itself and for the duplicate tests performed on the same soil sample. A plot of error variation and search for convergence during a typical optimization process is illustrated in Figure 5.14. The error (objective function) is plotted in semi-log form to demonstrate the full range of the convergence. The final error achieved at the end of this convergence is 0.009593.

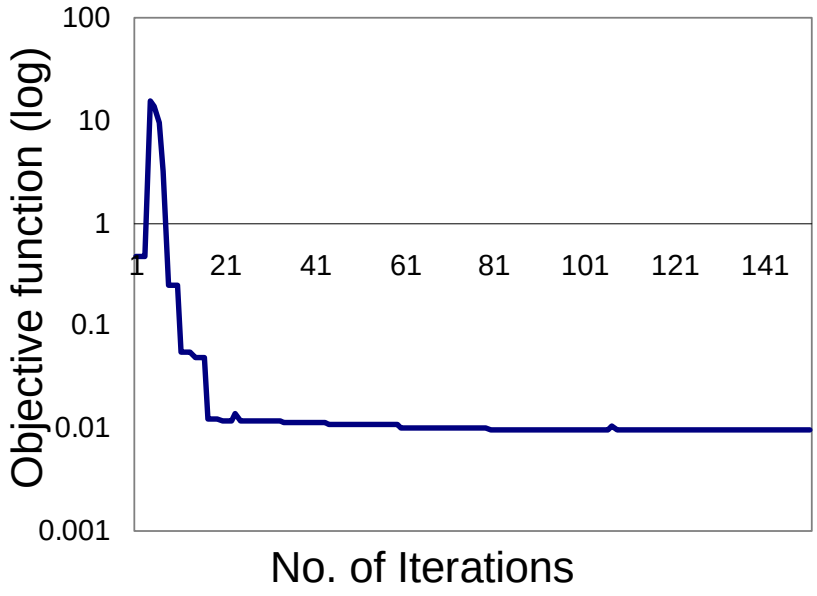


Figure 5.14: Typical convergence plot during a parameter estimation process.

### Other sources of error

As illustrated in Figure 5.15, many performance measures can be obtained and monitored to evaluate the parameter identification approach. The error between

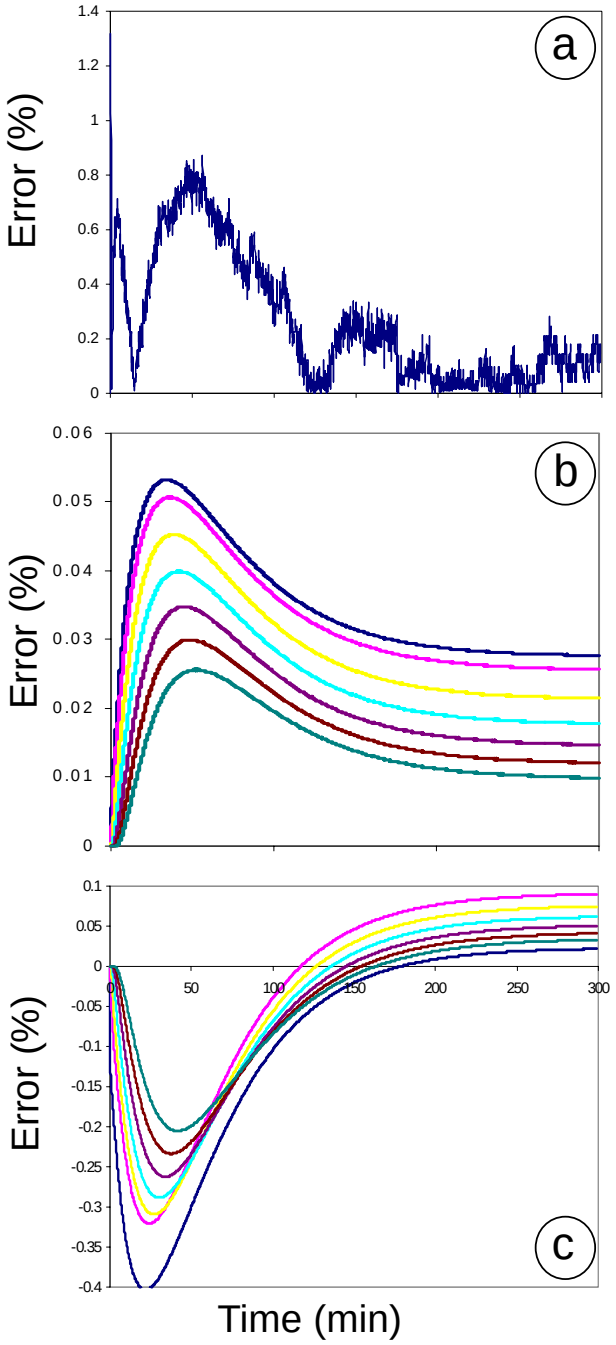


Figure 5.15: Typical errors; a) station 2 (401 nodes-experimental), b) all stations (101 - 201 nodes), c) all stations (101-401 nodes).

the optimized numerical solution and the experimental result is one of the most critical measures. A typical plot of the percent error between the numerical and experimental temperature response at one of the stations is shown in Figure 5.15a. The overall error term for all stations is computed and printed at the end of each parameter estimation process.

It should be noted that the parameter estimation for temperature response is only based on partial data obtained from a segment of the sample. This partial data is collocated with the corresponding segment of the numerical solution obtained for the entire sample. It is also indicated that a constant single parameter is used to represent the entire porous medium, which assumes homogeneous media and does not consider variations with other properties. Therefore the relatively small magnitude of the error and the convergence of the system to the experimental response is a measure of success of the process.

The variations in the numerical response due to the spatial discretization and their comparison with each other is shown in Figure 5.15b and 5.15c for 101 vs. 201 nodes and 101 vs. 401 nodes respectively. In all cases, the magnitude of the percent error, is well below 2% as shown in Figure 5.15.

# Chapter 6

# Summary and conclusion

A non-destructive system approach to the classical heat and mass transfer problem is studied. The goal of this study was to measure the transient response of the saturated porous media in terms of the temperature and pressure values, and illustrate the application of the developed system approach consisting of analytical, experimental and numerical components in obtaining the corresponding soil parameters. The closed material boundaries were used with small magnitude gradient applications to preserve the original properties of the porous media.

The ability to apply various combinations of gradients at the boundaries of the same sample under non-destructive testing conditions provided the necessary data to obtain the required parameters. These experimental tasks were conducted using a one-dimensional test set-up specifically constructed for non-destructive testing.

The coupled, transient governing equations are derived and used in a numerical simulation scheme to generate the numerical temperature and pressure distributions along the sample with an initial set of estimated coupled coefficients. The numerically generated responses are compared to the experimental set obtained under the similar boundary conditions. A parameter estimation routine is constructed based on the deviation between these two data sets. This routine performs optimization on the objective function defining the error term resulting from the collocation of the experimental and numerical responses in the spatial and temporal planes.

The analytical model describing the transient coupled process in a multi-phase

porous medium is applied to the particular two-phase, single component case studied under the experimental conditions. The governing equations are then numerically solved by methods of lines programmed in FORTRAN90.

Finally, the optimization routine was used to collocate the numerical and experimental results and solve for the desired coupled coefficients related to heat and mass transfer problem in saturated porous media. This approach was based on a sound analytical model rather than empirical evaluation. The real-time on-line capabilities of the automated test, numerical method and optimization environment could easily be geared to handle closed-loop control based on implementations of various feedback and prediction scenarios.

A unified system of experimental, numerical and parameter estimation method is developed and its validity is demonstrated in solving select problems under applied thermal and hydraulic gradients in porous media. The heat and hydraulic diffusivity coefficients are obtained under various conditions.

Further improvements to the experimental set-up are needed to capture the minute contributions from the cross coupling effects. The deformation characteristics of a two-phase saturated system can be directly included by experimental modifications at the boundaries to include piezo-electric elements as micro actuator-receiver components. The numerical simulation environment can be extended to include the equations of state and conservations for multi-component system that can address issues in three-phase unsaturated porous media.

# Bibliography


[1] *IMSL FORTRAN Subroutines for Mathematical Applications*, *2*.

[2] Bear, J. and J. M. Buchlin. *Modelling and Applications of Transport Phenomena in Porous Media*, *5*. Lecture Series Presented at the Von Karman Institute for Fluid Dynamics, Rode-Saint-Genese, Belgium, Nov. 30-Dec. 4, 1987. Kluwer Academic Publishers, 1987. Theory and Applications of Transport in Porous Media.

[3] Berzins, M., Dew P.M. and R.M. Furzeland. "Developing Software for Time Dependent Problems Using the Method of Lines and Differential-Algebraic Integrators," *Applied Numerical Mathematics*, *5*:375–397 (1989).

[4] Biot, M.A. "General Theory of Three-Dimensional Consolidation," *Journal of Applied Physics*, *12*:155–164 (February 1941).

[5] Biot, M.A. "Theory of Elasticity and Consolidation for a Porous Anisotripic Solid.," *Journal of Applied Physics*, *26*(2):182–185 (February 1955).

[6] Biot, M.A. "Theory of Stability and Consolidation of a Porous Medium under Initial Stress," *Journal of Mathematics and Mechanics*, *12*(4):521–541 (1963).

[7] Dakshanamurty, V. and D.G. Fredlund. "A Mathematical Model for Predicting Moisture Flow in an Unsaturated Soil under Hydraulic and Temperature Gradients," *Water Resources Research*, *17*(3):714–722 (June 1981).

[8] de Groot, S.R. and P. Mazur. *Non-Equilibrium Thermodynamics*. North-Holland, Amsterdam: Wiley, New York, 1962.

[9] Del Rio P., J. A. and M. Lopez De Daro. "Extended Irreversible Thermodynamics as a Framework of Transport Phenomena in Porous Media," *Transport in Porous Media*, *9*:207–221 (1992).

[10] Eckert, E. R. G. *Analysis of Heat and Mass Transfer*. McGraw-Hill Book Company, 1972.

[11] Edgar, T. V. *Moisture Movement in Nonisothermal Deformable Media*. PhD dissertation, Colorado State University, 1983.

[12] Farouki, O. T. *Thermal Properties of Soils*, *11*. Series on Rock and Soil Mechanics. Trans Tech Publications, 1986.

[13] Fitts, D. D. *Nonequilibrium Thermodynamics*. McGraw-Hill Book Company, 1962.

[14] Fletcher, R. *Practical Methods of Optimization*. John Wiley Sons, 1986.

[15] Forsythe, G.E., Malcolm M.A and C.B. Moler. *Computer Methods for Mathematical Computations*. Englewood Cliffs, NJ: Prentice Hall, 1977.

[16] Fox, R. L. *Optimization Methods for Engineering Design*. Addison-Wesley Publishing Company, 1971.

[17] Freeze, R.A. and J.A. Cherry. *Groundwater*. Prentice-Hall, 1979.

[18] Gear, C.W. *Numerical Initial Value Problems in Ordinary Differential Equations*. Englewoor Cliffs, NJ: Prentice-Hall, 1971.

[19] Gray, D. H. *Coupled Flow Phenomena in Clay-Water Systems*. PhD dissertation, University of California, Berkley, 1966.

[20] Hestenes, M. R. *Optimization Theory The Finite Dimensional Case*. John Wiley Sons, 1975.

[21] Hindmarsh, A.C. "ODEPACK, A Systematized Collection of ODE Solvers," *Scientific Computing*, 55–64 (1983).

[22] Jumikis, A. R. *Thermal Geotechnics*. Rutgers University Press, 1977.

[23] Jumikis, A. R. *Thermal Soil Mechanics*. Rutgers University Press, 1996.

[24] Katchalsky, A. *Nonequilibrium Thermodynamics in Biophysics*. Harvard University Press, 1967.

[25] Miyazaki K., Kitahara K., Bedeaux D. "Nonequilibrium Thermodynamics of Multicomponent Systems," *Physica A*, *230*:600–630 (1996).

[26] Narasimhan, T.N. and P.A. Witherspoon. "Numerical Model for Saturated-Unsaturated Flow in Deformable Porous Media 1. Theory," *Water Resources Research*, *13*:657–664 (June 1977).

[27] Onsager, L. "Reciprocal Relations in Irreversible Processes, I.," *Physical Review*, *37*(4):405–426 (1931).

[28] Onsager, L. "Reciprocal Relations in Irreversible Processes, II.," *Physical Review*, *38*(12):2265–2279 (1931).

[29] Philip, J. R. and D. A. De Vries. "Moisture Movement in Porous Materials under Thermal Gradients," *American Geophysical Union Transactions*, *38*(2):222–232 (April 1957).

[30] Polak, E. *Computational Methods in Optimization*. Academic Press, 1971.

[31] Prigogine, I. *Thermodynamics of Irreversible Processes*. Interscience Publishers, 1961.

[32] Rowley, R. L.. "Application of Nonequilibrium Thermodynamics to Heat and Mass Transport Properties: Measurement and Prediction in Nonelectrolyte Liquid Mixtures," *Flow, Diffusion, and Rate Processes*, 82–109 (1992).

[33] Schiesser, W. E. *The Numerical Method of Lines, Integration of Partial Differential Equations*. Academic Press, Inc., 1991.

[34] Schiesser, W. E. *Computational Transport Phenomena*. Cambridge University Press, 1997.

[35] Sposito, G. *The Thermodynamics of Soil Solutions*. Oxford Clarendon Press, 1981.

[36] Taylor, S. A. and J. W. Cary. "Analysis of the Simultaneous Flow of Water and Heat or Electricity with the Thermodynamics of Irreversible Processes," *International Cong. of Soil Science*, 80– 90 (1960).

[37] Terzaghi, K. *Theoretical Soil Mechanics*. New York: Wiley, 1943.

[38] Wouwer, A. V. *Simulation, Parameter and State Estimation Techniques for Distributed Parameter With Real-Time Application to a Multizone Furance*. PhD dissertation, Faculte Polytechnique de Mons, 1994.

[39] Wrobel, M. A. "Head and Mass Flows Coupled With Stress in a Continuous Medium," *International Journal of Heat Mass Transfer*, *40*(1):191–207 (1997).

# Vita

Mesut Pervizpour was born in 1967 in Tehran, Iran. After finishing Alborz high school in Tehran, he and his father, Mehrnouche Parvizpoor, mother, Fugen Pervizpour and sister, Arzu Pervizpour moved to Turkey, where he attended Bogazici University and received a Bachelor of Science in Civil Engineering with honors in 1990.

Mesut received his first Masters of Science degree in Engineering Management from Portland State University in 1992. His second Masters of Science degree was received in Civil and Environmental Engineering from Lehigh University in 1994. He pursued his work at Lehigh University and received his Ph.D. in Civil and Environmental Engineering in January 2000.

Mesut has been appointed as a teaching assistant and adjunct instructor for many undergraduate and graduate courses in civil engineering, computer programming and numerical methods courses throughout his graduate studies. He has been recognized and awarded for his teaching efforts at both Portland State University and Lehigh University. Furthermore, he has been recognized as a leading research scholar in his field and he has published in topics related to coupled flow, non-destructive testing, electrokinetic decontamination, and use of medical imaging technologies such as NMR in porous media.

Mesut is currently working as a research associate at the Drexel Intelligent Infrastructure and Transportation Safety Institute at Drexel University in Philadelphia.